Research on models for the transient system of the visual system

Wong, K.H.

Award date:
1986

5083.

Department of Electrical Engineering.
Eindhoven University of Technology.
Group "Measurement and Control".

RESEARCH ON MODELS FOR THE TRANSIENT SYSTEM OF THE VISUAL SYSTEM.

by K.H.Wong

This report is submitted in partial fulfillment of the requirements for the degree of electrotechnical engineer (M.Sc.) at the Eindhoven University of Technology.
The work was carried out from May 1985 untill August 1986 in charge of Prof.dr.ir.P.Eykhoff and under supervision of ir.H.A.L.Piceni and ir.A.C.den Brinker.

Summary

The purpose of this research is to construct a spatio-temporal model for the transient channel of the human visual system. With this model predictions can be made for the detection of relatively large, and fast changing stimuli.

The model considered in this report consist of two parts: a spatio-temporal filter and (in cascade) a temporal filter. The spatio-temporal filter is called the lateral membrane. This lateral membrane is a two-dimensional spatial structure modelled as an electric transmission line.

For simplicity reasons the transmission line is chosen of a very low temporal order. Several electric circuits (equivalents for the transmission line) with appropriate order are investigated. From these circuits one is chosen on qualitatively similarities to the measurement data.

Quantitatively the membrane and the temporal filter are parametrized on basis of the impulse response of disks with relatively large diameter (1° - field).

Hereafter we simulate the transient system on a computer and compare the simulations with the known measured data.

For not too large stimulus disk diameter our model gives good results compared with the measured data.

Contents:

Chapter 1: Introduction

Nowadays visual perception takes an important place in a man-machine relation. In various situations it is interesting and often important to know, how the perception occurs in the human visual system.
Having a model for the human visual system, predictions can be made for the perception of an arbitrary stimulus. In this way one can state technical demands, which have to be fulfilled by visual apparatuses. For instance one could make predictions, how well certain details on a display can be observed.
Another example is in the area of the print- and reproduction techniques; here one is interested in the recognition of letters and symbols, which often are distinctive by the presence of a small detail. Here one wants to predict how the size, the shape and the luminance of the letters and symbols influence the observation.
Therefore a model of the visual perception is developed.

In the visual observation the spatial as well as the temporal luminance variations of the detail are of importance.
Models of the human visual system usually are spatial or temporal only. Both spatial and temporal models mostly are split into several channels operating in parallel, each tuned to specific stimuli.
In the temporal domain there usually are two channels postulated: the sustained and the transient channel. The first channel gives responses mainly to low temporal variations, the second to relatively high temporal variations (see Roufs and Blommaert, 1981).
The spatial models consist of four (e.g. Wilson and Bergen, 1979) or more (e.g. Koenderink and van Doorn, 1978) parallel operating channels, operating at every place of the retina.
It also is known that a coupling exists between temporal and spatial characteristics of a channel. Spatially high tuned channels (for detail vision) have sustained characteristics, spatially low tuned channels are transient of character.
We think a unifying view might give more insight in the operations of the visual system. Therefore a spatio-temporal model is proposed. For the time being, this model is used for the transient channel only. The reason for this is that a spatio-temporal coupling is to be expected to be most pronounced for channels that operate on spatially extended stimuli. For instance a limited velocity of the transmission of signals from one place of the retina to another would be particularly influential for large distances.
To obtain insight in the processing in the visual system many experiments are done using detection tasks at a certain background level of luminance. The operation of the visual system is then approached in a system-analytic manner; see figure 1.-1.
We have a certain input signal (the stimulus) of specified spatial and temporal luminance course. Furthermore an output signal exists in the form of answers of some subject signalling he did or did not see the stimulus.
Between this in- and output we suppose some detection rule and the blackbox of the system-analytic approach.

In this blackbox all the important features of the visual system are to be modelled.

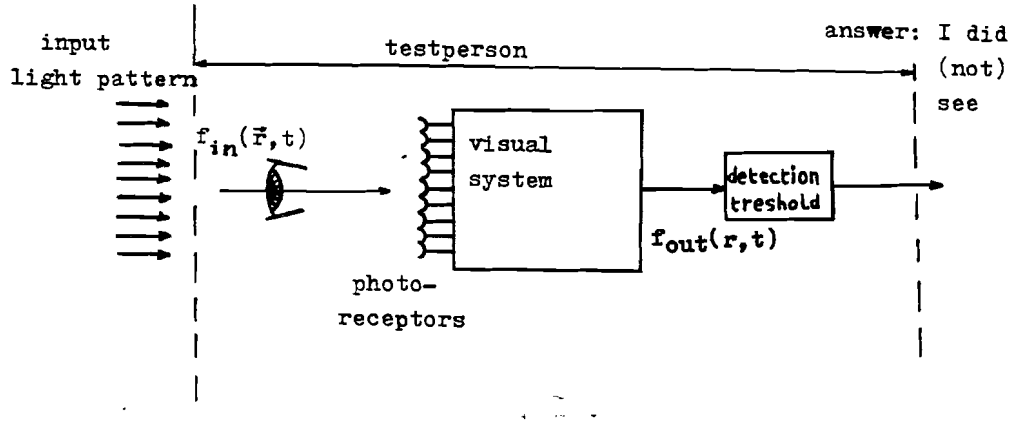

Figure 1.-1. The model of the human visual system for detection tasks.

In this report we will discuss the following items:
The chapter 2 is used to give a short overview of existing (important) spatial and temporal models and subsequently our model for the transient channel.
Then, in chapter 3, the measurement data are considered, that we think are part of the transient channel and thus should be incorporated in our model. From these data a qualitative notion of the operation of the transient channel can be obtained.
In chapter 4 part of the already outlined data is quantitatively analyzed. These analyses will later on be used to parametrize the suggested model.
In chapter 5 the basic postulates of the model are stated and discussed. Starting from these postulates a (quite general) theory of system analysis in three dimensions (two spatial and one temporal) is outlined.
Having a general theory, this is applied to a transmission line, in the consequent section. This transmission line is a model for the connections between the different receptors in the retina. The transmission line itself can be modelled by different electrical circuits. Several of these circuits are discussed. On qualitative grounds one structure for the transmission line is chosen. This transmission line is then parametrized on the basis of the analysis of chapter 4.
In chapter 8 simulations of the chosen transmission line, which we will call the lateral membrane, are shown. From the analysis of chapter 4 it follows that in series with the lateral membrane a pure temporal filter is needed. This temporal filter is discussed and also parametrized in chapter 9.
Finally the total model can be simulated and the overall responses are calculated. These can be compared to the measured data.
As a last chapter the conclusions and recommendations on the model analyzed so far, are given.

Chapter 2: Several models for human vision

In this chapter we will discuss three models of the human vision. As already stated in the introduction most models are spatial or temporal only. Two of the models dicussed here are spatial (Wilson and Bergen, 1979; Koenderink and van Doorn, 1978) and one is temporal (Roufs, 1974; Roufs and Blommaert, 1981). These models give some idea along which lines most of the present modelling of the visual perception runs.
As a last part of this chapter we will introduce the model we are going to investigate in the rest of this report. We will look at the simularities and differences of this model with respect to the others.

2.1) Temporal model (J.A.J.Roufs and F.J.J.Blommaert).

Here the visual system is analysed according to the temporal properties. The visual system is assumed to consist of two systems operating in parallel (figure 2.-1). A lowpass filter, associated with the physiologically defined "sustained" cells and a strict bandpass type of filter associated with "transient" cells. In the case of sinusoidal modulation the output of the former is suggested to cause the homogeneous brightness variations at low frequencies ("swell") and the typical percept seen at the high frequencies ("agitation"). The bandpass filter is found to process quasi-linearly at threshold level.

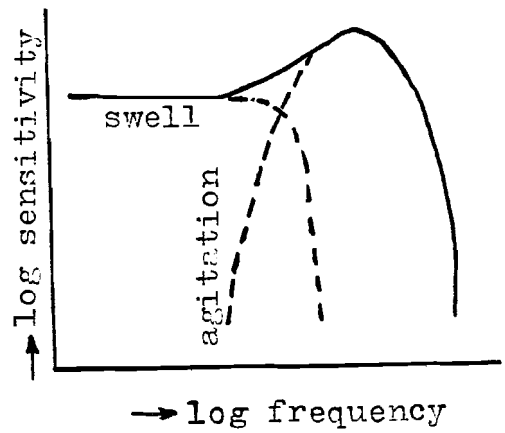

Figure 2.-1. Schematic representation of the amplitude sensitivity curves harmonically modulated light of a 1°-field as a composite of the curves of two constituent processes.

Changes of retinal illumination caused by a stimulus on a steady background level E will be described by $f_{in}(t) = \epsilon_f f(t)$. ϵ_f is the amplitude factor and $f(t)$ the normalized time function.
We shall only consider small and fast changes of retinal illuminance (transients).
For sufficiently large fields (1°-fields and larger) these evoke perceptual changes in the visual field ("agitation"), which cannot be identified as brightness changes. For small fields clear brightness increments or decrements may be observed.

The model used is illustrated in figure 2.-2.

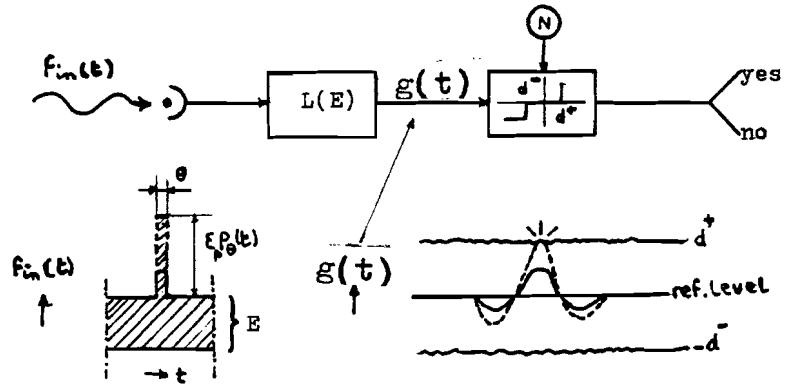

Figure 2.-2. The operation of the hypothetical mechanism for detecting fast luminance variations.

At the lower left an example of such a variation of retinal illumination is shown. The signal, which is proportional to a luminance variation, is processed linearly by the first part L of the system. Response g(t) leads to perception, if the deviation from the stationary state exceeds a certain amplitude d^+ or $-d^-$. Two deterministic systems properties are postulated. First small changes are processed linearly:

$$L\{\epsilon_f f(t)\} = \epsilon_f g_f(t) = g_\beta(t) \qquad (2.-1)$$

L is a linear operator (dependent on E; see figure 2.-2) and $g_f(t)$ the response from the linear system to f(t).
Second the stimulus $\epsilon_f f(t)$ is seen, if its response deviates at least by a magnitude m from the stationary reference level (peak detection). This might be a signal-to-noise criterion or an internal threshold. Thus at threshold:

$$\epsilon_f \, \mathrm{extr}\{g_f(t)\} = m \qquad (2.-2)$$
$$m=d^+ \text{ or } -d^-;\ d^+, d^- > 0$$

If the extremum happens to be positive $m=d^+$, otherwise $m=-d^-$. Equation (2.-2) states that if $g_f(t)/m$, the response of f(t) expressed in m units is known, the threshold value of the amplitude factor ϵ_f can be calculated. The magnitude d is in fact thought to be a stochastic variable. Here the intrinsic stochastic properties are not essential and therefore d will be treated for convenience as a deterministic quantity. For all stimuli the values ϵ_f corresponding with a 50% detection probability will be defined as threshold (see chapter 3: psychometric function).
As an example let us take a rectangular flash with an intensity increment ϵ_p and a duration θ, which is short compared to the time constant of system L. Denote this flash by $\epsilon_p p(t)$. From its response, $\epsilon_p g_p(t)$, we obtain the threshold value by applying equation (2.-2):

$$\epsilon_\rho \text{extr}\{g_\rho(t)\} = m \qquad (2.-3)$$

The linear system L is fully characterized by its unit impulse response $g_\delta(t)$. If the flash is short, the response $\epsilon_\rho g_\rho(t)$ can be approximated by $\epsilon_\rho \theta g_\delta(t)$.
The threshold condition becomes in this case

$$\epsilon_\rho \theta \,\text{extr}\{g_\delta(t)\} = \epsilon_\rho \theta\, g_\delta(t_{ex}) = m \qquad (2.-4)$$

t_{ex} is the time after the stimulus onset, at which $g_\delta(t)$ attains its extreme value. Thus at threshold the stimulus factors are related to the extreme of the impulse response by :

$$\frac{1}{\epsilon_\rho \theta} = \frac{g_\delta(t_{ex})}{m} \qquad (2.-5)$$

$g_\delta(t_{ex})/m$ will be referred to as the norm factor of the unit impulse response.
In order to predict thresholds of arbitrary fast changing stimuli by means of (2.-2) only $g_\delta(t)/m$ and not the value m is needed. This easily can be seen by rewriting (2.-2) in the next form:

$$\epsilon_f \,\text{extr}\{g_f(t)/m\} = 1$$

The function $g_f(t)/m$ can be written as a convolution with the impulse response according to

$$\frac{g_f(t)}{m} = \int_0^t f(t-\tau)\,\frac{g_\delta(\tau)}{m}\,d\tau \qquad (2.-6)$$

The function $g_\delta(t)/m$ can be directly measured as is shown in the article of Roufs and Blommaert (1981). In chapter 3 we will show some impulse responses measured in the way described by Roufs and Blommaert, and use these data for the parametrization of our model.

2.2) The Wilson-Bergen model (the four channel model).

This model is based on results, which are obtained from measurements of linespread functions (LSF). A linespread function is the response of the visual system on a small, lineshaped stimulus.
Wilson and Bergen assume that at each location of the retina more detection mechanisms contribute to the detection of a stimulus. Each mechanism has a distinctive LSF.
They say that there are four different detection mechanisms and so there are four different LSF's at each location of the retina. The strength of the response of a mechanism is determined by the way of stimulation: each mechanism has its own "preference stimulus". Dependent on the temporal course of the stimulus the so-called S- or T-mechanism gives the strongest response (S=sustained, T=transient). The two used modulation forms are drawn in figure 2.-3.

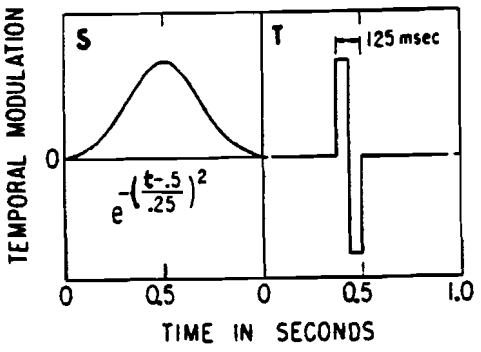

Figure 2.-3.The two used modulation forms.

The spatial shape of the stimulus is also important: in the high spatial frequencies the N-mechanism is stronger influenced, in the low spatial frequencies the U-mechanism (N=narrow, U has no special meaning).
These four mechanisms, or channels, always work in parallel. The total response is a kind of co-operation of all four the responses of the individual mechanisms.
The response of each mechanism can be calculated from its linespread function. This LSF can be described as the difference of two Gauss-functions. The LSF of the i^{th} mechanism has the following shape:

$$LSF_i(x,x') = A_i(x)\{\exp - \frac{(x-x')^2}{\sigma_i^2(x)} - \beta_i \exp - \frac{(x-x')^2}{\gamma_i^2 \sigma_i^2(x)}\} \qquad (2.-7)$$

x=location of the centre of the LSF on the retina.
x-x'=distance to the centre of the LSF.
A (x)= amplitude factor: $A_i(x) = A_i(0)/(1+a_i|x|)$
σ_i (x) =width factor: $\sigma_i(x) = \sigma_i(0)(1+K|x|)$.
β_i and γ_i are constants for a certain i.
i=N,S,T or U = index for a certain mechanism.
The factors A_i, σ_i, β_i and γ_i are different for each of the four mechanisms. Further σ_i, β_i and γ_i seem to be invariant for different testpersons, so that for one testperson still 9 parameters have to be measured: A_N, A_S, A_T, A_U, a_N, a_S, a_T, a_U and K. These 9 factors are dependent on the way of modulation.
The LSF's of the four mechanisms on the same location of the retina are different of shape and magnitude. The LSF of one mechanism also varies with the excentricity. This is shown schematically in figure 2.-4.

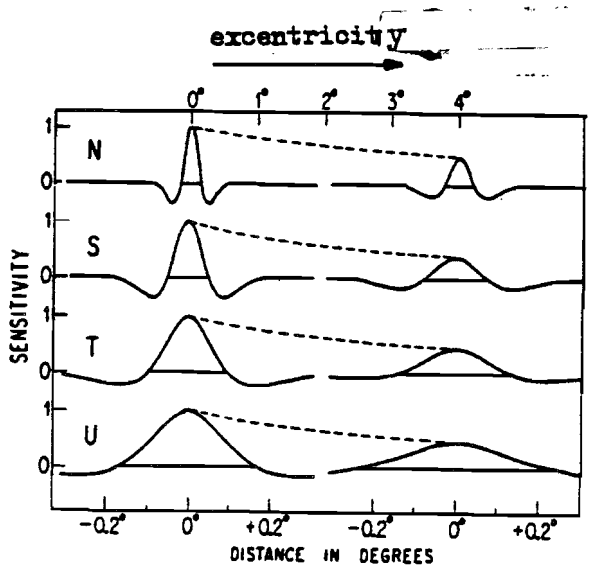

Figure 2.-4. The linespread functions of the four mechanisms.

The response $R_i(x)$ of a mechanism i on a stimulus with a lumination $L(x')$ is given by the convolution of $L(x')$ and the LSF:

$$R_i(x) = \int_{-\infty}^{\infty} LSF_i(x,x')\ L(x')\ dx' \qquad (2.-8)$$

Assume now that only one mechanism responds. The stimulus will be detected, when the response exceeds the internal signal threshold. The detection value is then $R_i(x) \geq d$.
The threshold d is stochastic; the probability distribution is assumed as Gaussian shaped. The probability that this "early" detection occurs is bigger, if the area of the response is bigger. Therefore one must account for this "spatial probability summation".
For example instead of 1 N-mechanism now two or more nearby N-mechanisms will respond. For the other channels holds the same. Because the relation between the response on a certain point and the contribution to the spatial probability summation is not linear, Wilson and Bergen take a number of arithmetic rules in their model to describe this non-linearity. These arithmetic rules (see Heynen, 1980) read as follows:
-the response $R_i(x)$ of each mechanism is raised to the fourth power (the power 4 is in accordance with the steepness of the psychometric curve of Wilson and Bergen). By this operation the relation between response magnitude and the contribution to the probability summation is linearized. (It is in fact a transformation to a linear probability space).
-after that the response values of all response mechanisms of one kind are summed over the whole visual field.
-finally the fourth root is taken of the sum (because of the first operation this inverse transformation is needed).

In this way the total effect of all the mechanisms i are created (it is assumed that the mechanisms are not correlated spatially). In formula:

$$R_i = \left[\sum_{\substack{\text{visual} \\ \text{field}}} \left\{ \int_{-\infty}^{\infty} LSF_i(x,x')\ L(x')\ dx' \right\}^4 \right]^{1/4} \qquad (2.-9)$$

With this formula the effective magnitude of the responses of the i^{th} mechanisms together on a stimulus $L(x')$ can be calculated. Because in reality the four kind of mechanisms work in parallel and so all respond, these four R_i's are summed. The total response of the visual system on one certain stimulus can be described as:

$$R_{total} = (R_N^4 + R_S^4 + R_T^4 + R_U^4)^{1/4} \qquad (2.-10)$$

By the value of R_{total} a "thresholdmeter" determines, if the threshold has been exceeded or not. In figure 2.-5 the model is shown schematically in bloc form.

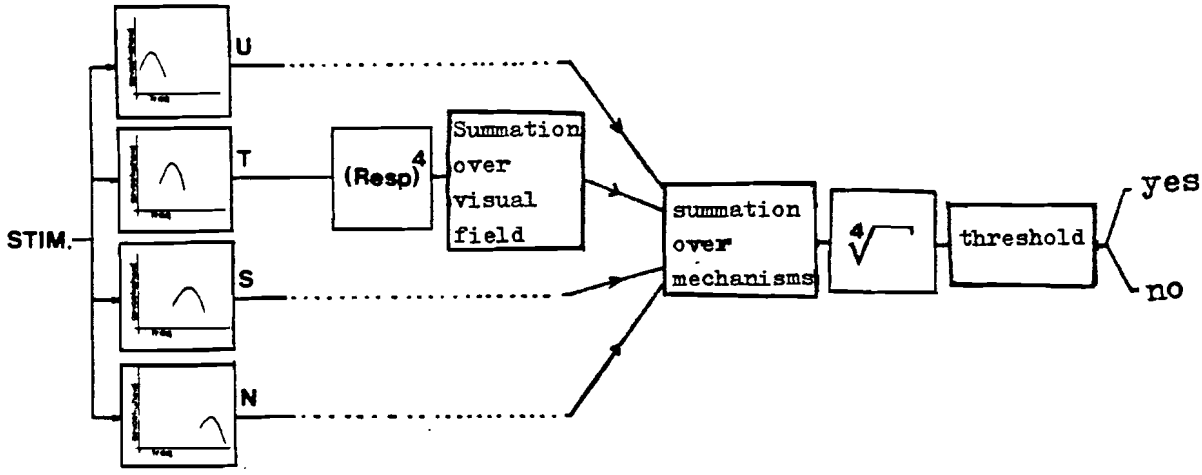

Figure 2.-5. Schematic representation of the four channel model.

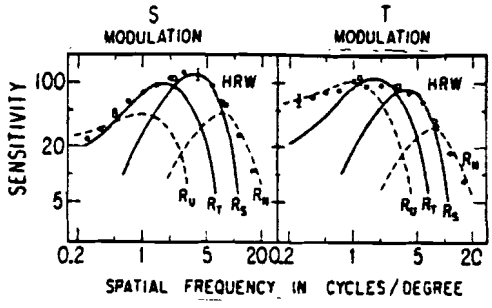

Figure 2.-6. The summation over the four mechanisms (in MTF-form). The lines are the calculated, the dots the measured values. (MTF=Modulation Tranfer Function).

In figure 2.-6 for each LSF the Fourier transform is drawn. The horizontal axis is the spatial frequency axis and the vertical axis the sensitivity (this is the reciprocal value of the luminance threshold). This graph is called the (Spatial) Modulation Transfer Function (MTF).

The four channel model can be seen as an "arithmetic model", with which predictions of threshold values are obtained by a number of arithmetic rules.

2.3) The Koenderink-Van Doorn model (the sunflower model).

This spatial model is more a "think model", by which a likely more real situation is described, but by which quantitive predictions are more difficult to obtain. Therefore here follows only a qualitive description of this model. This so-called "layer-model" is based on psychophysical, physiological and electrophysiological experimental data.
The most important (electro-) physiological result that is incorporated in the model, is the fact that receptive fields are measured. This means that one certain receptor cell in the retina is not represented at one point of the visual cortex, but that by all kinds of connections between the cells, which the signal passes on its way to the brain, finally a bigger field of the cortex is stimulated.
These receptive fields have been shown to exist at cortex level, but also at points closer to the receptor cells, for example at ganglion cell level. One receptor cell stimulates thus more ganglion cells. Reversed one ganglion cell is stimulated by a small group of retina receptor cells. This small group is assumed circular-shaped. The centre of this small group of cells has a positive action on the activity of the ganglion cell (see figure 2.-7).

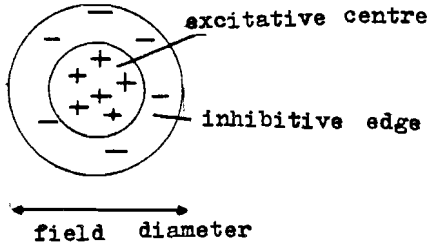

Figure 2.-7. Schematic construction of a receptive field: centre-surround structure.

In the edge of this small group the effects of the receptor cells work against the activity of the ganglion cells. This is also experimentally confirmed by measurements of signals of ganglion cells.

The model is derived from the fact, that near each location on the retina receptive fields with different sizes are measured. The receptive fiels, called "units", are presumed circular-shaped. The unit diameter varies continuous between a minimum value (for the fovea about 20 seconds of arc) and a maximum value (about 1 degree).
In the model the units are divided into a number of groups, dependent of the unit diameter. Such a "subset" contains units with almost equal extension. There are 40 subsets. In a subset all the units lie next to each other, such that an imaginary layer arises that is constructed of equal units (thus 1 subset=1 layer). The number of units in a layer is always the same and equal to 4.10^4.
All units within one layer join to each other and lie circle symmetric round the centre of the fovea. The result is that consecutive layers will always be more extensive. The layer with the smallest units will have a total extension of about 1 degree; a measure which is comparable with the measure of the central fovea.
In figure 2.-8 this is schematically shown. This figure also shows that units of all kind of sizes appear in the centre of the visual field. From the centre to the periphery with increasing excentricity continually more small units drop out.
The minimal unit magnitude ϕ increases also as a function of the excentricity according to $\phi_{min}(exc.) = \lambda.exc$, in which exc (the excentricity) and λ are constants.

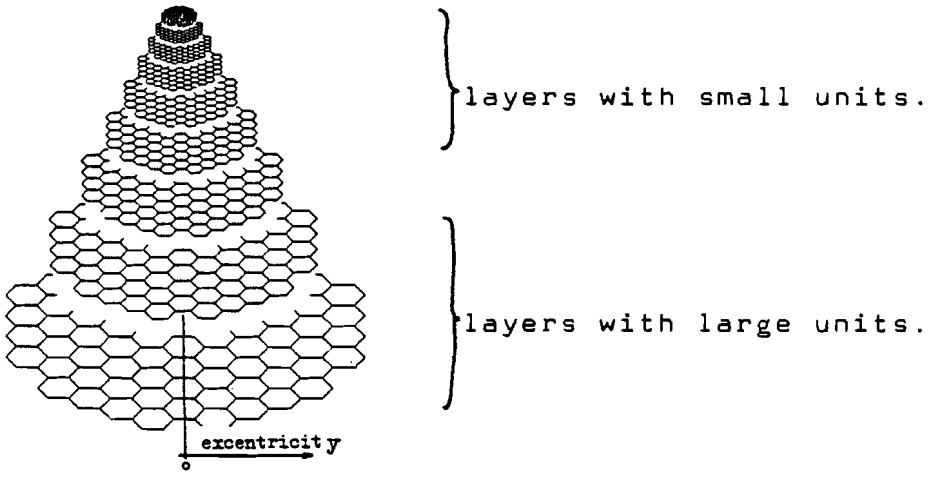

Figure 2.-8. Schematic presentation of the layer-model. Drawn are parts of nine successive layers. The units are for the simplicity drawn as six angles instead of dots.

The response of one unit.
Each unit has a "centre-surround" structure: it consists of an excitation centre, surrounded by an inhibitation margin area (see figure 2.-6). This also has the following consequences: if a stimulus only acts on the centre of an unit, then the unit will respond strongly. If also a part of the inhibitation edge is stimulated, then the response is smaller.

If both edge and centre are completely covered by the stimulus, then the actions of both parts are cancelled, so that there is no response. This means that units which are smaller than the stimulus (and are covered completely) give no contribution to the response.
It will be obvious that the pointspread function and the response of one unit are related to each other: the point spread function is strongly determined by the neural (unit) action.
Koenderink and Van Doorn approximate the action of a unit with the following function (see figure 2.-9): the excitation part has an action, which is constant over the area; the inhibitation part is "infinitely" narrow and has an "infinitely" negative action. The total integral over both parts is however equal to zero.

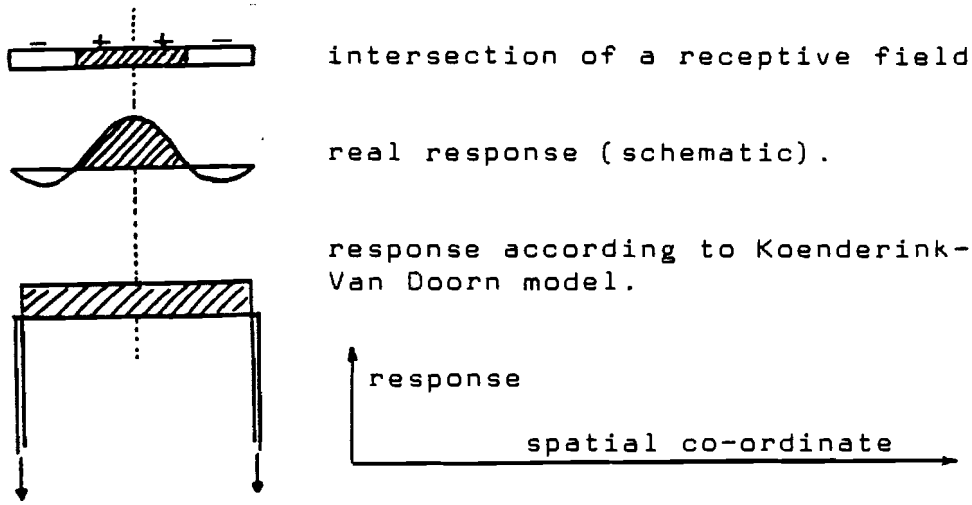

Figure 2.-9. Response of a receptive field.

Through the combination of the both preceding models the results of Wilson and Bergen are more reasonable:
a. The linespread function will be wider with increasing of the excentricity, because there are continually less small units.
b. There will be more mechanisms active, because at one location of the retina there are more unit sizes present. Wilson and Bergen have explained their experimental data by assuming, that there are four mechanisms present. This is the minimum to come to satisfactory results. These four mechanisms correspond with the 40 layers of the Koenderink-Van Doorn model. One mechanism is thus in fact an average over about 10 unitlayers.
c. The spatial probability summation is a certain co-operation of units, as well within one layer as between the layers mutually.

A disadvantage of the Wilson and Bergen model is that the model is based on linespread functions instead of pointspread functions. According to the Koenderink-Van Doorn model the use of pointspread functions is preferable.

2.4) A spatio-temporal model for the transient system.

The visual system is here analysed according to both dimensions: spatial and temporal. The light which goes into the human eye, is spatially sampled by the photo receptors (light sensitive elements) on the retina. In figure 2.-10 a model is shown of the spatio-temporal model.

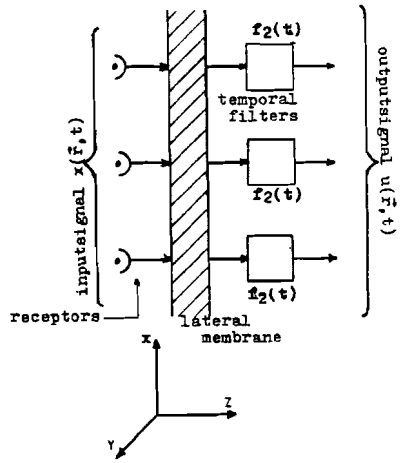

Figure 2.-10. Schematic presentation of the spatio-temporal visual model.

The signals $f_{in}(r,t)$ are input to a layer of neural elements, on which the filaments lie in a lateral (parallel to the retina) plane, where they make synaptic connection with each other.
We assume that the density of these neural elements is so large, that the layer may be looked upon as a continuum (in lateral direction). We shall call this layer the lateral membrane of the visual system. Then the signals will be processed further by filters with an impulse response $f_2(t)$.
In this report it is assumed that the lateral membrane can be compared with a passive electrical transmission line: these lines usually conduct the signal with a limited velocity and damp the signal. This damping relates the interaction between two spatially seperated inputsignals in the transmission line. Therefore it is a measure of the distance, for which signals are integrated through the transmission line.

The similarities and differences between the several models:
-a subdivision in parallel operating channels is used in every model, each operating at every point of the retina.
-each channel is linear.
-we do not present a total model for vision, but we only consider one channel.
-this one channel is simultaneously parametrized in the temporal and spatial domain.

-the model is spatio-temporal, i.e. its spatial and temporal properties are interdependent. (The Wilson Bergen model is in a certain sense also spatio-temporal: they used another parametrization for each of the two different time modulation methods, with which the experiments were performed).
-we do not go parafoveally, as the two spatial models.
-in our model no stochastic properties are incorporated.

Note that:
-the broadest channel of Wilson and Bergen changes with the excentricity.
-the broadest channel of Koenderink and van Doorn stays the same.

We do not make any assumptions about changes going from fovea to parafovea.
Secondly the Wilson and Bergen and also the Koenderink and van Doorn model have two antagonistic parts even in their broadest channel. Although this antagonistic part is very shallow in the Wilson and Bergen model for the broadest channel (see figure 2.-4), it still exists. We have no (spatial) inhibition in our model.

Chapter 3: Measurement data

In this chapter all the available data concerning the transient system is presented. These consist of measurement of different temporal variations to disk-formed stimuli of different diameter. The following experiments are dicussed:
-temporal impulse response measurements.
-sensitivity measurements of impulse with different disk diameter.
-sensitivity measurements of sinusoidal temporal modulation of disks.
-phase characteristics of sinusoidal temporal modulation.
-sensitivity measurements of temporal pulse modulation with variable duration.
The data shown here are from different subjects, and different background luminances (E). And there is no surround luminance. All data are obtained from psycho-physical measurements, which are performed at the IPO (Institute for Perception Research).

Psychometric curve.
Offering any stimulus of a certain intensity a testperson can be asked, if he sees, or does not see the stimulus. Doing this with the same stimulus several times and also at different intensities a psychometric curve is obtained; for certain small intensities the testperson never detects the stimulus, for certain larger stimulus intensities the stimulus is always seen. In between there exists a range of intensities, where the stimulus is sometimes seen and sometimes not. For these intensities the percentage of seen stimuli can be plotted against the intensity. A monotonically increasing curve is then obtained as shown in figure 3.-1. The intensity at which 50% of the stimuli is observed, is often called the threshold value.
All experments discussed in this chapter involve the measurement of psychometric curves and its threshold value.

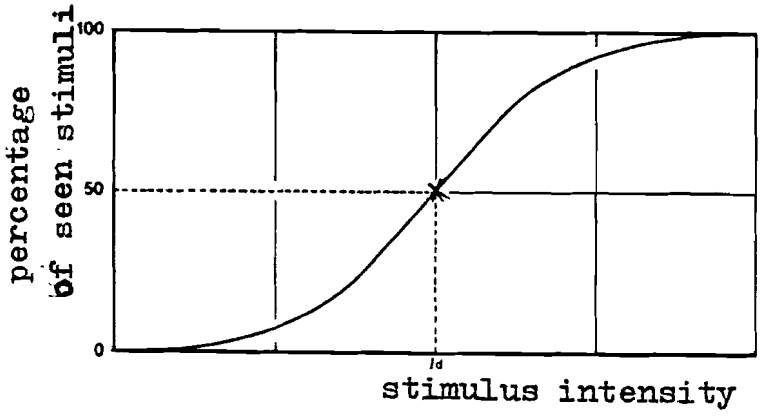

Figure 3.-1. A psychometric curve.

The physical value at which 50% of the stimuli is observed, is often called the threshold value.

3.1) Impulse response measurements of disks.

The transient system of the visual system is assumed to be linear: a filter in cascade with a peak detector. By this assumption one can measure the impulse response of this linear filter by using a perturbation technique. We will not discuss this technique here. For more information about this perturbation technique one can consult the article of Roufs and Blommaert (1981).
The consequence of this technique is that the measured impulse responses are all normalized at an extremum equal to one and have a time axis, which has its origin exactly at the moment of this extremum. The starting point of the impulse response is lost. The black dots are the mean values of the measurements. The vertical lines through the dots are twice the value of the mean variance of the mean value of the measurements.
In figure 3.-2 we show the impulse response of two different subjects with two different background luminances and three different disk diameters.

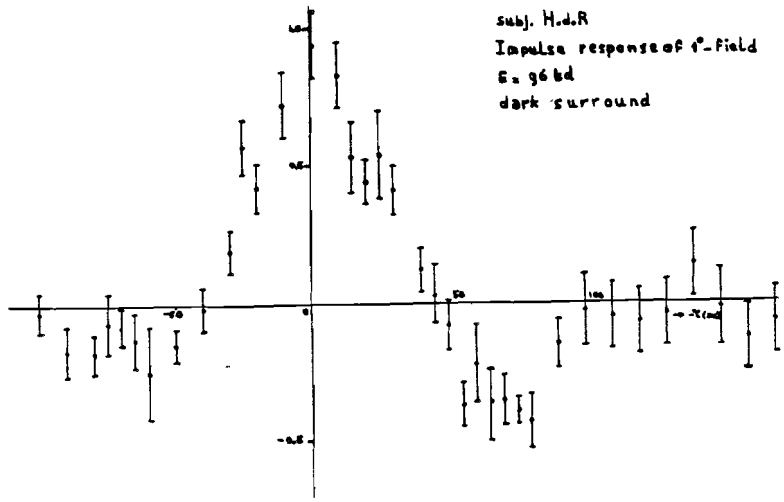

Figure 3.-2a)

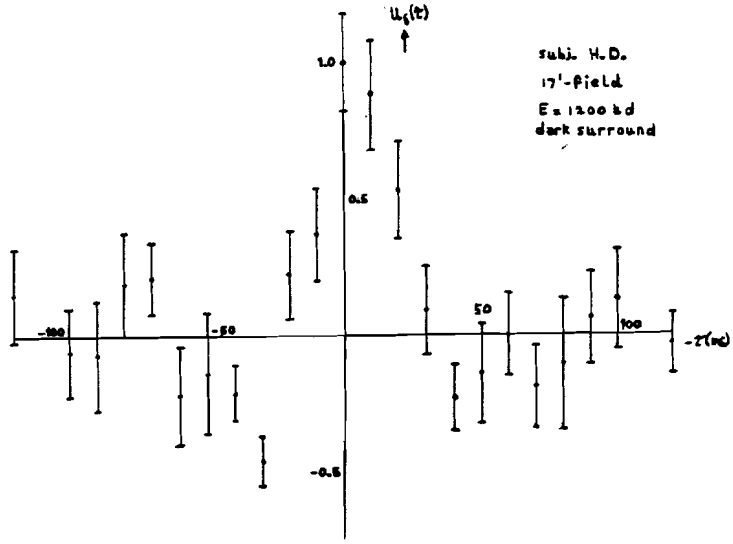

Figure 3.-2b)

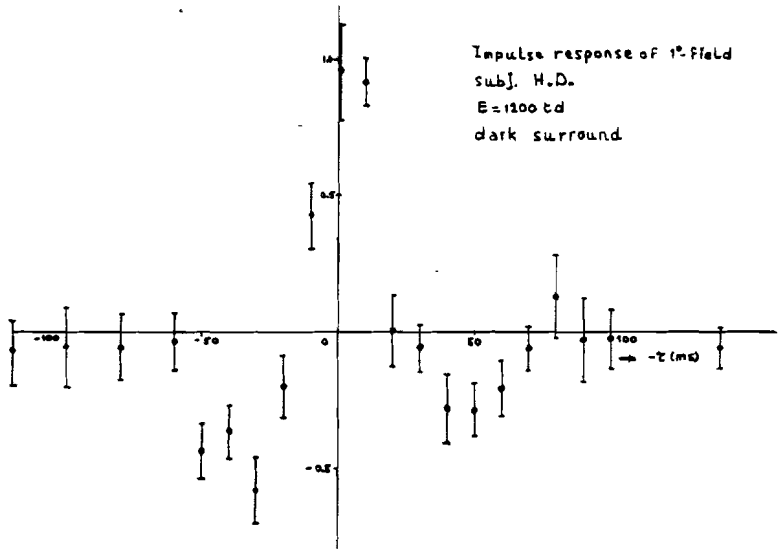

Figure 3.-2c)

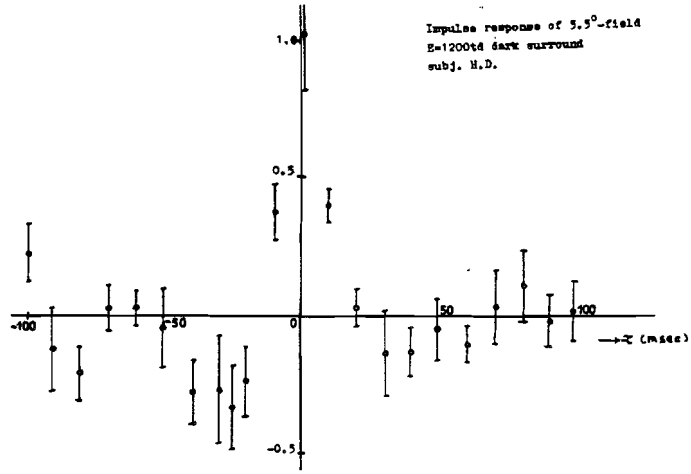

Figure 3.-2d)
figure 3.-2. The impulse response of the visual system as a function of the time.

Figure 3.-2a shows the impulse response of 1 degree field of subject H.d.R. and a background luminance E=96td.
Figures 3.-2b, c and d show the impulse responses of subject H.D. with a background luminance E=1200td and with different stimulus disk diameters.
From these figures we see that for different background levels E and different subjects the impulse response has essentially the same form: a triphasic impulse response. Compare figure 3.-2a and 3.-2c.
Figure 3.-2b, c and d show the impulse responses for different disk diameters (different spatial configurations). We see here that the form remains the same but that the impulse response gets faster for larger disks: larger time constants.
The negative phases increase and later decrease with the increasing of the stimulus disk diameter.
From these figures we can conclude that the transient system must be a spatio-temporal model, because temporal impulse response depends on spatial configuration.

3.2) Sensitivity measurements of the transient system of the visual system to impulses with variable disk diameter.

In figure 3.-3 the amplitude ϵ of the impulse response is measured for which a detection probability of 50% occurs, as a function of the disk diameter. The inputsignal is here also a Dirac-function as temporal modulation: a pulse with a small duration θ =2ms.
For subject H.d.R. and a background luminance of E=100td the experimental data are shown in figure 3.-3. From this figure we can conclude that in the intermediate values 1-3 degrees the sensitivity (defined as $1/\epsilon$) is here the strongest.

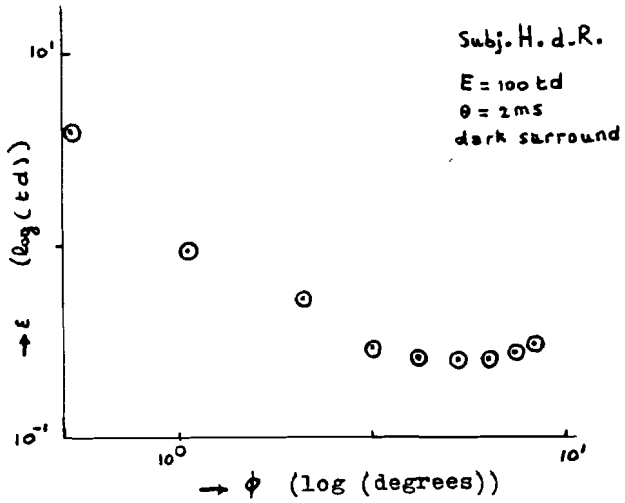

Figure 3.-.3. The threshold measurement of flashed disks as function of the stimulus diameter.

3.3) Sensitivity of the transient system to temporal sinusoidal modulation of disks.

The input signal has now a sinusoidal time modulation and has an amplitude e. The reciprocal of the amplitude e is called amplitude sensitivity (1/e). The amplitude e is measured of the sinusoids, for which 50% peak detection occurs.
In figure 3.-4 the sensitivity 1/e as a function of the temporal frequency is illustrated with the stimulus disk diameter as parameter. These curves are called the De Lange curves. The subject is H.J.M. and the background luminance E=62td.

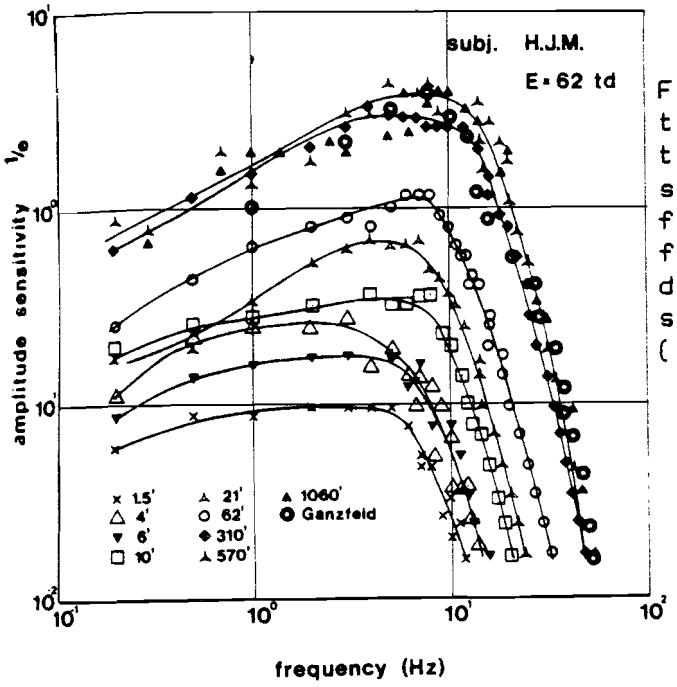

Figure 3.-4: temporal modulation transfer as measured by 50% theshold amplitudes of a sinusoidal modulation as a function of the temporal frequency. The parameter is the diameter of the foveal circular stimulus (E=60td; dark surround). (from Roufs and Bouma, 1980)

From this figure we see that for smaller disk diameter the curve is more smooth for small temporal frequency: there is less bandpass characteristic for smaller disks. The bandwidth also decreases with smaller disks.
Because the temporal properties shift with the variation of the spatial configuration (changing of stimulus disk diameter) we again see that the transient system of the visual system is spatio-temporal.

3.4) Phase characteristic of the transient system.

In figure 3.-5 the phase difference between the sinusoidal stimulus and its response of the visual system is shown as function of the temporal frequency. The phase characteristic is measured using a pertubation technique (this is not discussed here, see Roufs, Piceni, Pellegrino van Stuyvenberg, 1984).

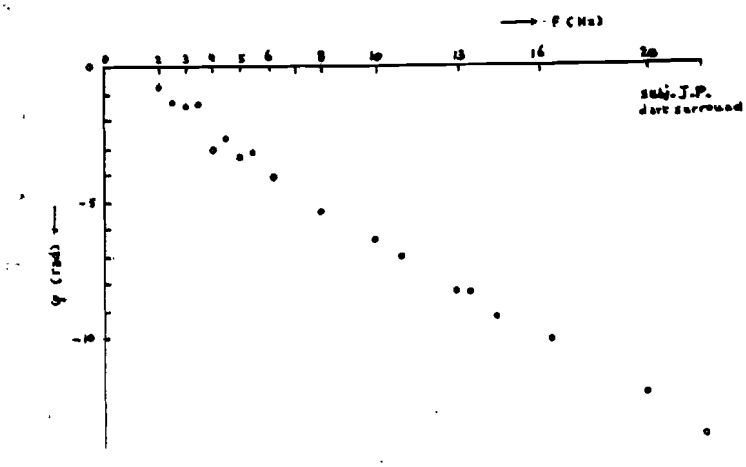

Figure 3.-5. The phase characteristic as a function of the temporal frequency for the human visual system.

The measurement of figure 3.-5 is done for subject J.P. at one luminance level (E=1200td) and with one stimulus disk diameter (1^{o}).
We see that the phase curve decreases nearly linear with the increasing of the temporal frequency. This is in agreement with the nearly symmetrical impulse response shown in a) of this chapter.
From Fourier analysis it can be shown that signals symmetrical with respect to some vertical axis $t=T_1$, have a linear phase characteristic, $\phi = \omega T_1$.

3.5) Sensitivity measurements using temporal pulse modulation with different pulse duration.

As in 3.2) and 3.3) of this chapter the sensitivity ϵ is measured according to the 50% peak detection method for a certain stimulus disk diameter and a certain pulse duration θ in the time domain. In figure 3.-6 the sensitivity ϵ is measured as a function of the pulse duration θ for different stimulus disk diameter and three different subjects at three different background level E.

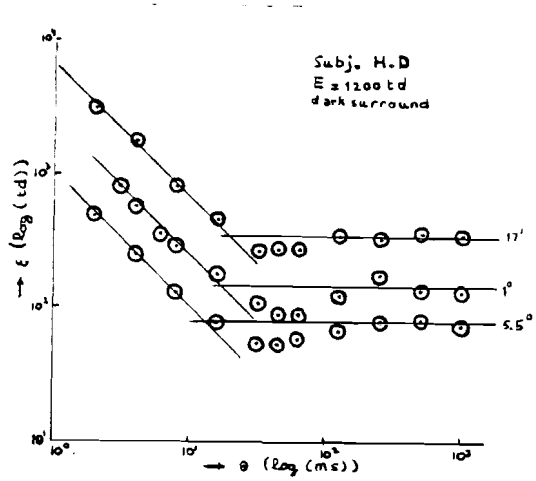

Figure 3.-6a)

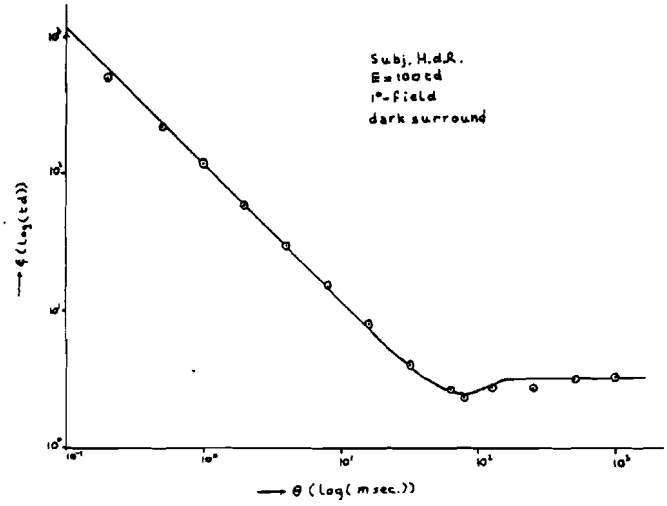

Figure 3.-6b)

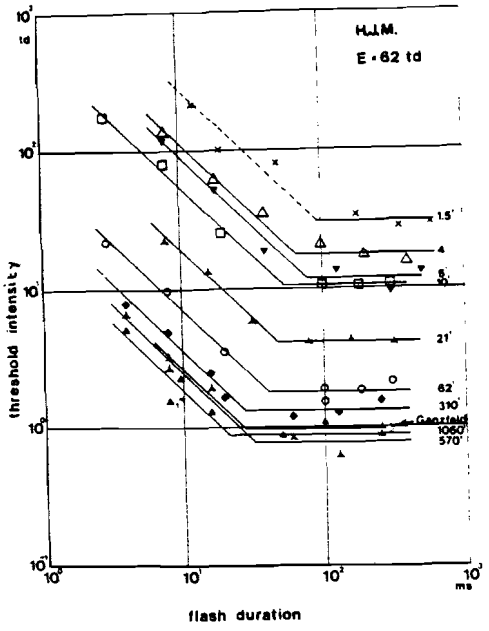

Figure 3.-6c) (From Roufs and Bouma, 1980)
Figure 3.-6. The threshold sensitivity ϵ as a function of the pulse duration for different stimulus disk diameter and three different subjects at three different background levels E.

In figure 3.-6a the data for subject H.d.R. is shown with a background luminance E=100td and a stimulus disk of 1°; figure 3.-6b shows data of subject H.D. with E=1200td and 3 stimulus disks 17', 1° and 5.5°; in figure 3.-6c we have subject H.J.M. with E=62td and different stimulus disks.
We see in these figures that for short pulse duration θ the sensitivity curves decrease linear with the increase of the pulse duration: the detection is dependent on the area of the pulse (Bloch's law).
For example if a pulse of sensitivity ϵ_1 and duration θ_1 is detected, then a pulse of sensitivity $\frac{1}{2}\epsilon_1$, and duration $2\theta_1$ will be also detected for small pulse durations. The angle of the sensitivity curve and the vertical axis is 45° for small pulse duration. This relation holds for any linear filter for durations much smaller than the time constants of the observed filter.
For long pulse duration the sensitivity curve is constant, thus independent of the pulse duration θ. The two transients of the on-set and the off-set of the rectangular pulse don't influence each other anymore for long pulse duration.

For intermediate values of the pulse duration we see a dip; the sensitivity curve goes down, comes up and becomes constant with increasing pulse duration. This is called Broca-Sulzer effect. From simulations of different subjects at different background levels it can be shown that the measured impulse response is in good quantitative agreement with the strength of the Broca-Sulzer dip (Blommaert,F.J.J., J.A.J.Roufs and A.C.den Brinker, 1986).

Furthermore we see that with the variation of the disk diameter the dip also varies. The dip has a largest value at 1°-field for subject H.D. (see figure 3.-6b) (figure 3.-6c contains not enough data-points to observe this effect).
The largest dip for 1°-field of the measurement of subject H.D. is also in accordance with negative phases of the triphasic impulse response for 1°-field (see figures 3.-2b, c and d); for the negative phases of the impulse response also have their largest values for 1°-field.

3.6) Comparison of pulse measurements and the frequency domain measurements.

We are going to seek, if the frequency response measurements and the pulse duration measurements are in accordance with each other with the changing of the stimulus disk diameter.
The maximum of the amplitude sensitivity curve (for an interpretation see Roufs and Bouma, 1980) in figure 3.-4 is defined as the sensitivity-factor S. In figure 3.-7 this sensitivity S is illustrated as a function of the stimulus disk diameter (upper curve).
The lower curve is the sensitivity factor $F=1/\epsilon$, this is defined as the reciprocals of thresholds of the pulse response for long pulse duration. Thus in figure 3.-4 there is also shown the sensitivity factor F as a function of the stimulus disk diameter.

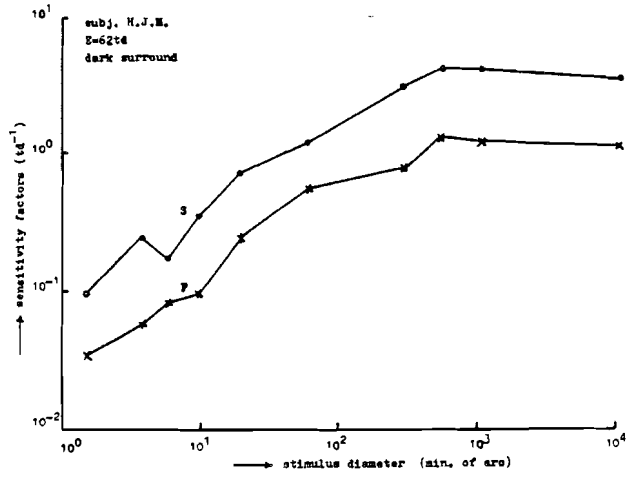

Figure 3.-7. Sensitivity characterized by the top, S, of the curves of figure 3.-4 or by F, the reciprocal of the threshold ϵ of long pulse duration flashes of figure 3.-6 as a function of stimulus disk diameter (from Roufs and Bouma, 1980).

In this figure we see that both curves have the same form: both increase and for a certain stimulus disk diameter are constant with a further increase of the disk diameter.

In figure 3.-8 the reciprocal of the cutoff frequency f_h is given as a function of the stimulus disk diameter. This cutoff frequency f_h is the frequency at which the amplitude sensitivity has dropped to S/2.
The lower curve is the critical duration T_c as a function of the stimulus disk diameter. The critical duration T_c is the pulse duration at the intersection of the constant line and the decreasing line with a slope of 45° in figure 3.-6.

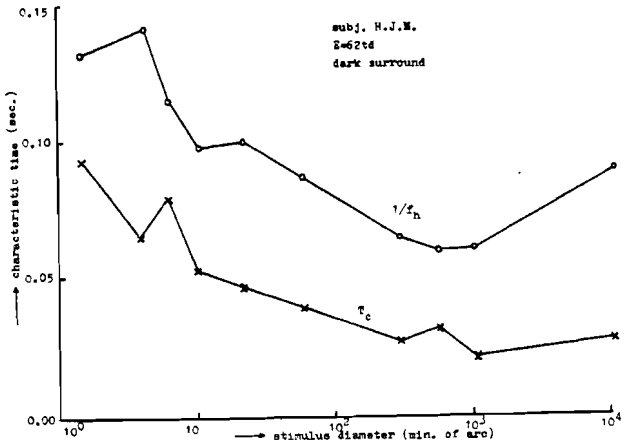

Figure 3.-8. The time constants of the visual system characterized by either the reciprocal of the cutoff frequency f_h of figure 3.-4 or the critical duration T_c of figure 3.-6 (from Roufs and Bouma, 1980).

From figure 3.-8 we see that both curves have the same form: both curves have a minimum for a certain stimulus disk diameter.
We conclude from this two last figures that the pulse and frequency response measurements are in good agreement with each other as a function of the stimulus disk diameter (see Roufs and Bouma, 1980). This is to be expected for a linear system.

3.7) Perceptual data.

When the impulse response of the stimulus disk is viewed above the threshold level a brightness is then seen which is largest in the middle of the disk and zero at the border.
On the basis of this kind of considerations a transmission line is suggested as a model for the transient system of the visual system (see den Brinker and van Aalst, 1984 and van Aalst, 1981). This transmission line has a load impedance at the edge of the disk, which has a value equal to zero. The signals, travelling along the transmission line and reaching this impedance are reflected and are reversed of sign. The response at the edge will therefore always be zero.

Chapter 4: Analysis of temporal data

At the moment there are two different description available for the triphasic impulse responses: as a fourth order filter, or as a pseudo-matched filter configuration (see den Brinker, 1985A and 1985B).

4.1) Fourth-order model.

Here we want to show that the triphasic impulse response of the visual system can be modelled as a linear fourth order filter. The response to an impulse of a 1°-field with a dark surround can be modelled as a fourth order filter with four poles and three zeroes according to:

$$G(s) = K^{*} \frac{\prod_{i=1}^{3} (s - z_i)}{\prod_{i=1}^{4} (s - p_i)} \qquad (4.-1)$$

with $G(s)$ the Laplace transform of the impulse response, while z_i are the zeroes of the system, p_i the poles and K^{*} is a multiplication factor.

The parameters of this model (K^{*}, z_i, p_i) were estimated from the measurement data of subject H.D. using a Hankel estimation for two different stimulus disk-sizes (1° and 5.5°). The plots are shown in figure 4.-1a and 4.-1b together with the measured responses for the same stimulus disk-sizes.

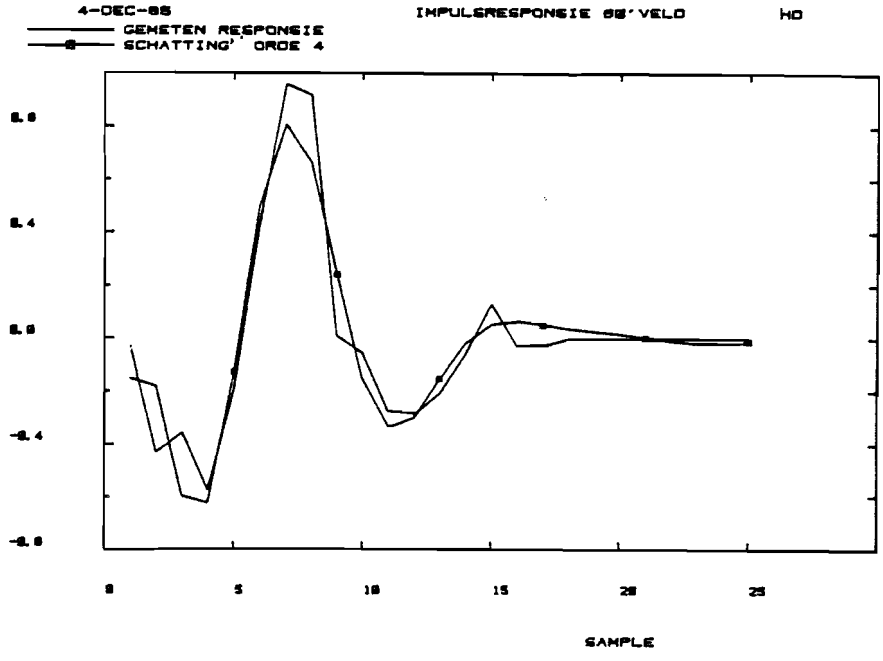

Figure 4.-1a)

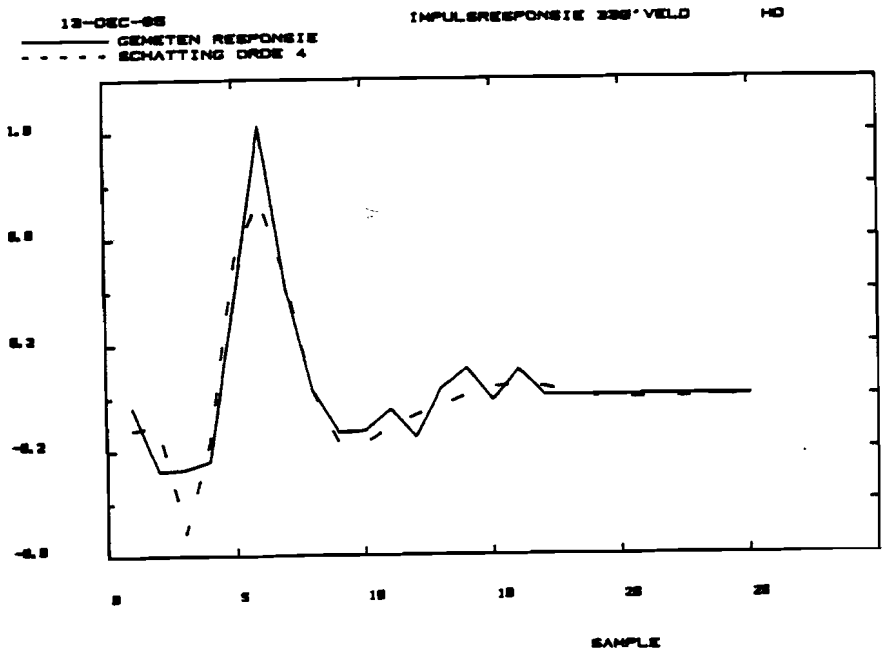

Figure 4.-1b)
Figure 4.-1. The measurement data and the fourth order estimation of the measurement data of subject H.D. at a background luminance E=1200td for two different stimulus (a: 1^{o}-field, b: 5.5^{o}-field) disk sizes.

The approximated poles are:

1^{o}-field		5.5^{o}-field		ratio of the imaginary parts
$Re\{p_i\}$	$Im\{p_i\}$	$Re\{p_i\}$	$Im\{p_i\}$	
-25.99	93.78	-37.61	123.0	1.31
-20.87	56.41	-25.23	60.31	1.07

In the first column are the real parts of the two pole pairs at a 1^{o}-field and in the second column the imaginary parts.
In the third column are the real parts of the two pole pairs at a 5.5^{o}-field is given and in the fourth column their imaginary parts.
The last column shows the ratio of the imaginary parts with the changing of the disk sizes.

From the table we conclude that the smallest imaginary part ($Im\{p_i\}$) doesn't change much with the increasing of the disk size: the ratio of the imaginary parts is here 1.07. Meanwhile the highest imaginary part does change very much with increasing stimulus size: the ratio of the imaginary parts is 1.31. Thus one pole pair seems stationary and the other pole pair seems dependent on the spatial configuration.

4.2) Matched filter model.

The triphasic impulse response of the visual system can also be

modelled as a system with a matched filter configuration. It is shown that the impulse response of a 1°-field with a dark surround can be approximated by four in serie connected filters with impulse responses $f_1(t)$, $f_2(t)$, $f_3(t)$ and $f_4(t)$ (see den Brinker, 1985B).

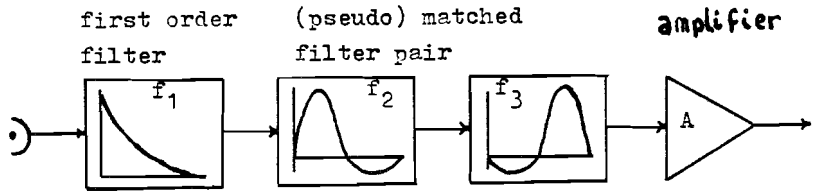

Figure 4.-2. The pseudo-matched filter model.

$$
\begin{aligned}
f_1(t) &= a e^{-a t}\, U(t) \\
f_2(t) &= e^{-b_1 t}\, \sin(\omega t)\{U(t)-U(t-T)\} \\
f_3(t) &= -e^{-b_2 t}\, \sin(\omega t)\{U(t)-U(t-T)\} \\
f_4(t) &= A\delta(t)
\end{aligned}
\qquad (4.-2)
$$

with $T = 2\pi/\omega$

$U(t)$ is the unit step function

a, b_1, $A > 0$ and $b_2 < 0$.

If $b_2 = -b_1$ then $f_2(t)$ and $f_3(t)$ form a matched pair. If b_2 lies in the order of $-b_1$ we call this a pseudo-matched filter pair. This matched filter model is applied to the measurement data of subject H.d.R. at a background luminance of E=100td. Figure 4.-3 shows this estimation of the matched filter model with the measured data of H.d.R.

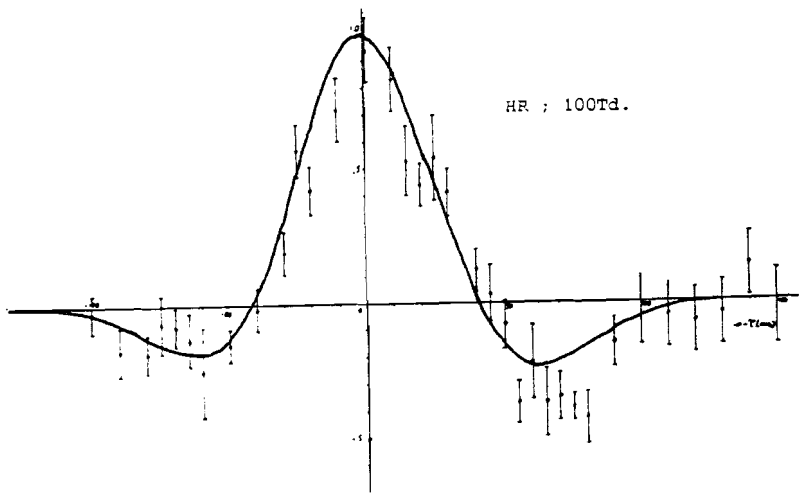

Figure 4.-3. The estimation of the matched filter model from the impulse response data of the subject H.d.R. at a background luminance E=100td. (from den Brinker, 1985C).

4.3) Conclusion.

The resemblance between the measurements and the response of the two models is reasonable. The fourth-order model is better to show the third phase of the measured impulse response, the pseudo-matched filter model gives a better representation of the dominant phase.
Further the fourth order analysis suggests that one complex pole pair is dependent on the spatial configuration. We can see this changing pole pair as a part of a spatio-temporal filter. The other complex pole pair is stationary. This complex pole pair we can think of as a pure temporal filter independent of the spatial form of the stimulus.
Thus we derive from these analysis at a model of the transient visual system which consists of a spatio-temporal filter in cascade with a temporal filter. As seen from this analysis this model is capable of producing a triphasic signal as a response to a Dirac at the input of this model.
From parameter estimations for the matched filter model it can be shown that the damping and frequency of the filter f_2 are very similar to the parameters of the largest pole in the fourth order estimates.
This means that in case the pseudo-matched filter model is to be elaborated into a spatio-temporal model, only the filter f_2 has to be changed into a spatio-temporal filter.
So we can use the pseudo-matched filter principle in our model; the pseudo-matched filter principle gives an optimum signal/noise in case of noise in the system (see Papoulis, 1968). This noise is thought to be injected between f_2-filter and the f_3-filter.

Chapter 5: Theory

In this attempt to model the processing of the stimulus by the human eye we make the following assumptions:
1) quasi linearity; we only look at small luminance variations, this assumption we already used in chapter 4.
2) local homogeneity; we assume the fovea to be homogeneous and all stimuli are so small that they fall within the fovea, all experiments are foveally focused disks.
3) radial symmetry; within the fovea all the directions have the same characteristics.
4) peak detection; this is a simplest detector, we already used this assumption in chapter 3: the measurement of the impulse response (see 3.1) and the phase characteristic (see 3.4).

5.1) General theory.

Following assumptions 1) and 2) we can use linear theory with time and space invariance properties. This means a partial differential equation (p.d.e.) for a spatio-temporal filter can be postulated with constant (time- and space-independent) coefficients:

$$\sum_{k=1}^{n_1}\sum_{l=1}^{n_2}\sum_{m=1}^{n_3} a_{klm}\,\frac{\partial^{k+l+m} f_{in}(x,y,t)}{\partial^k x\,\partial^l y\,\partial^m t} = \sum_{k=1}^{n_1'}\sum_{l=1}^{n_2'}\sum_{m=1}^{n_3'} b_{klm}\,\frac{\partial^{k+l+m} f_{out}(x,y,t)}{\partial^k x\,\partial^l y\,\partial^m t} \qquad (5.-1)$$

$f_{in}(x,y,t)$ is the input signal of the visual system and $f_{out}(x,y,t)$ the output signal in x-, y- and t-domain. a_{klm} and b_{klm} are coefficients. $k,l,m,n_1,n_2,n_3,n_1',n_2'$ and n_3' are integers. The relation between input and output signal is shown in figure 5.-1 as a blackbox.

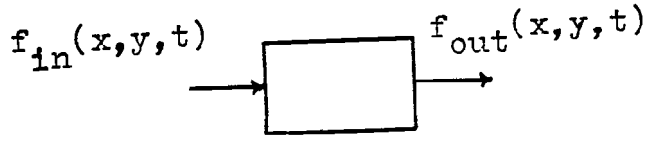

Figure 5.-1. The human visual system drawn as a blackbox.

For the input signal $f_{in}(x,y,t) = \delta(x)\delta(y)\delta(t)$ we define the causal fundamental solution as $h(x,y,t) = f_{out}(x,y,t)$. With $\delta(x)$ as an impulse in the x-domain and $x,y,t \in \mathbb{R}$ and as causality-condition: $h(x,y,t)=0$ for $\forall_{x,y,t}\ t<0$.
The relation between input and output signal for an arbitrary input is the convolution integral:

$$f_{out}(x,y,t) = \int_{-\infty}^{\infty}\int_{-\infty}^{\infty}\int_{-\infty}^{\infty} h(x-\nu,y-\eta,t-\tau)\,f_{in}(\nu,\eta,\tau)\,d\nu\,d\eta\,d\tau$$
$$= h(x,y,t) \overset{x}{*}\overset{y}{*}\overset{t}{*} f_{in}(x,y,t) \qquad (5.-2)$$

For a causal system and an input signal, which starts at t=0 the convolution integral is:

$$f_{out}(x,y,t) = \int_{-\infty}^{\infty}\int_{-\infty}^{\infty}\int_{0}^{t} h(x-\nu, y-\eta, t-\tau) f_{in}(\nu,\eta,\tau)\, d\nu\, d\eta\, d\tau \qquad (5.-3)$$

The system is completely described by the causal fundamental solution. It is difficult to find the causal fundamental solution $h(x,y,t)$ by solving of the p.d.e. for an input signal $f_{in}(x,y,t) = \delta(x)\delta(y)\delta(t)$. Therefore we will use some transformation to frequency domain.

The Fourier transformation is defined by:

$$G(\omega_p) = \mathcal{F}\{g(p)\} = \int_{-\infty}^{\infty} g(p)\, e^{-i\omega_p p}\, dp \qquad (5.-4)$$

Applying this to the spatial variables x and y we get the transformation variables ω_x and ω_y, which are spatial frequencies.

The single side Laplace transformation of f(t) is defined by:

$$F(s) = \int_{0}^{\infty} f(t)\, e^{-st}\, dt = \mathcal{L}\{f(t)\} \qquad (5.-5)$$

s is the variable in the Laplace domain.

We define now the following signals:

$$F_{in}(\omega_x,\omega_y,s) = \mathcal{F}^2\,\mathcal{L}\{f_{in}(x,y,t)\}$$
$$F_{out}(\omega_x,\omega_y,s) = \mathcal{F}^2\,\mathcal{L}\{f_{out}(x,y,t)\}$$
$$H(\omega_x,\omega_y,s) = \mathcal{F}^2\,\mathcal{L}\{h(x,y,t)\}$$

From the convolution relation (5.-3) follows the relation between the three transforms:

$$F_{out}(\omega_x,\omega_y,s) = H(\omega_x,\omega_y,s)\, F_{in}(\omega_x,\omega_y,s) \qquad (5.-6)$$

Further we assume now that the visual system is isotrope, this means that the causal fundamental solution is rotation symmetric: $h(x,y,t)$ is only dependent of the radius $r = \sqrt{x^2 + y^2}$.
The consequence is that the transform $H(\omega_x,\omega_y,s)$ is also no longer dependent of ω_x and ω_y separately, but of the norm $w = \sqrt{\omega_x^2+\omega_y^2}$.
w is called the spatial frequency. The angles Θ and α don't play any role here; $\Theta = \arctan(x/y)$ and $\alpha = \arctan(\omega_x/\omega_y)$.

$$h(x,y,t) = h(\sqrt{x^2 + y^2}, t) = h(r,t)$$

$$H(\omega_x,\omega_y,s) = H(\sqrt{\omega_x^2+\omega_y^2}, s) = H(w,s)$$

Instead of the double Fourier transformation to x- and y-variables we will use the Hankel transformation. This transformation is specially defined for rotation symmetric signals and is completely equivalent to a double Fourier transformation for a rotatic symmetric signal (except for a factor 2π).
The Hankel transformation is defined by:

$$\tilde{G}(w) = \int_0^\infty g(r)\, r J_0(wr)\, dr = \mathcal{H}\{g(r)\} \qquad (5.-7)$$

with J_0 the zero order Bessel function of the first kind.

J_0 is a real function for real arguments, w is a real argument, thus $\tilde{G}(w)$ is a real function.
We can write the zero order Bessel function as:

$$J_0(wr) = \frac{1}{2\pi} \int_{-\pi}^{\pi} e^{irw\cos(\theta-\alpha)}\, d\theta \qquad (5.-8)$$

with $\theta = \arctan(x/y)$ and $\alpha = \arctan(\omega_x/\omega_y)$.

The inverse Hankel transformation $\mathcal{H}^{-1}$ has the same form as the Hankel transformation: $\mathcal{H}^{-1} = \mathcal{H}$.
By using the Hankel transformation we get the following relation:

$$H(w,s) = \mathcal{F}[2\pi \mathcal{H}\{h(r,t)\}] \qquad (5.-9)$$

We only consider input signals that are rotation symmetric. The result is then that the output signal is rotation symmetric.
The input signal is thus

$$f_{in}(x,y,t) = f_{in}(r,t)$$

and the transform of the input signal:

$$F_{in}(w,s) = 2\pi \mathcal{F}\{\mathcal{H}\{f_{in}(r,t)\}\}$$

The output signal is

$$f_{out}(x,y,t) = f_{out}(r,t)$$

and its transform is:

$$F_{out}(w,s) = F_{out}(\sqrt{\omega_x^2+\omega_y^2}, s) = 2\pi \mathcal{F}\{\mathcal{H}\{f_{out}(r,t)\}\}$$

The Hankel transformation tables are defined without the factor 2π, so we define the following functions; $\tilde{H}$, $\tilde{F}_{in}$, $\tilde{F}_{out}$ to distinguish them from the double Fourier transforms H, F_{in}, F_{out}.

$$\begin{aligned}
\tilde{H}(w,s) &= \mathcal{F}\{\mathcal{H}\{h(r,t)\}\} = \tfrac{1}{2\pi} H(w,s) \\
\tilde{F}_{in}(w,s) &= \mathcal{F}\{\mathcal{H}\{f_{in}(r,t)\}\} = \tfrac{1}{2\pi} F_{in}(w,s) \\
\tilde{F}_{out}(w,s) &= \mathcal{F}\{\mathcal{H}\{f_{out}(r,t)\}\} = \tfrac{1}{2\pi} F_{out}(w,s)
\end{aligned}$$

Extended tables of Hankel transforms can be found in the book "Tables of Bessel Transforms" by F.Oberhettinger.
The relation between the Hankel transforms follow from the earlier given relation between the Fourier transforms (5.-6):

$$\tilde{F}_{out}(w,s) = 2\pi \tilde{H}(w,s)\tilde{F}_{in}(w,s) = H(w,s)\tilde{F}_{in}(w,s) \qquad (5.-10)$$

5.2) Eigenfunction.

Just as for a linear time invariant system sinus functions form the eigenfunctions, so a linear place and time invariant system has the zero order Bessel function as eigenfunction.

We assume the input signal $f_{in}(r,t)$ is separable in a function $T(t)$ and a Bessel function $J_o(w_o r)$:

$$f_{in}(r,t) = J_o(w_o r)\,T(t) \qquad (5.-11)$$

Then we get by transformations (see Papoulis, 1968, page 147):

$$\tilde{F}_{in}(w,s) = w_o^{-1}\,\delta(w-w_o)\,\bar{T}(s) \qquad (5.-12)$$

with $\bar{T}(s) = \mathcal{L}\{T(t)\}$

The output signal now becomes:

$$\tilde{F}_{out}(w,s) = 2\pi\tilde{H}(w,s)\,\tilde{F}_{in}(w,s) = 2\pi\tilde{H}(w,s)\,w_o^{-1}\,\delta(w-w_o)\,\bar{T}(s)$$

$$= \frac{2\pi}{w_o}\,\delta(w-w_o)\,\tilde{H}(w_o,s)\,\bar{T}(s) \qquad (5.-13)$$

The output signal is now:

$$f_{out}(r,t) = 2\pi J_o(w_o r)\,\mathcal{L}^{-1}\{H(w,s)\,\bar{T}(s)\} \qquad (5.-14)$$

Input and output signal have the same shape (Bessel function) with the same spatial frequency w_o. For a general input signal the time modulation of each Bessel function is different!
We assume now as time modulation a sinus (cosinus) function then:

$$f_{in}(r,t) = J_o(w_o r)\sin(\omega_o t) \qquad (5.-15)$$

With formula (5.-13) we get now:

$$f_{out}(r,t) = |H(w_o, i\omega_o)|\,J_o(w_o r)\sin(\omega_o t - \phi(w,\omega_o)) \qquad (5.-16)$$

with $H(w,i\omega_t) = 2\pi|H(w,i\omega_t)|\,e^{-i\phi(w,\omega_t)}$ and $s = i\omega_t$.

Thus input and output signal are of the same shape, they are only different in amplitude and are delayed in the time domain.

5.3) Excitations on uniform backgrounds.

We are going to derive some formulas, which we are going to use for the simulation on the computer (see chapter 8).
Assume that the parameters of the visual system are dependent on the mean illumination. We now consider the case of a completely uniform background and excitation with disks (see figure 5.-2).

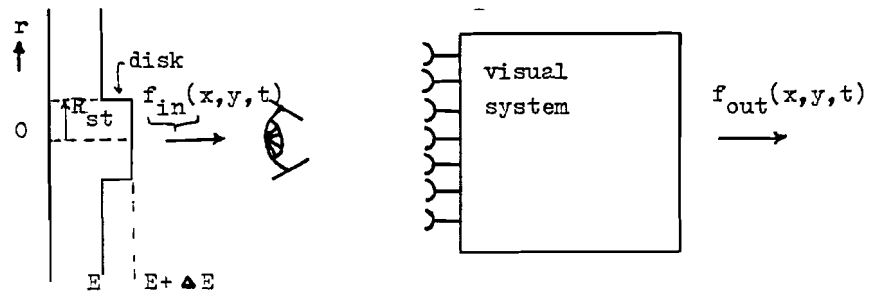

Figure 5.-2. Experiments with the visual system on an uniform background with a disk stimulus. R_{st} is the radius of the disk.

We can write the input signal $f_{in}(r,t)$ as:

$$f_{in}(r,t) = \Delta E\{U(r)-U(R_{st}-r)\}T(t) \qquad (5.-17)$$

The transform of the input signal is:

$$\tilde{F}_{in}(w,s) = \Delta E \frac{R_{st}}{w} J_1(wR_{st})\bar{T}(s) \qquad (5.-18)$$

The transform of the output signal is then:

$$\tilde{F}_{out}(w,s) = (2\pi R_{st}\Delta E)w^{-1} J_1(wR_{st})\tilde{H}(w,s)\bar{T}(s) \qquad (5.-19)$$

If the disk is sinusoidally modulated in the time:

$$f_{in}(r,t) = \Delta E\{U(r)-U(R_{st}-r)\}\sin(\omega_o t) \qquad (5.-20)$$

$$\tilde{F}_{out}(w,i\omega_t) = (2\pi R_{st}\Delta E)w^{-1} J_1(wR_{st})H(w,i\omega_o)\frac{1}{2i}\{\delta(\omega_t-\omega_o)-\delta(\omega_t+\omega_o)\} \qquad (5.-21)$$

$$f_{out}(r,t) = (2\pi R_{st}\Delta E)\,[w^{-1}J_1(wR_{st})|H(w,i\omega_o)|\sin(\omega_o t-\phi(w,\omega_o))] \qquad (5.-22)$$

5.4) Excitations on disk shaped background.

The parameters of the visual system are dependent of the mean lumination at the location (see den Brinker and van Aalst, 1984). The response on the edge of the disk is always zero: in den Brinker/Aalst (1984) is assumed that the linear filter characteristics (lateral membrane parameters) are dependent on the mean luminance.
For disk shaped background luminances with no surround luminances it was assumed that the impedances seen from the disk to surround side is zero. Consequently all responses at the border from background illumination to no illumination are equal to zero. Therefore this response can be written as a summation of Bessel functions according to the theory of the Fourier-Bessel series. Each Bessel function has its own time function.
Because Bessel functions are eigenfunction, we write the input signal also in the form of a summation of Bessel functions.

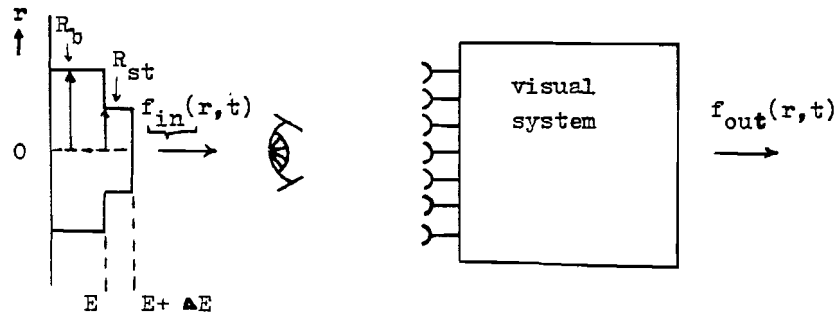

Figure 5.-3. Experiments with the visual system on disk shaped background with also a disk stimulus. R_b is the radius of the background disk.

We can write the input signal $f_{in}(r,t)$ on a disk shaped background in the size of R_b as a summation of Bessel functions:

$$f_{in}(r,t) = R(r)T(t) \qquad (5.-23)$$

$$R(r) = \sum_{m=1}^{\infty} A_m J_o\left(\frac{r}{R_b} j_m\right) \qquad (5.-24)$$

(5.-24) is called a Fourier-Bessel series and j_m is the m^{th} positive zero of the zero order Bessel function.
The coefficient A_m is determined by the integral-relation (see Papoulis, 1968 and Boersma, 1981):

$$\int_0^{R_b} R(r) r J_o\left(j_m \frac{r}{R_b}\right) dr = \int_0^{R_b} A_m J_o\left(j_m \frac{r}{R_b}\right) r J_o\left(j_m \frac{r}{R_b}\right) dr = A_m \tfrac{1}{2} J_1^2(j_m) R_b^2 \qquad (5.-25)$$

The transform of $f_{in}(r,t)$ is:

$$\tilde{F}_{in}(w,s) = \{\sum_{m=1}^{\infty} \frac{A_m}{w_m} \delta(w-w_m)\}\bar{T}(s) \qquad (5.-26)$$

$$\text{with } w_m = \frac{j_m}{R_b} \quad \text{and} \quad \bar{T}(s) = \mathcal{L}\{T(t)\} \qquad (5.-27)$$

The Bessel functions are eigenfunctions of the visual system. The output signal contains thus the same spatial frequencies and can therefore be written as

$$f_{out}(r,t) = \sum_{m=1}^{\infty} B_m(t) J_o\left(j_m \frac{r}{R_b}\right) \qquad (5.-28)$$

$$\text{with coefficient } B_m(t) = 2\pi A_m \mathcal{L}^{-1}\{\tilde{H}(w_m,s)\bar{T}(s)\}$$

Notice that though each Bessel function of the input signal is modulated in the same way in the time, this doesn't apply to the Bessel functions of the output signal. This is a direct result of the inseparability of the transfer of the system.

We will derive the Fourier-Bessel series for a disk of size R_{st} on a background disk with radius R_b.
The input signal is:
$R(r) = \Delta E\{U(r)-U(R_{st}-r)\}$
and can be written as a Fourier-Bessel series with frequency $w_m = j_m/R_b$:

$$R(r) = \Delta E \sum_{m=1}^{\infty} A_m J_o\left(j_m \frac{r}{R_b}\right)\} \qquad (5.-29)$$

with $R_{st} < R_b$.
From (5.-25) we obtain:

$$A_m = \frac{2R_{st} J_1\left(j_m \frac{R_{st}}{R_b}\right)}{j_m R_b J_1^2(j_m)} = \frac{2R_{st} J_1(w_m R_{st})}{w_m R_b^2 J_1^2(j_m)} \qquad (5.-30)$$

In case of $R_{st} = R_b$ we get:

$$A_m = \frac{2}{j_m J_1(j_m)} \qquad (5.-31)$$

5.5) Disk excitations and a dirac pulse in the time.

The input signal for a disk stimulus and a dirac pulse in the time domain is:

$$f_{in}(r,t) = \Delta E\{U(r)-U(R_{st}-r)\}\delta(t) \qquad (5.-32)$$

The transform of the input signal is now:

$$\tilde{F}_{in}(w,s) = \Delta E\sum_{m=1}^{\infty}\frac{A_m}{w_m}\delta(w-w_m)$$

The transform of the output signal is:

$$\tilde{F}_{out}(w,s) = 2\pi\,\Delta E\sum_{m=1}^{\infty}\frac{A_m}{w_m}\tilde{H}(w_m,s)\delta(w-w_m)$$

This leads to the output signal:

$$\begin{aligned} f_{out}(r,t) &= 2\pi\,\Delta E\mathcal{L}^{-1}\Big[\sum_{m=1}^{\infty}A_m\tilde{H}(w_m,s)J_0(w_m r)\Big] \\ &= 2\pi\,\Delta E\sum_{m=1}^{\infty}\Big[A_m J_0(w_m r)\mathcal{L}^{-1}\{\tilde{H}(w_m,s)\}\Big] \end{aligned} \qquad (5.-33)$$

5.6) Disk excitation and sinusoidal modulation in the time.

For a disk exitation in the spatial domain and a sinusoidal modulation we get the following input signal:

$$f_{in}(r,t) = \Delta E\{U(r)-U(R_{st}-r)\}\sin\omega_0 t = \Delta E\{\sum_{m=1}^{\infty}A_m J_0(w_m r)\}\sin\omega_0 t \qquad (5.-34)$$

Its transform is:

$$\tilde{F}_{in}(w,i\omega_t) = \Delta E\sum_{m=1}^{\infty}\frac{A_m}{w_m}\delta(w-w_m)\,\frac{1}{2i}\,\{\delta(\omega_t-\omega_0)-\delta(\omega_t+\omega_0)\}$$

Hereby we get the transform of the output signal:

$$\begin{aligned} \tilde{F}_{out}(w,i\omega_t) &= \Delta E\sum_{m=1}^{\infty}\frac{A_m}{w_m}\delta(w-w_m)\,\frac{1}{2i}\,\{\delta(\omega_t-\omega_0)H(w_m,\omega_0) - \\ &\qquad -\delta(\omega_t+\omega_0)H(w_m,-\omega_0)\} \\ &= \Delta E\sum_{m=1}^{\infty}\frac{A_m}{w_m}\delta(w-w_m)\,\frac{|H(w_m,\omega_0)|}{2i}\{\delta(\omega_t-\omega_0)e^{-i\phi} - \delta(\omega_t+\omega_0)e^{i\phi}\} \end{aligned}$$

with $H(w,i\omega_t) = |H(w,i\omega_t)|\,e^{-i\phi(w,\omega_t)}$

and $H(w,-i\omega_t) = H^{*}(w,i\omega_t)$.

Now we derive the following output signal:

$$f_{out}(r,t) = 2\pi\sum_{m=1}^{\infty}\{A_m J_0(w_m r)|H(w_m,i\omega_0)|\sin(\omega_0 t - \phi(w_m,\omega_0)\} \qquad (5.-35)$$

Remark: In the cases when the stimulus disk is sinusoidal modulated in the time, we have used the Fourier transformation instead of the Laplace transformation. Therefore the spectral functions have an argument $i\omega_t$ in stead of s.

Chapter 6: Construction of the model for the transient system

In this chapter a model is outlined for the transient system. As already shown in the introduction the model consists of two parts: a spatio-temporal filter and a pure temporal filter. The reason for this subdivision is given in the analysis of the impulse response of disks of variable diameter (see chapter 4). We will now discuss the spatio-temporal filter, for which a transmission line is chosen as a model. Subsequently some rules are given of how to evaluate the spatio-temporal properties of such filter. Then the temporal filter is shortly discussed.

6.1) Model for the spatio-temporal filter.

As a model for the spatio-temporal filter an electric transmission line is used. This is a quite common model for the connections between light receptor cells.
The lateral membrane of the visual system is a two-dimension neural network. The neural network that consists of many elements, can be considered as spatially continuous. The spatio-temporal filter will be modelled as an electric transmission line for the two dimensional case.

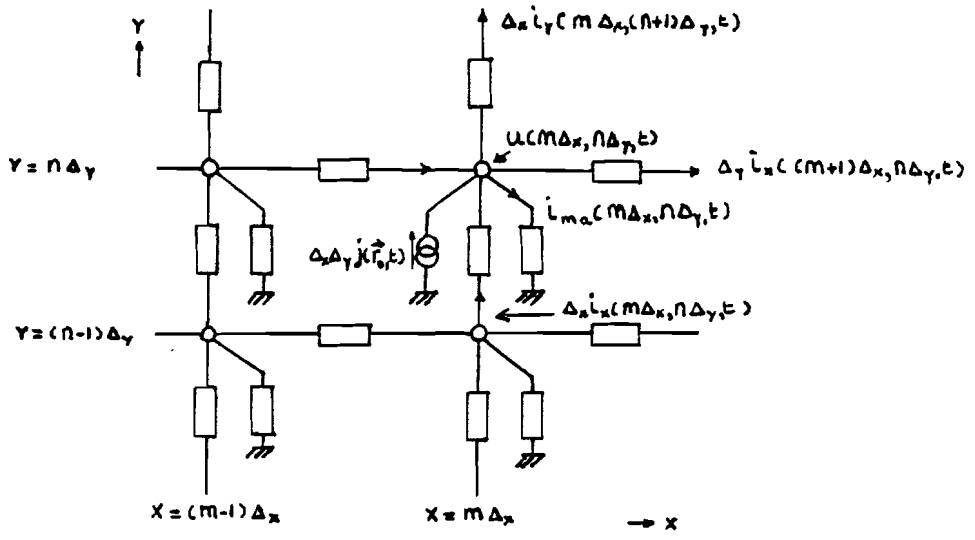

Figure 6.-1. The electric analogy of the lateral membrane.

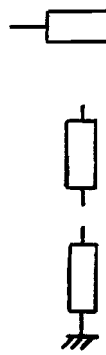

$= \frac{\Delta_x}{\Delta_y} Z_{1,x}$ $Z_{1,x}$ is the impedance of the length=1 in the x-direction with a width=1 in the y-direction.

$= \frac{\Delta_y}{\Delta_x} Z_{1,y}$ $Z_{1,y}$ is the impedance of the length=1 in the y-direction with a width=1 in the x-direction.

$= \frac{Z_2}{\Delta_x \Delta_y}$ Z_2 is the impedance for an area=1 to "earth".

m and n are integers; t is the time.
$\vec{r}$ is the radius with $r=|\vec{r}| = \sqrt{x^2 + y^2}$.
Δ_x is a infinitesimal piece of length of a unit in the x-direction and Δ_y in the y-direction.
For convenience we now assume $\Delta = \Delta_x = \Delta_y$.

In the figure 6.-1 the current source $j(\vec{r}_o, t)$ suggests a synaptic transmission: this transmission results in current going throughout the membrane. In each of the junctions such a current source exists, but for convenience we leave them out in the figure 6.-1. $j(\vec{r}_o, t)$ is viewed as continuous in the r-domain. It must be assumed as a space current density.
The current which goes through Z_2/Δ^2 at the location $(m\Delta, n\Delta)$ is called $\Delta^2 j_{ma}(m\Delta, n\Delta, t)$. This current is directed to earth.

The vector $\vec{I}(\vec{r}, t) = \begin{bmatrix} i_x(\vec{r}, t) \\ i_y(\vec{r}, t) \end{bmatrix}$ is an area current density.

Now we apply the one-side Laplace transformation and define the next functions:

$$
\begin{aligned}
J(\vec{r}_o, s) &= \mathcal{L}\{j(\vec{r}_o, t)\} \\
J_{ma}(\vec{r}_o, s) &= \mathcal{L}\{j_{ma}(m\Delta, n\Delta, t)\} \\
U(m\Delta, n\Delta, s) &= \mathcal{L}\{u(m\Delta, n\Delta, t)\} \\
I_x(m\Delta, n\Delta, s) &= \mathcal{L}\{i_x(m\Delta, n\Delta, s)\} \\
I_y(m\Delta, n\Delta, s) &= \mathcal{L}\{i_y(m\Delta, n\Delta, s)\}
\end{aligned}
$$

The parameter $\vec{r}$ doesn't play any role during the Laplace transformation.
From the Kirchhoff current equation we get from figure 6.-1 at point $(m\Delta, n\Delta)$:

$$
\Delta I_x(m\Delta, n\Delta, s) + \Delta I_y(m\Delta, n\Delta, s) - \Delta I_x((m+1)\Delta, n\Delta, s) - \Delta I_y(m\Delta, (n+1)\Delta, s) - \Delta^2 J_{ma}(m\Delta, n\Delta, s) + \Delta^2 J(m\Delta, n\Delta, s) = 0 \qquad (6.-1)
$$

This formula we can write as:

$$-\left[\frac{I_x((m+1)\Delta,n\Delta,s)-I_x(m\Delta,n\Delta,s)}{\Delta}\right]-\left[\frac{I_y(m\Delta,(n+1)\Delta,s)-I_y(m\Delta,n\Delta,s)}{\Delta}\right]=$$

$$= J_{ma}(m\Delta,n\Delta,s)-J(m\Delta,n\Delta,s)$$

For $\Delta\to 0$ we get:

$$-\frac{\partial I_x(\vec{r},s)}{\partial x}-\frac{\partial I_y(\vec{r},s)}{\partial y}=-\nabla\vec{I}(\vec{r},s)=J_{ma}(\vec{r},s)-J(\vec{r},s) \qquad (6.-2)$$

From the Kirchhoff voltage equation follows:

$$U(m\Delta,n\Delta,s)=Z_2(s)J_{ma}(m\Delta,n\Delta,s) \qquad (6.-3)$$

$$\begin{aligned}
\Delta I_x(m\Delta,n\Delta,s) &= Z_1^{-1}(s)\{U((m-1)\Delta,n\Delta,s)-U(m\Delta,n\Delta,s)\}\\
\Delta I_x((m+1)\Delta,n\Delta,s) &= Z_1^{-1}(s)\{U(m\Delta,n\Delta,s)-U((m+1)\Delta,n\Delta,s)\}\\
\Delta I_y(m\Delta,n\Delta,s) &= Z_1^{-1}(s)\{U(m\Delta,(n-1)\Delta,s)-U(m\Delta,n\Delta,s)\}\\
\Delta I_y(m\Delta,(n+1)\Delta,s) &= Z_1^{-1}(s)\{U(m\Delta,n\Delta,s)-U(m\Delta,(n+1)\Delta,s)\}
\end{aligned} \qquad (6.-4)$$

From formula (6.-2) and (6.-3):

$$-\nabla\vec{I}(\vec{r},s)=Z_2^{-1}(s)U(\vec{r},s)-J(\vec{r},s) \qquad (6.-5)$$

For $\Delta\to 0$ we get from formula (6.-4):

$$\vec{I}(\vec{r},s)=-Z_1^{-1}(s)\nabla U(\vec{r},s) \qquad (6.-6)$$

From (6.-5) and (6.-6) follow then:

$$Z_1^{-1}(s)\nabla^2U(\vec{r},s)=Z_2^{-1}(s)U(\vec{r},s)-J(\vec{r},s)$$

or

$$-\nabla^2U(\vec{r},s)+Z_1(s)Z_2^{-1}(s)U(\vec{r},s)=Z_1(s)J(\vec{r},s) \qquad (6.-7)$$

According to the third basic postulate (see page 4) we can drop the arrow above $\vec{r}$: the angle-dimension doesn't play any role in our modelling. Therefore we can use the Hankeltransformation. For the Hankeltransformation the next property holds (see Papoulis, 1968):

$$\nabla^2f(r)=f''(r)+\frac{1}{r}f'(r)\overset{\mathcal{H}}{\longleftrightarrow}-w^2\tilde{f}(w)$$

We apply the Hankel transformation on the differential equation (6.-7):

$$w^2\tilde{U}(w,s)+Z_1(s)Z_2^{-1}(s)\tilde{U}(w,s)=Z_1(s)\tilde{J}(w,s)$$

with

$$\tilde{U}(w,s)\overset{\mathcal{H}}{\longleftrightarrow}U(r,s)$$

$$\tilde{J}(w,s)\overset{\mathcal{H}}{\longleftrightarrow}J(r,s)$$

We now define the following function $H_1(w,s)$:

$$H_1(w,s) = \frac{\tilde{U}(w,s)}{\tilde{J}(w,s)} = \frac{Z_1(s)}{w^2 + Z_1(s)Z_2^{-1}(s)} \qquad (6.-8)$$

and according to (5.-10):

$$\tilde{H}_1(w,s) = \frac{1}{2\pi} H_1(w,s)$$

The parameter s plays no role in the Hankel transformation. By applying the inverse Hankel- and the inverse Laplace transformation on $\tilde{H}_1(w,s)$ we can obtain the causal fundamental function $h_1(r,t)$.
The inverse Laplace transformation is:

$$f(t) = \frac{1}{2\pi i} \int_{-i\infty}^{i\infty} F(s) e^{st}\, ds = \mathcal{L}^{-1}\{F(s)\} \qquad (6.-9)$$

$$h_1(r,t) = \mathcal{L}^{-1}\{\mathcal{H}^{-1}\{\tilde{H}_1(w,s)\}\} \qquad (6.-10)$$

Remark: in our modelling most of the inverse transformations are not solvable analytically, for they lead to too complex forms. Therefore they must be determined numerically by the computer.

6.2) Spatio-temporal characteristics: root-locus.

Root-locus analogy.
We will call the characteristic equation of $H_1(w,s)$ the equation with the denominator of $H_1(w,s)$ equal to zero:
$1+w^{-2} Z_1(s) Z_2^{-1}(s) = 0$
The solutions $s=p$ of this equation are the poles of the transmission and dependent on w: $p=p(w)$. The roots of the characteristic equation can be plotted in the s-domain with w as parameter. This is a root-locus plot, which follows the same arithmetic rules as the construction of the root-locus of a feedback system.
To show the simularities we rewrite (6.-8):

$$H_1(w,s) = \frac{\frac{1}{w^2} Z_1(s)}{1 + \frac{1}{w^2} Z_1(s) Z_2^{-1}(s)}$$

Suppose $K=1/w^2$, $G_1(s) = Z_1(s)$ and $G_2(s) = Z_2^{-1}(s)$.

$$\text{Thus } H_1(w,s) = \frac{KG_1(s)}{1 + KG_1(s)G_2(s)} \quad \text{with } K = 1/w^2 \geq 0.$$

This can be regarded as a feedback system. In figure 6.-2 we have drawn the bloc-scheme of this system.

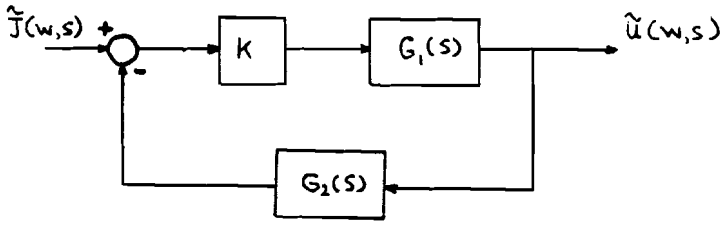

Figure 6.-2. $H_1(w,s)$ is here illustrated as a feedback system. K is here a function of the spatial frequency frequency w.

The poles of H (w,s) are found by the solution of the equation $1+KG_1(s)G_2(s)=0 \longrightarrow G_1(s)G_2(s) = -1/K$.
By variation of K one can sketch the root-loci of the system. From the course of the root-loci we get an impression of the behaviour of the visual system with the changing of the spatial frequency w.
The root-locus which arises hereby, gives an image of the position of the poles of the impulse response with a Bessel function that has a spatial frequency w as input signal.

Remark: $K=1/w^2$. Thus K is inversely proportional to w^2: if w increases, K becomes smaller. K and w go the opposite directions. From the analogy $G_2(s)=Z_2^{-1}(s)$ we see that the poles of $Z_2(s)$ are the zeroes of $G_2(s)$ and the zeroes of $Z_2(s)$ are the poles of $G_2(s)$.

The zeroes of $H_1(w,s)$ are the zeroes of $G_1(s)$ and the poles of $G_2(s)$. The poles of $H_1(w,s)$ are:
for w=0 the poles of $Z_1(s)$ and the zeroes of $Z_2(s)$
for $w=\infty$ the zeroes of $Z_1(s)$ and the poles of $Z_2(s)$

6.3) Impedances in the transmission line.

Parametrisation.
We want to construct a two dimensional membrane, so that all important properties fit in the model of figure 6.-6.
As electric network equivalence of the lateral membrane we use the model from figure 6.-1. The transfer function $H_1(w,s)$ must be in approximation of the second order in s, because $f_2(t)$ (see figure 4.-2) is biphasic and $f_2(t)$ is generated by $H_1(w,s)$ (the convolution of two biphasic signals gives a triphasic signal). Thus there may be at most two non-resistive elements (the spool L and the capacitor C) in the circuit (see figure 6.-3). Because of this limitation and parsimony principle we demand: maximum 2 elements in Z_1 and 2 elements in Z_2.

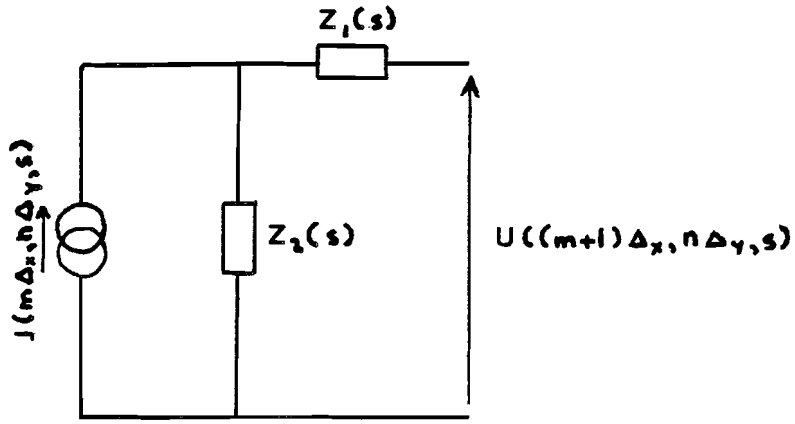

Figure 6.-3. A segment of the transmission.

We can connect the two elements in the impedance in serie or parallel. Thus there are the following possibilities to construct the impedance.

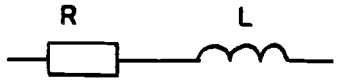

$$Z = R + sL$$

a)

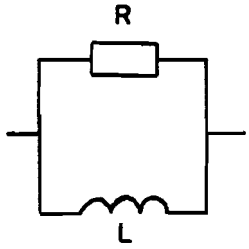

$$Z = \frac{sRL}{R+sL}$$

b)

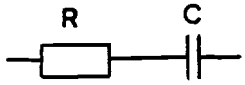

$$Z = \frac{1+sRC}{sC}$$

c)

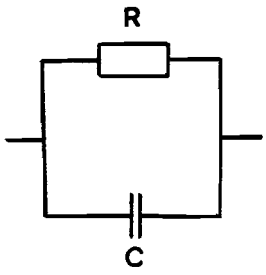

$$Z = \frac{R}{1+sRC}$$

d)

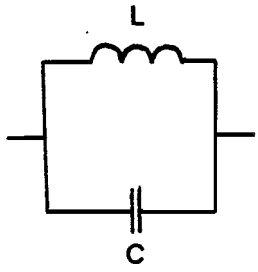

$$Z = \frac{sL}{1+s^2LC}$$

e)

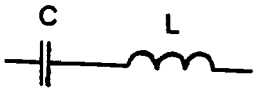

$$Z = \frac{1+s^2LC}{sC}$$

f)

Case e) and f) drop off: these are resonance circuits and lead to high resonance peaks, because these systems lie on the edge of stability. This doesn't occur in the data (see chapter 3). The other cases can be combined arbitrary. This gives 16 possibilities. The properties of each of the 16 combinations considered in the next chapter.

6.4) Model for the temporal filter.

The temporal behaviour of 1°-fields (dark surround) can be characterized by the impulse response. This can be measured with the aid of the perturbation technique. The impulse response has a triphasic course (see figure 6.-4).

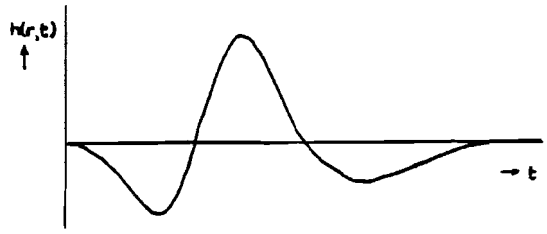

Figure 6.-4. 1° -field impulse response determined by threshold measurements with the aid of a perturbation technique.

This impulse can be considered as a convolution of the response of two filters, which are connected in serie . The impulse responses of these two filters are adapted to each other by the matched filter principle (see Papoulis, 1968 and den Brinker, 1985 and chapter 4).

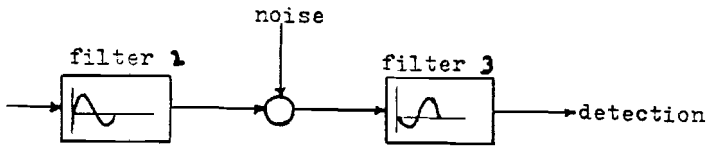

Figure 6.-5. The matched-filter model.

In case of detection problems the influence of additive noise, which is introduced between the two filters, is then minimum. Filter 2 we suppose at the retina level and filter 3 at cortex level. Between both levels there are connections of neural cells, which cause noise.
The response of filter 2 is biphasic corresponding with the physiologic measurements at the retina.
It has been shown that in the matched-filter model filter 2 and filter 3 can be described respectively by the impulse response $f_2(t)$ and $f_3(t)$.

$$f_2(t) = e^{-b_1 t} \sin(\omega t)\{U(t) - U(t - T)\}$$
$$f_3(t) = -e^{-b_2 t} \sin(\omega t)\{U(t) - U(t - T)\}$$

with $T=2\pi/\omega$, $b_1>0$ and $b_2<0$.
$U(t)$ is the unit step function.

Besides a temporal character we assume that filter 2 has a spatial character. So that we can substitute filter 2 through the lateral membrane (see figure 6.-6).

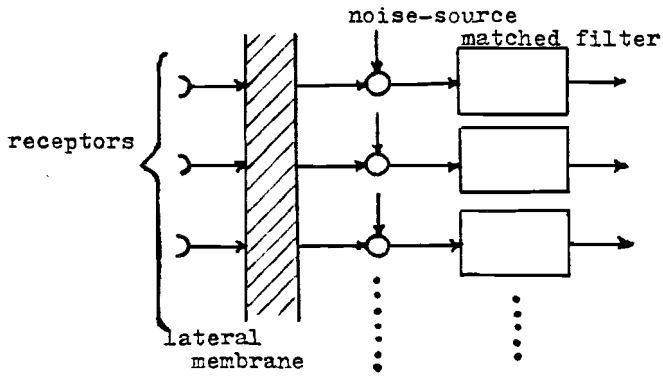

Figure 6.-6. Signal processing in a spatio-temporal model.

Notice that the original pseudo-matched filter scheme contained an extra first order filter. This was for simplicity reasons left out in the construction of the spatio-temporal model.

Chapter 7: Examined models for the lateral membrane

In chapter 6 it was shown that several choices exist for the impedances within the transmission line that is our model for the spatio-temporal filter.
In this chapter all these specific choices are evaluated on their spatio-temporal properties, using the root-locus plots as suggested in chapter 6.
From these analysis it is possible to make a choice for the impedances that are to be used for the transmission line, on basis of qualitative agreement with measurement data. Next the parameter values for all impedances are chosen.

Here we consider only one specific choice of the impedances. All the other cases are given in appendix 1.

Case II (see Appendix 1)

In figure 7.-1 a segment of the transmission line (see figure 6.-1) is drawn with the following impedances:

$$Z_1(s) = \frac{1 + sR_1C_1}{sC_1} \; ; \; Z_2(s) = R_2 + sL_2$$

The current source is left out in this figure and also the second dimension (originally there were four $Z_1(s)$ in figure 6.-1).
The dimensions of the elements in these two impedances are:
$R_1 = [\Omega]$; $C_1 = [F]$; $L_2 = [Hm^2]$; $R_2 = [\Omega m^2]$.

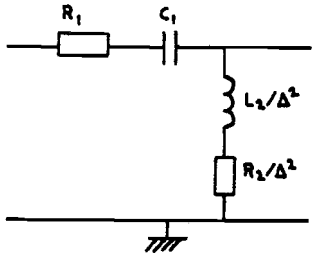

Figure 7.-1. A segment of the transmission line is drawn here, where $Z_1(s)$ consists of R_1 and C_1 in series connected and $Z_2(s)$ of R_2 and L_2also in series.

According to formula (6.-8) the transfer function can be given by:

$$H_1(w,s) = \frac{\{1 + sC_1R_1\}\{R_2 + sL_2\}}{L_2C_1w^2s^2 + \{R_1C_1 + R_2C_1w^2\}s + 1} \qquad (7.-1)$$

The two zeroes are: $z_1 = -\frac{1}{R_1C_1}$ and $z_2 = -\frac{R_2}{L_2}$

The two poles are:

$$p_{1,2} = \left\{ \frac{-\{R_2 C_1 w^2 + C_1 R_1\} \pm \sqrt{\{R_2 C_1 w^2 + C_1 R_1\}^2 - 4 L_2 C_1 w^2}}{2 L_2 C_1 w^2} \right\}$$

These poles are dependent on the spatial frequency w. For two special cases w=0, w→∞ it is found:

For w=0 we get: $p_1 = -\frac{1}{R_1 C_1}$ and $p_2 = -\infty$.

For w→∞: $p_1 = 0$ and $p_2 = -\frac{R_2}{L_2}$

We can draw the root-locus $1+KG_1(s)G_2(s)=0$ with

$$G_1(s) = Z_1(s) = \left\{ \frac{1 + sR_1C_1}{sC_1} \right\} \quad \text{and} \quad G_2(s) = \{Z_2(s)\}^{-1} = \left\{ \frac{1}{R_2 + sL_2} \right\}$$

This root-locus of case II is drawn in figure 7.-2.
Note: the indicated poles and zeroes (with crosses and little circles) are those of a system the transfer function $Z_1(s)/Z_2(s)$.

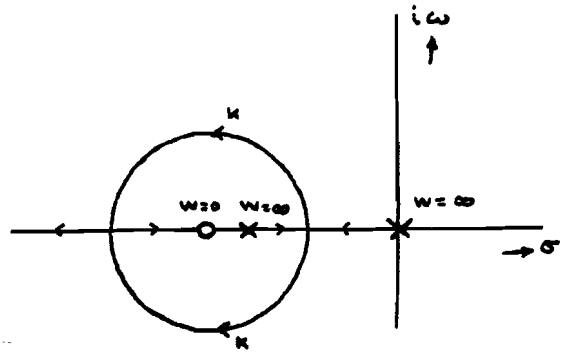

Figure 7.-2. Root-locus of case II for $\frac{1}{R_1C_1} > \frac{R_2}{L_2}$.

The arrows illustrate the increase of K, thus the decrease of the spatial frequency w.
x is the pole of $Z_1(s)$ or the zero of $Z_2(s)$,
o is the zero of $Z_1(s)$ or the pole of $Z_2(s)$.

We can prove that the root-locus has a circular shape for the complex solutions of the characteristic equation (see appendix 2).

The circle equation is:

$$\omega^2 + \left[\sigma + \frac{1}{R_1C_1}\right]^2 = \frac{1}{R_1C_1}\left[\frac{1}{R_1C_1} - \frac{R_2}{L_2}\right]$$

with $p_{1,2} = \sigma \pm i\omega$
and radius $\sqrt{\frac{1}{R_1C_1}\left[\frac{1}{R_1C_1} - \frac{R_2}{L_2}\right]}$ and centre $(-\frac{1}{R_1C_1}, 0)$, e.g. the zero of $Z_1(s)/Z_2(s)$.

For $\frac{R_2}{L_2} \geq \frac{1}{R_1C_1}$ we get the root-locus from figure 7.-3.

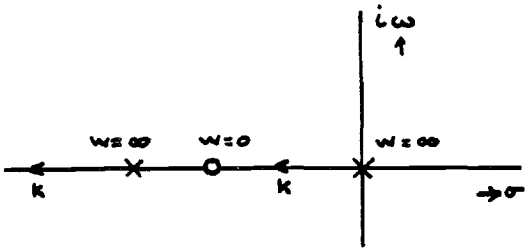

Figure 7.-3. Root-locus of case II for $\frac{R_2}{L_2} \geq \frac{1}{R_1 C_1}$.

In general we find that all the cases can be described by the transfer function $H_1(w,s)$ according to:

$$H_1(w,s) = \frac{D_1 s^2 + D_2 s + D_3}{(A_1 + w^2 B_1) s^2 + (A_2 + w^2 B_2) s + (A_3 + w^2 B_3)}$$

In all considered cases two of the A, B-parameters are equal to zero. This is summarized in table 7.-1, where also the zeroes z_1, z_2 (independent of w) are shown.

Table 7.-1: the coefficients of the models with their zeroes.

	case	s^2	s	1	zeroes z_1	zeroes z_2
RC-lateral RL to "earth"	I	$A_1 + w^2 B_1$	A_2	A_3	$-\frac{1}{R_1 C_1}$	0
	II	$w^2 B_1$	$A_2 + w^2 B_2$	A_3	$-\frac{1}{R_1 C_1}$	$-R_2/L_2$
	III	$w^2 B_1$	$w^2 B_2$	$A_3 + w^2 B_3$	∞	$-R_2/L_2$
	IV	$w^2 B_1$	$A_2 + w^2 B_2$	A_3	∞	0
RL-lateral RC to "earth"	V	A_1	A_2	$A_3 + w^2 B_3$	$-R_1/L_1$	∞
	VI	A_1	$A_2 + w^2 B_2$	$w^2 B_3$	$-R_1/L_1$	$-\frac{1}{R_2 C_2}$
	VII	$A_1 + w^2 B_1$	$w^2 B_2$	$w^2 B_3$	0	$-\frac{1}{R_2 C_2}$
	VIII	A_1	$A_2 + w^2 B_2$	$w^2 B_3$	0	∞
RC-lateral RC to "earth"	IX	$A_1 + w^2 B_1$	$A_2 + w^2 B_2$	-	$-\frac{1}{R_1 C_1}$	$-\frac{1}{R_2 C_2}$
	X	A_1	$A_2 + w^2 B_2$	A_3	$-\frac{1}{R_1 C_1}$	∞
	XI	$w^2 B_1$	$A_2 + w^2 B_2$	$w^2 B_3$	∞	$-\frac{1}{R_2 C_2}$
	XII	-	$A_2 + w^2 B_2$	$A_3 + w^2 B_3$	∞	∞
RL-lateral RL to "earth"	XIII	-	$A_2 + w^2 B_2$	$A_3 + w^2 B_3$	$-R_1/L_1$	$-R_2/L_2$
	XIV	A_1	$A_2 + w^2 B_2$	A_3	$-R_1/L_1$	0
	XV	$w^2 B_1$	$A_2 + w^2 B_2$	$w^2 B_3$	0	$-R_2/L_2$
	XVI	$A_1 + w^2 B_1$	$A_2 + w^2 B_2$	-	0	0

From this table we see that the coefficients A and B of case II and IV are identical, the coefficients A and B of case VI and VIII, and the coefficients A and B of case X and XIV. Thus the shape of the root-locus is the same in cases with same coefficients A and B.

Selection of the impedances of the transmission line.
For all the examined models there holds $H_1(w,s)=0$ for $w \to \infty$. For

increasing spatial frequency w the transfer function $H_1(w,s)$ goes to zero as expected from the transient system. The spatial frequency w is reversed proportional to the disk diameter . Thus for smaller disk diameter ϕ the amplitude transfer function $H_1(w,s)$ also is smaller.
In the analysis of the temporal impulse response only complex pole pairs occurred. Only in cases I to VIII complex pole pairs occur, this means we cannot use IX - XVI.
From 3.1) and 3.3) we have concluded a spatio-temporal model is needed with increasing bandpass character for decreasing spatial frequency w (i.e. increasing field diameter).
Cases V to VIII show an initially decreasing bandwidth for spatial frequency w going downward from $w=\infty$.
So only cases I to IV are suitable for our purposes.
Case I: almost unstable for very small field sizes (two poles in the origin).
Case III: straight lines resonance frequency always increasing with decreasing w, hereby the peak will always increase.
Case II and IV: identical possibilities for pole variations. Only the zeroes are different.

We shall examine case II further. Hereby we shall simulate model II on a computer and compare the simulations with the measured diagrams.

To obtain $f_2(t) = e^{-b_1 t} \sin\omega t$ (see chapter 4) we must remove the two zeroes of $H_1(w,s)$. Therefore we put a bloc with transfer function $H_2(s)$ in cascade with $H_1(w,s)$. The zeroes of $H_1(w,s)$ are the poles of $H_2(s)$ (see figure 7.-4).

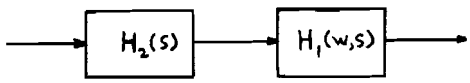

Figure 7.-4. Zero cancellation of $H_1(w,s)$ by the aid of $H_2(s)$.

$$H_1(w,s) = \frac{D_1 s^2 + D_2 s + D_3}{(A_1 + w^2 B_1) s^2 + (A_2 + w^2 B_2) s + (A_3 + w^2 B_3)}$$

$$H_2(s) = \frac{K_1}{(s - z_1)(s - z_2)} = \frac{K_1}{s^2 + \frac{D_2}{D_1} s + \frac{D_3}{D_1}}$$

The total transfer function is now:
$H(w,s) =$

$$H_1(w,s) H_2(s) = \frac{K_1 D_1}{(A_1 + w^2 B_1) s^2 + (A_2 + w^2 B_2) s + (A_3 + w^2 B_3)}$$

$H_2(s)$ we can see as the transfer function of the receptor.

With $K_2 = \frac{K_1 D_1}{A_3 + w^2 B_3}$, $\omega_0^2 = \frac{A_3 + w^2 B_3}{A_1 + w^2 B_1}$ and $\beta = \frac{1}{2}\omega_0 \frac{A_2 + w^2 B_2}{A_3 + w^2 B_3}$

We obtain: $H(w,s) = \dfrac{K_2}{\frac{s^2}{\omega_0^2} + 2\frac{\beta}{\omega_0}s + 1}$

for $\beta < 1$: $p_{1,2} = \omega_0\{-\beta \pm i\sqrt{1-\beta^2}\} = -b_1 \pm i\omega$
with $b_1 = \omega_0\beta$ and $\omega = \sqrt{1-\beta^2}$.

$$H(w,s) = \frac{K_2}{(s + b_1 + i\omega)(s + b_1 - i\omega)} = \frac{K_2}{\omega}\left\{\frac{\omega}{(s + b_1)^2 + \omega^2}\right\}$$

By the inverse Laplace transformation we obtain:

$$h(w,t) = \frac{K_2}{\omega}e^{-b_1 t}\sin(\omega t) \quad \text{for } t>0.$$

b_1 is the damping; ω is the eigenfrequency; ω_0 is the natural eigenfrequency; β is the relative damping (see figure 7.-5). K_2, b_1 and ω are dependent of the spatial frequency w.

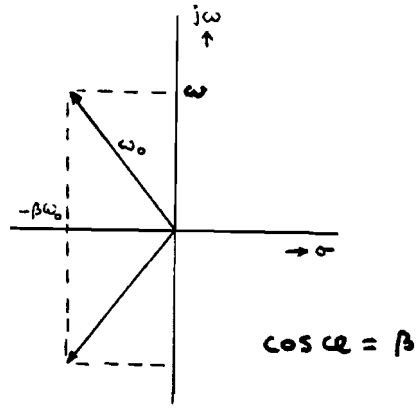

Figure 7.-5. The poles of a damped second order system.

The amplitude equation of $H(w,s)$ is

$$|H(w,i\omega_t)| = \frac{K_2}{\sqrt{\{1-(\frac{\omega_t}{\omega_0})^2\}^2 + 4\beta^2\frac{\omega_t^2}{\omega_0^2}}}$$

The static amplification is $|H(w,0)| = K_2$.

$$\left.\frac{\partial |H(w,i\omega_t)|}{\partial \omega_t}\right|_{\omega_m} = 0 \rightarrow \omega_m = \sqrt{1-2\beta^2}$$

For real ω_m: $\beta^2 < \frac{1}{2}$
The maximum of $|H(w,i\omega_t)|$ is the:

$$|H(w,i\omega_m)| = \frac{K_2}{2\beta\sqrt{1-\beta^2}}$$

The ratio of the maximum and the static amplification is:

$$Q_R = \frac{|H(w, i\omega_t)|}{|H(w,0)|} = \frac{1}{2\beta\sqrt{1-\beta^2}}$$

This value indicates the peak in the Bode amplitude diagram.

$$\frac{\partial Q_R}{\partial \beta}\Big|_{\beta_m} = 0 \rightarrow \beta_m = \frac{1}{\sqrt{2}} = 0.7071 \quad \text{and } \omega_m = 0$$

$$\varphi = \arccos \beta_m = 45^\circ$$

Beneath $\varphi = 45^\circ$ no peak will occur in the Bode amplitude diagram.

To simulate our model of case II on the computer we must have suitable values for the parameters R_1, R_2, C_1 and L_2. From measurements the following values can be assumed:

for 1°-field: $w \approx 0.08$ (min of arc.)$^{-1}$

$y_1 = \omega = 70$ rad/s

$x_1 = \beta\omega_0 = -15$

for 5°-field: $w \approx 0.016$ (min of arc.)$^{-1}$

$y_2 = 93.33$ rad/s

$x_2 = -20$

The circle equation for model II is:

$$\omega_t^2 + \left(\sigma + \frac{1}{R_1C_1}\right)^2 = \frac{1}{R_1C_1}\left(\frac{1}{R_1C_1} - \frac{R_2}{L_2}\right)$$

assume: $y^2 + (x + a)^2 = r^2$

$$y_1^2 + (x_1 + a)^2 = y_2^2 + (x_2 + a)^2 \rightarrow a = \frac{1}{R_1C_1} = 398.6$$

$$y_1^2 + (x_1 + a)^2 = (390) \rightarrow r = 390 \rightarrow \frac{R_2}{L_2} = 17.14$$

$$\left.\begin{array}{l} \omega = \omega_0\sqrt{1-\beta^2} = 70 \\ \beta\omega_0 = -15 \end{array}\right\} \rightarrow \begin{array}{l} \beta = 0.2095 \\ \omega_0 = 71.59 \text{ rad/sec} \end{array}$$

$$\omega_0^2 = \frac{A_3 + B_3w^2}{A_1 + B_1w^2} = (L_2C_1w^2)^{-1} \rightarrow L_2C_1 = 0.03049$$

$$\frac{2\beta}{\omega_0} = \frac{A_2 + B_2w^2}{A_3 + B_3w^2} = R_2C_1w^2 + C_1R_1 \rightarrow R_2C_1 = 0.5226$$

By choosing one parameter the other three are also determined. We choose arbitrary $R_1 = 2\Omega$, then $R_2 = 416.7\,\Omega m^2$, $L_2 = 24.31$ Hm^2 and $C_1 = 0.001254$ F.

Chapter 8: Simulation of the lateral membrane model

The membrane structure found most suitable according to chapter 7 is

$$H(w,s) = \left\{ \frac{R_1 C_1 L_2}{L_2 C_1 w^2 s^2 + \{R_1 C_1 + R_2 C_1 w^2\} s + 1} \right\} \qquad (8.-1)$$

with parametrization:

$R_1 = 2 \ \Omega$; $R_2 = 416.7 \ \Omega m^2$

$C_1 = 0.001254$ F; $L_2 = 24.31$ Hm^2

The response of this membrane to various excitations is simulated on a computer and discussed in this chapter.

8.1) Response to Bessel functions in the space domain.

The response to an excitation given as $F_{in}(r,t) = J_0(w_s r)\sin(\omega_0 t)$ was already considered in chapter 5 and calculated as $F_{out}(r,t) = |H(w_s; i\omega_0)| J_0(w_s r)\sin(\omega_0 t - \phi)$, where $H(w_s, i\omega_0) = |H(w_s, i\omega_0)| e^{-i\phi}$.
The amplitude transfer function $|H(w_s, i\omega_0)|$ is plotted in figure 8.-1 with w_s as a parameter.

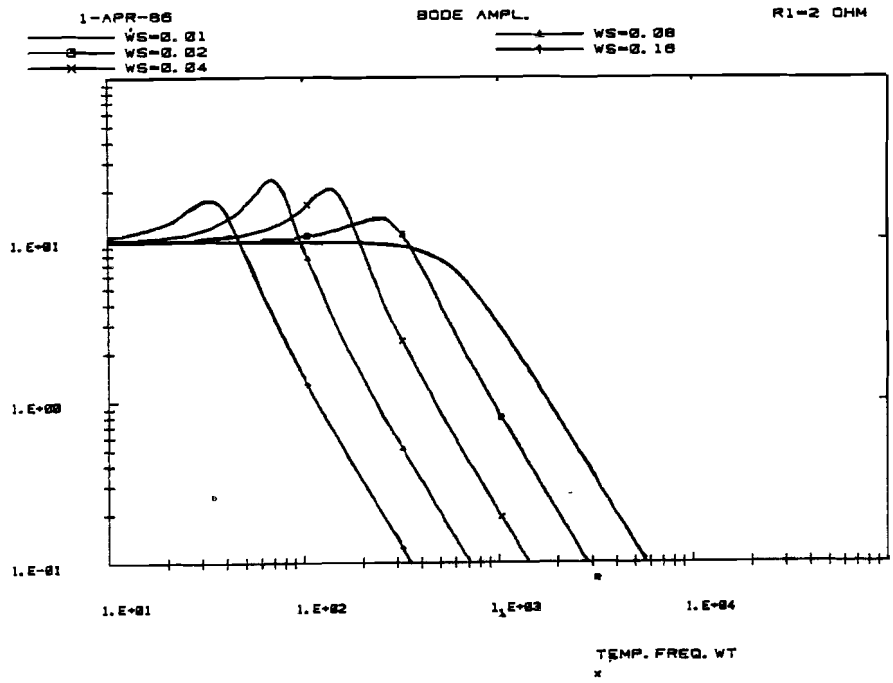

Figure 8.-1. Amplitude diagram as a function of the temporal frequency with the spatial frequency w_s as parameter.

From figure 8.-1 it can be seen that (as expected from chapter 7):
-first the peak increases, then decreases with decreasing spatial frequency w_s.
-the bandwidth monotonically increases with decreasing spatial frequency w_s.

The response to a flashed Bessel function given by $F_{in}(r,t) = J_0(w_s r)\delta(t)$ is $F_{out}(r,t) = J_0(w_s r)\mathcal{L}^{-1}\{H(w_s,s)\}$ and the inverse Laplace transform (the impulse response) to a Bessel function of spatial frequency w_s is plotted in figure 8.-2a and b.

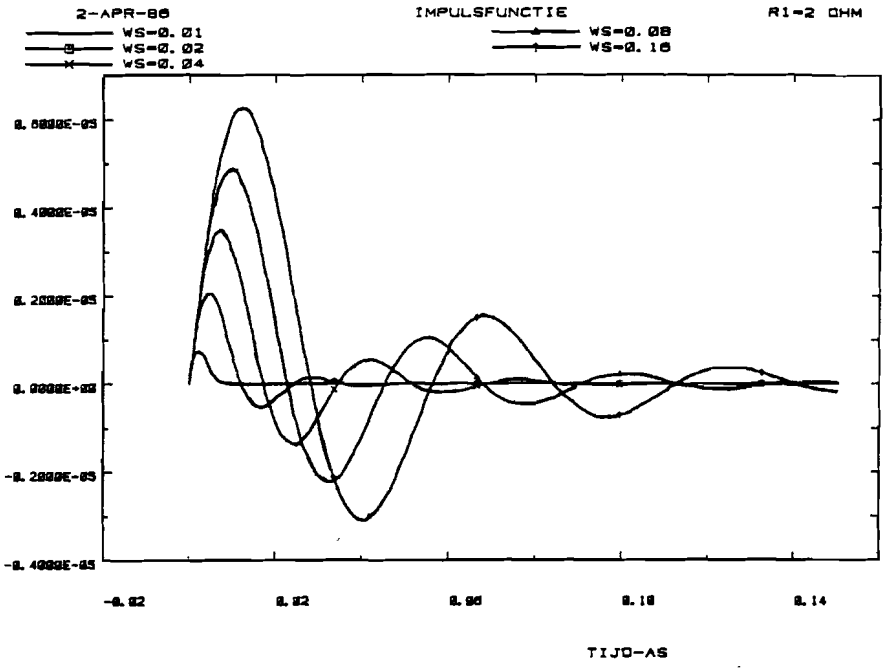

Figure 8.-2a)

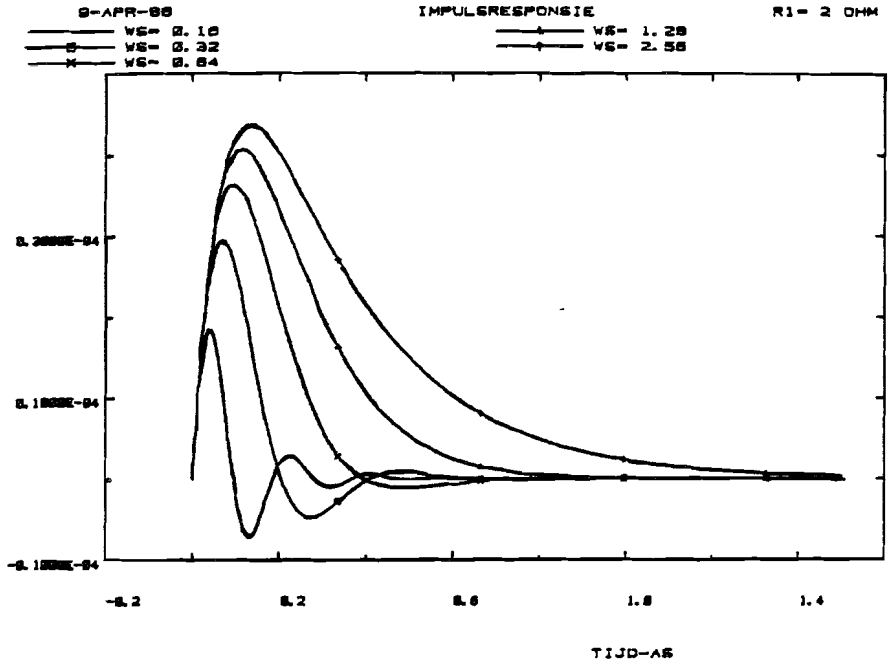

Figure 8.-2b)
Figure 8.-2. The impulse response $h(w_s,t)$ as a function of the time with parameter the spatial frequency. (in figure 8.-2a w_s is from 0.01 to 0.16 and in figure 8.-2b w_s is from 0.16 to 2.56).

In agreement with figure 8.-1 we see:
-faster responses for smaller frequency w_s.
-most oscillatory behaviour for intermediate value w_s from slow monophasic to damped sinusoid to fast monophasic impulse response.
-maximum of response increases with increasing w_s.

8.2) Responses to disk excitations in the spatial domain.

We now turn our attention to stimuli whose spatial form is a disk and with arbitrary time modulation. As shown in chapter 5 such stimulus can be considered as a summation of infinite series of Bessel functions in case of an experiment without surround. First the effect of truncation of the series is considered. In figure 8.-3 a summation of 10 Bessel functions is shown for R_b = R_{st} = 30 according to (5.-24). In figure 8.-4 the same summation is shown for R_b = 30 and R_{st}=15. In both figures we see that the truncation produces ripples on the input signal.

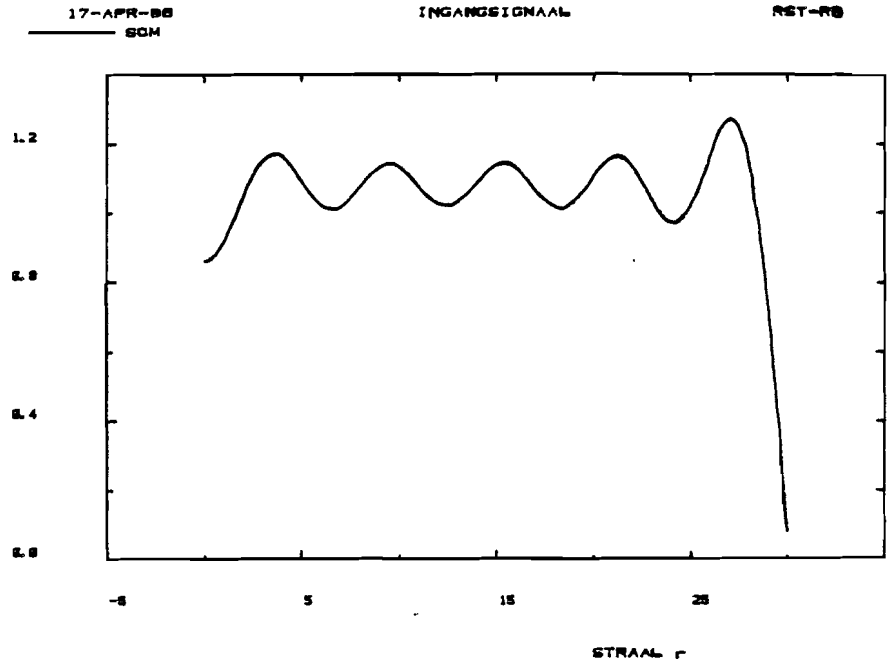

Figure 8.-3. Input signal as a summation of 10 Bessel functions with the stimulus diameter A_{st} equal to the background disk diameter A_b.

The peak on the edge of the disk is higher than in the middle of the disk stimulus.

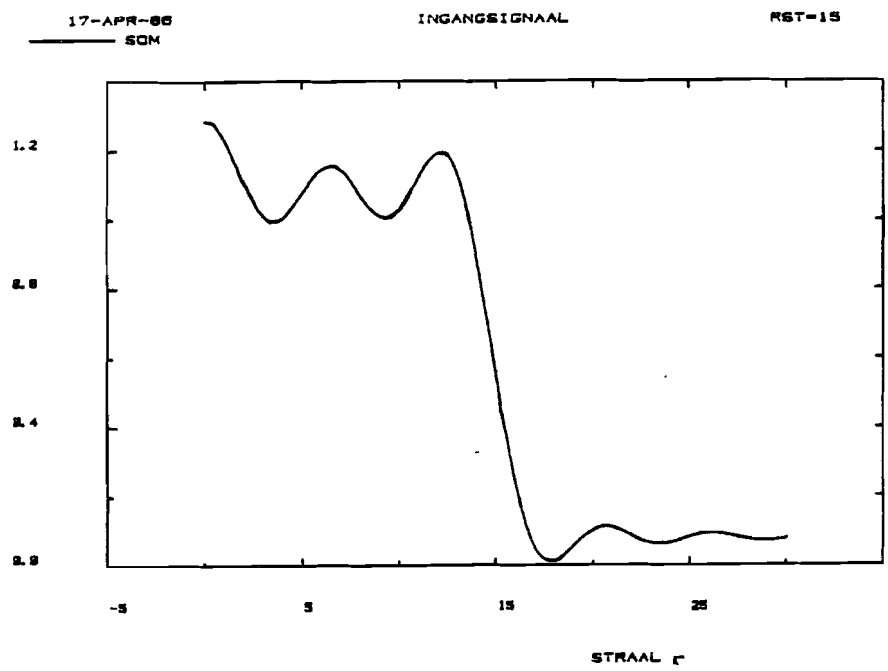

Figure 8.-4. Input signal as a function of the radius r with a smaller stimulus diameter R_{st} = 15.

We now consider a disk that is flashed. As shown in (5.-32) the response of the system will consist of a serie of Bessel function each with its own time course. This is shown in figure 8.-5. Figure 8.-5a shows the time course of the first Bessel function in this series ($J_0(\frac{r}{R_b} j_1)$) of a disk with $R_{st} = R_b = 30$, figure 8.-5b the second and figure 8.-5c the third in that series. In figure 8.-5d the time course of the first Bessel function of a disk with $R_{st} = R_b = 50$ is plotted.
For $R_b = 30$ the impulse responses are smaller in magnitude with smaller Bessel period $r=(j_1/j_m)R_b$; the impulse response of of an excitation with the form $J_0(\frac{r}{R_b} j_1)$ has the largest magnitude of the Bessel series.
The period in the time-domain increases with smaller Bessel period $r=(j_1/j_m)R_b$ in the function of the form $J_0(\frac{r}{R_b} j_m)$ with $m>1$; the impulse response of of an excitation with the form $J_0(\frac{r}{R_b} j_1)$ is the fastest.
The impulse response of the excitation with the form $J_0(\frac{r}{R_b} j_1)$ has the longest Bessel period; the impulse response of the excitation with form $J_0(\frac{r}{R_b} j_2)$ the second longest. The Bessel period decreases with higher m.

The sign of the impulse response of the excitation with the form $J_0(\frac{r}{R_b} j_2)$ is negative with regard to the impulse response of the excitation with the form $J_0(\frac{r}{R_b} j_1)$; the impulse response of of the excitation with the form $J_0(\frac{r}{R_b} j_2)$ starts with a negative phase instead of a positive phase like the impulse response of the excitation with the form $J_0(\frac{r}{R_b} j_1)$.

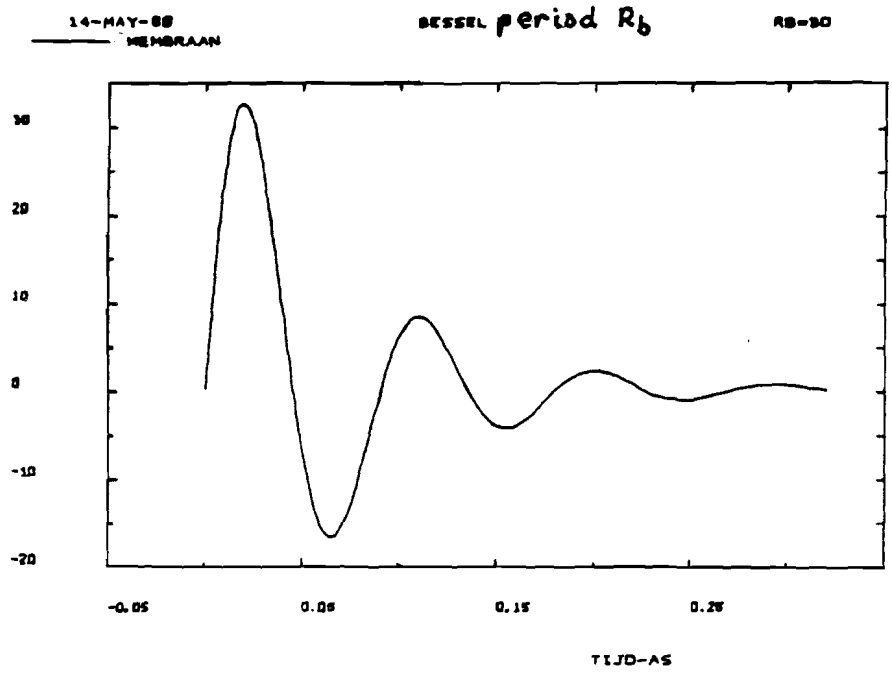

Figure 8.-5a)

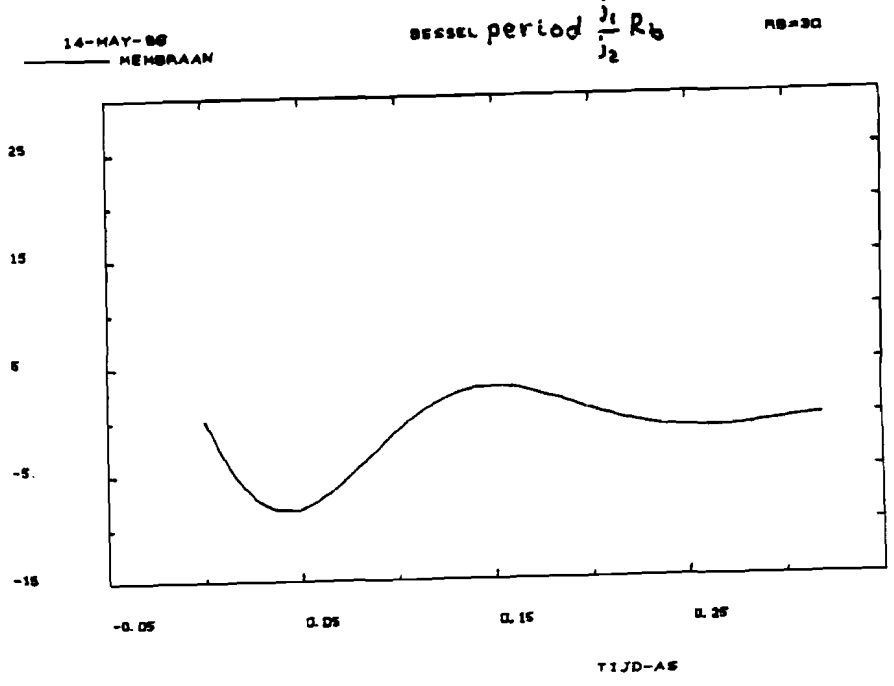

Figure 8.-5b)

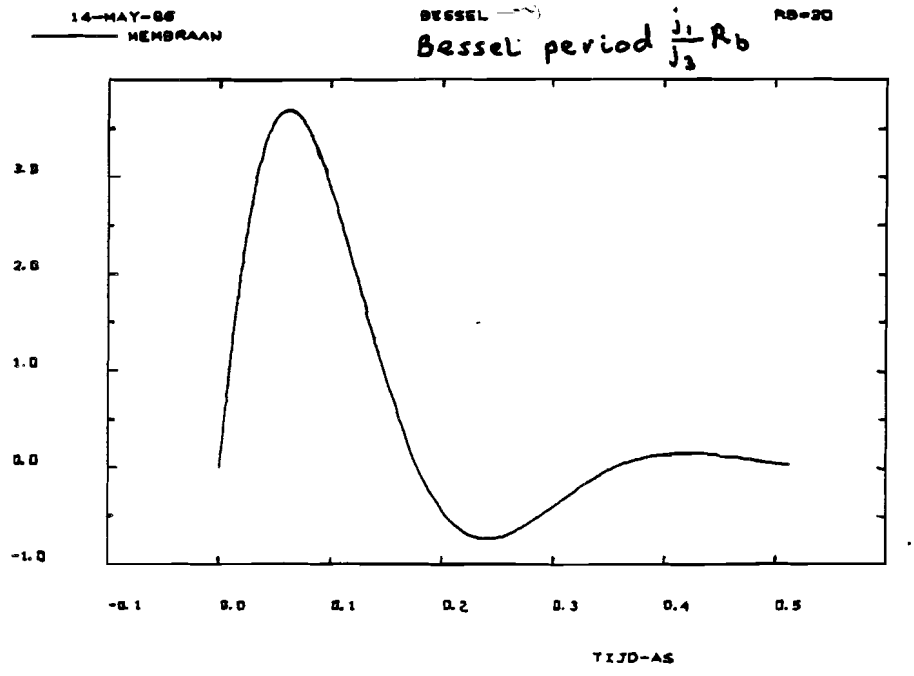

Figure 8.-5c)

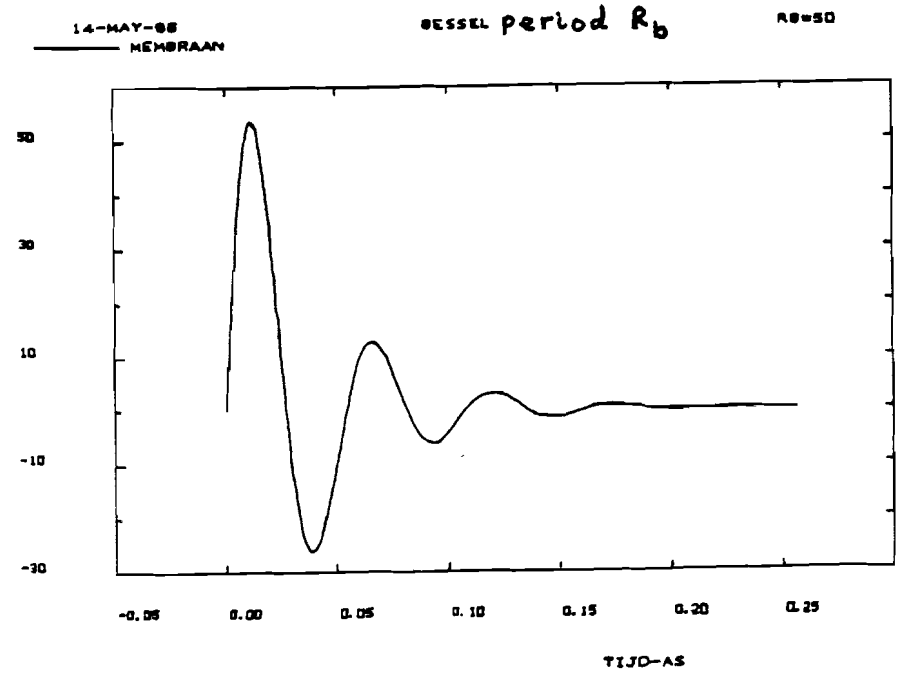

Figure 8.-5d)

The response of figure 8.-5d (larger excitation disk: R_b=50) is faster and higher than the impulse response of figure 8.-5a. The impulse response of the lateral membrane is dependent upon the coefficients A_m and the functions $J_0(w_m r)$ and $h(w_m t)$ (see formula 5.-33 and figure 8.-2).

In figure 8.-6 we plot the impulse responses as a function of the radius r with the time as parameter. The time is chosen in the neighbourhood of the maximum of the impulse response of the first Bessel function of the summation (see figure 8.2).

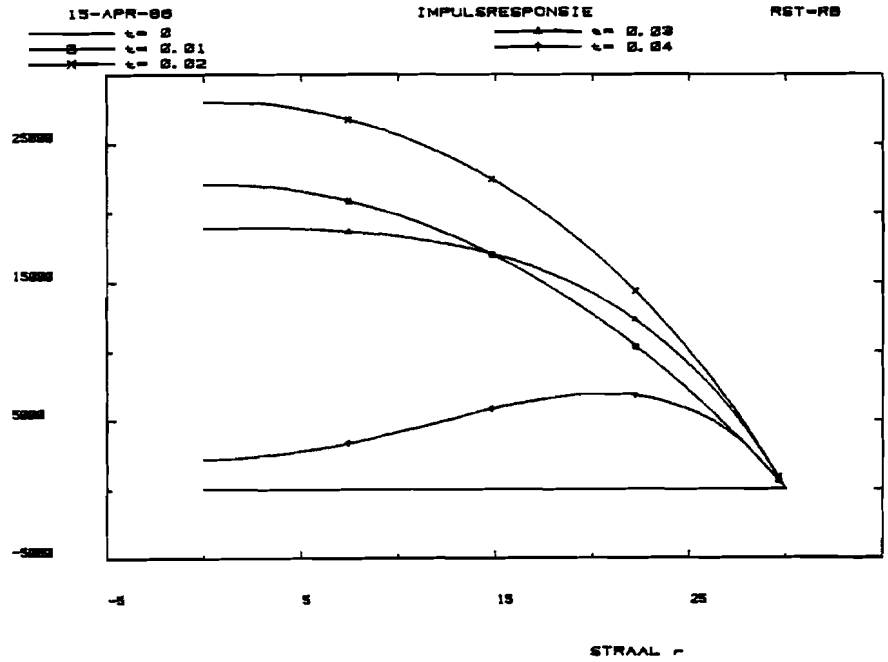

Figure 8.-6. The impulse responses as a function of the radius r with parameter the time.

Here the stimulus diameter R_{st} is equal to the background diameter R_b($R_{st} = R_b$=30). At t=0 the impulse response is zero. These curves move according to the curves of figure 8.-2. In figure 8.-7 the stimulus diameter R_{st} = 15 and R_b = 30.

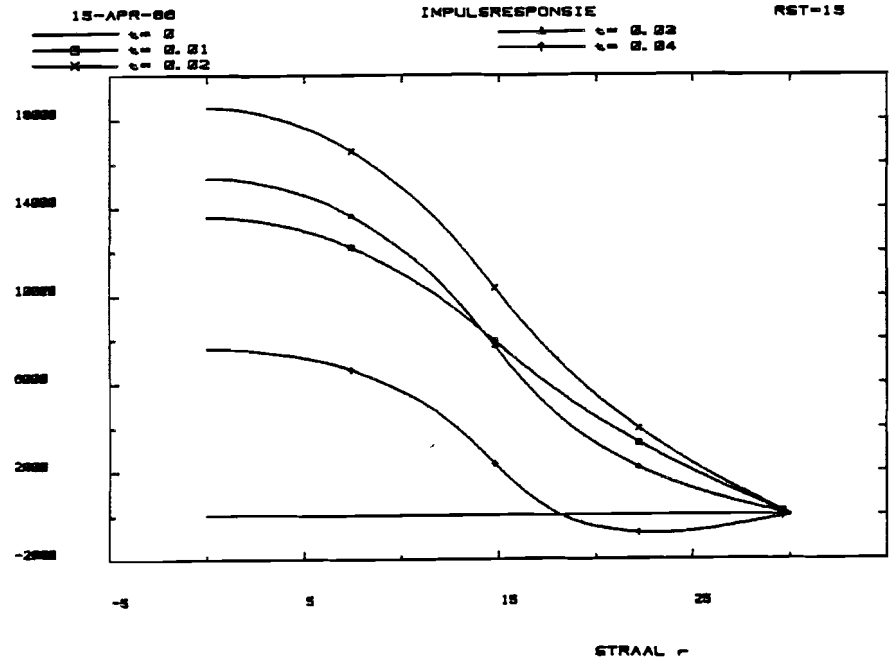

Figure 8.-7. Impulse responses as a function of the radius r with the time as parameter and a stimulus radius R_{st} = 15 and background radius R_b = 30.

In figures 8.-6 and 8.-7 the summation of the first 10 Bessel functions is shown.

In figure 8.-8 the amplitude diagrams of the impulse response (of figure 8.-5) are illustrated as a function of the temporal frequency. The input signal is a Bessel function. The plots are taken at a radius: r=0. The plots are taken with different spatial frequency $w=j_m/R_b$. The phase diagrams of these impulse responses are illustrated in figure 8.-9.

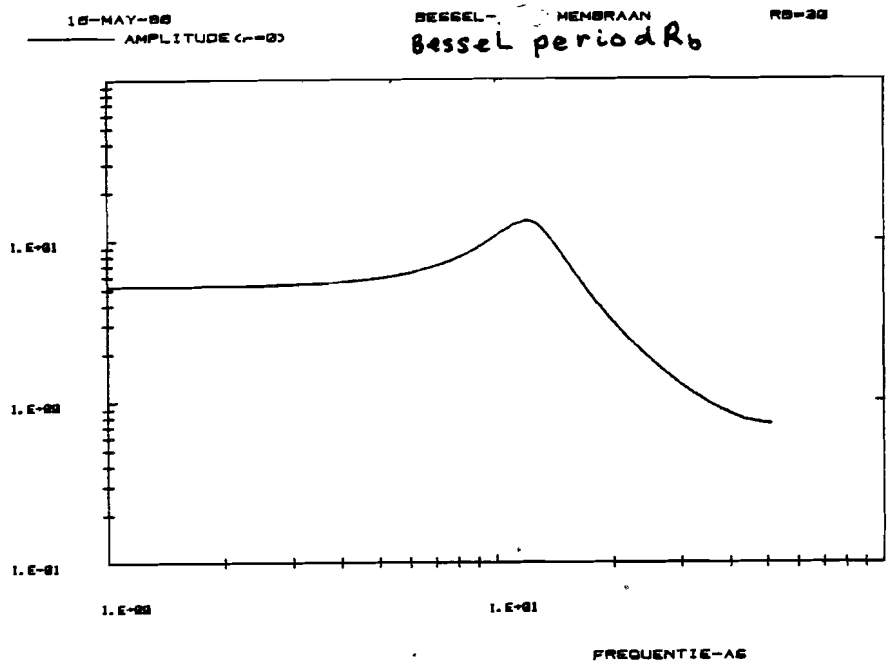

Figure 8.-8a)

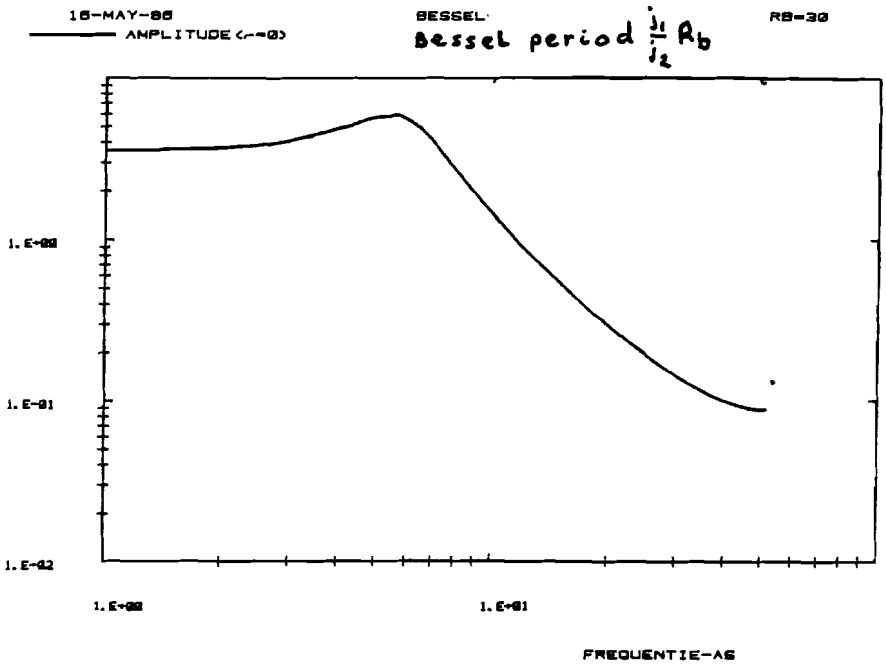

Figure 8.-8b)

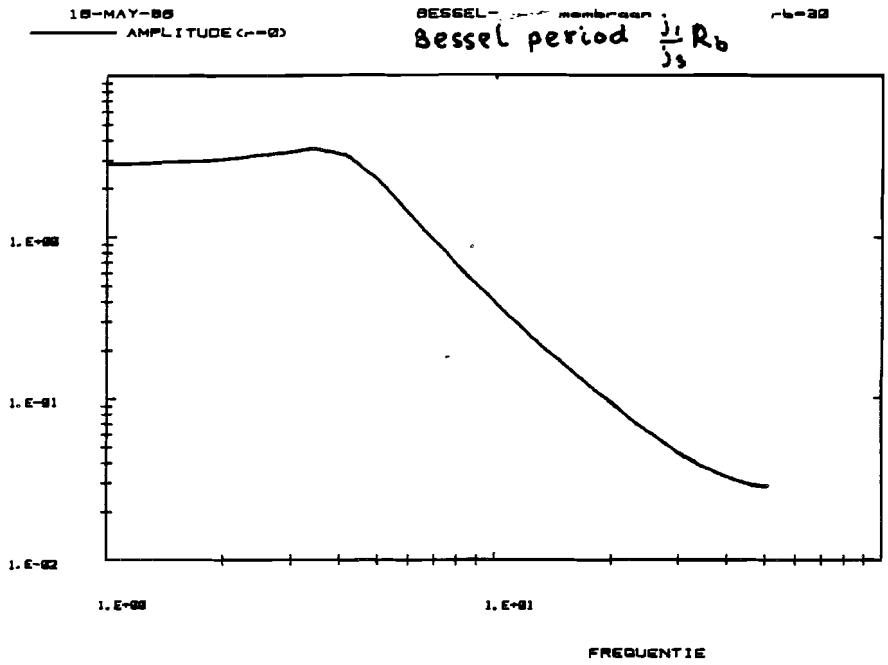

Figure 8.-8c)

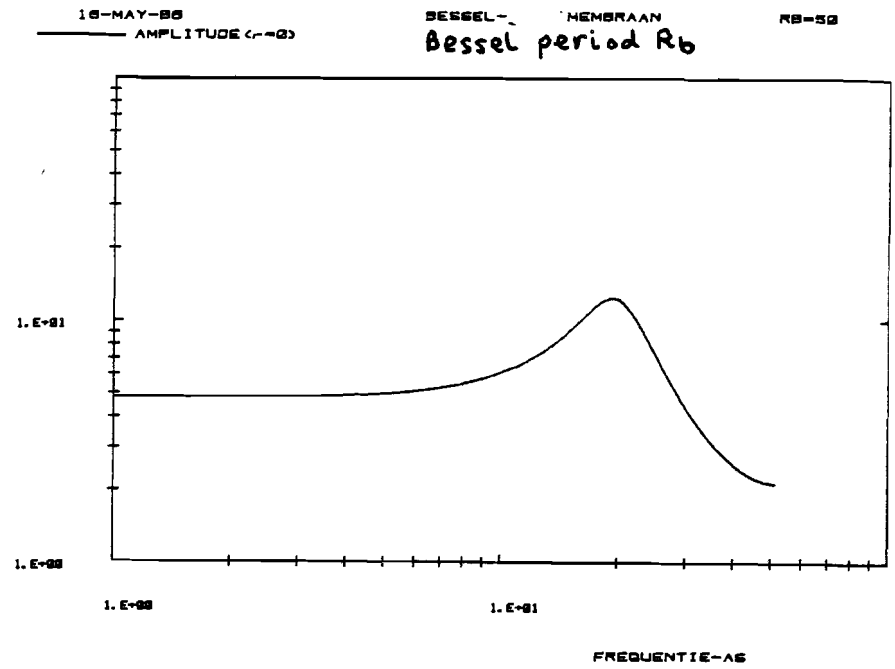

Figure 8.-8d)

These Bode diagrams are identical to the diagrams of figure 8.-1, because the Fourier transform of the input signal is a constant (the input signal is a Dirac function in the time domain).

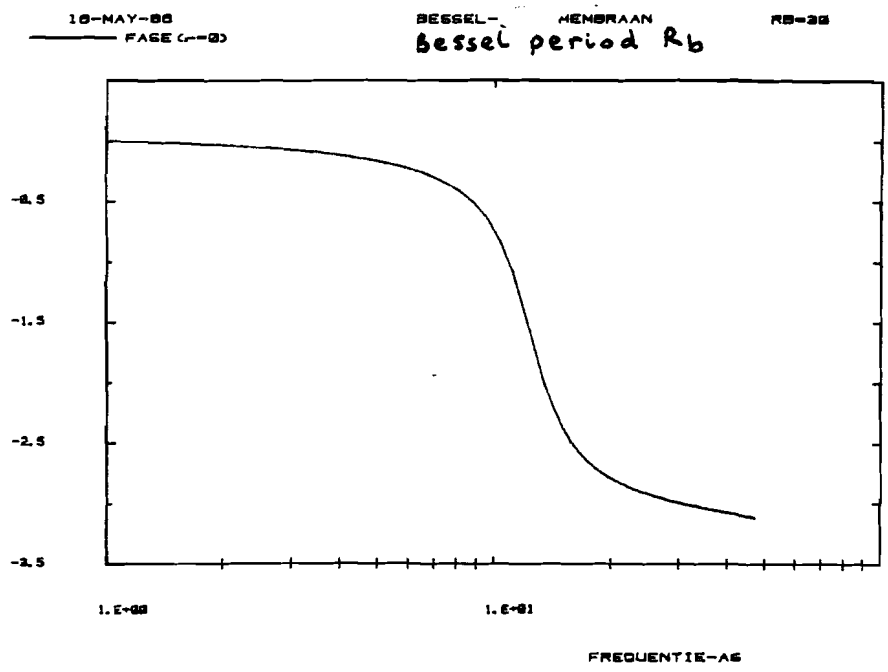

Figure 8.-9a

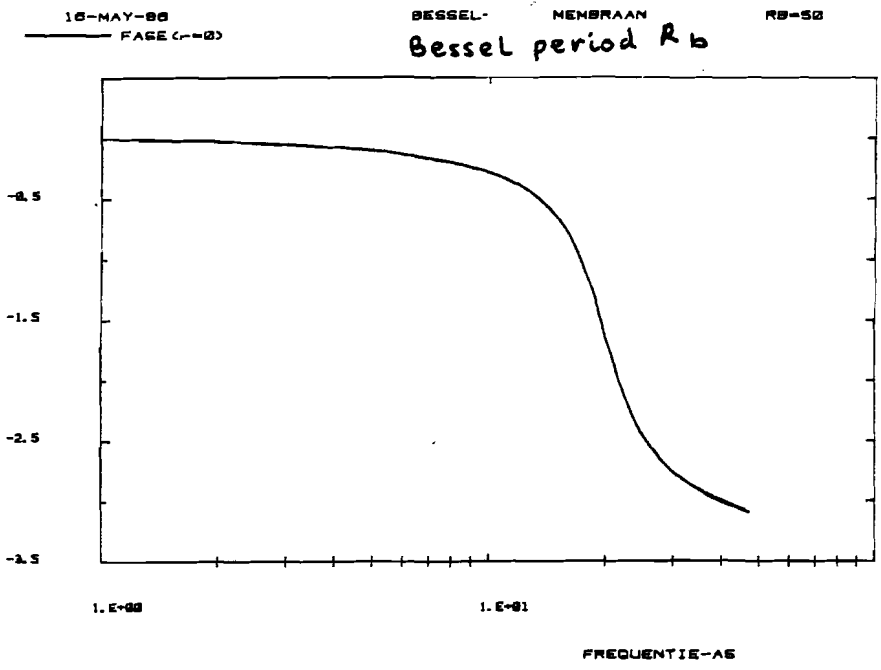

Figure 8.-9b

Remark: in the Bode amplitude diagrams of figure 8.-8 we see that the curve becomes a constant for higher temporal frequency. This is due to the limited area of the impulse response, in which we are sampling. The sampled impulse response is transformed then into the temporal frequency domain with the aid of a subroutine of the NAGD library. The subroutine uses the Fast Fourier Transformation.
Thus for higher frequency it looks like, there are zeroes present, but this is not the case. The slope of the amplitude diagram is approximately correct.

In figure 8.-10 the time course is plotted for r=0. From this we see that the first Bessel function has the most important contribution for r=0 (for this particular stimulus diameter). The second and higher order terms are relatively small.
For smaller diameters than $R_{st} = R_b = 30$ this is even more true: the first term is the dominant term. For larger diameters the higher order terms become relative more influential. See figure 8.-10a with $R_b = 10$ and figure 8.-10b $R_b = 20$.
Thus for even smaller disk diameters the first Bessel function is the most influential, for larger disk diameters the higher terms of the summation are more influential.
Larger fields have a faster response with smaller amplitude.

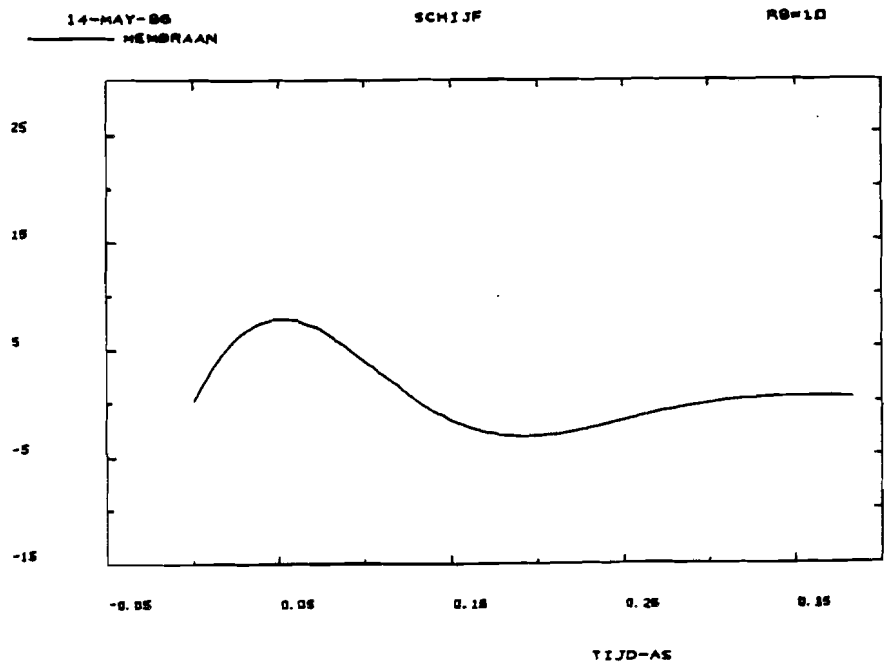

Figure 8.-10a

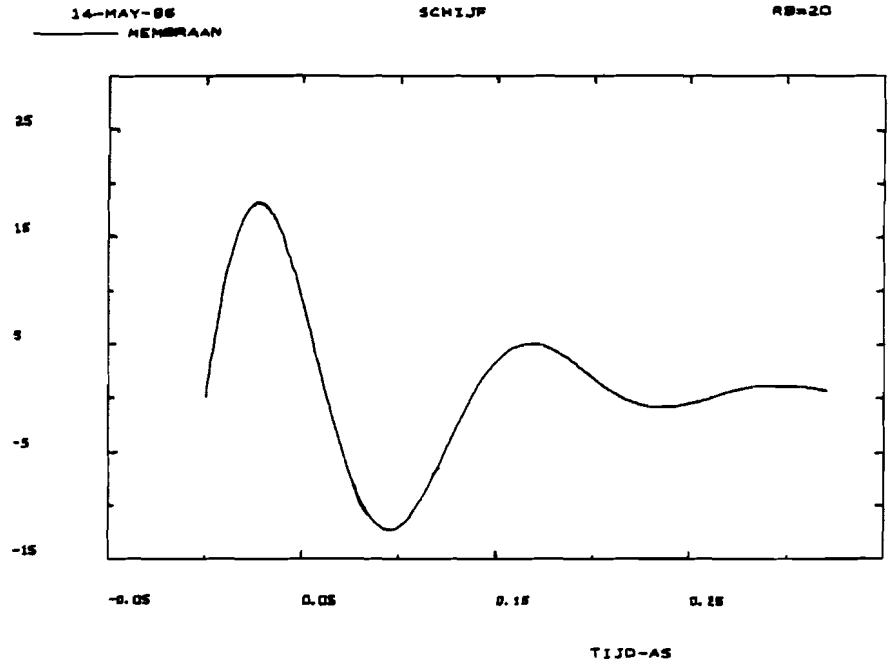

Figure 8.-10b

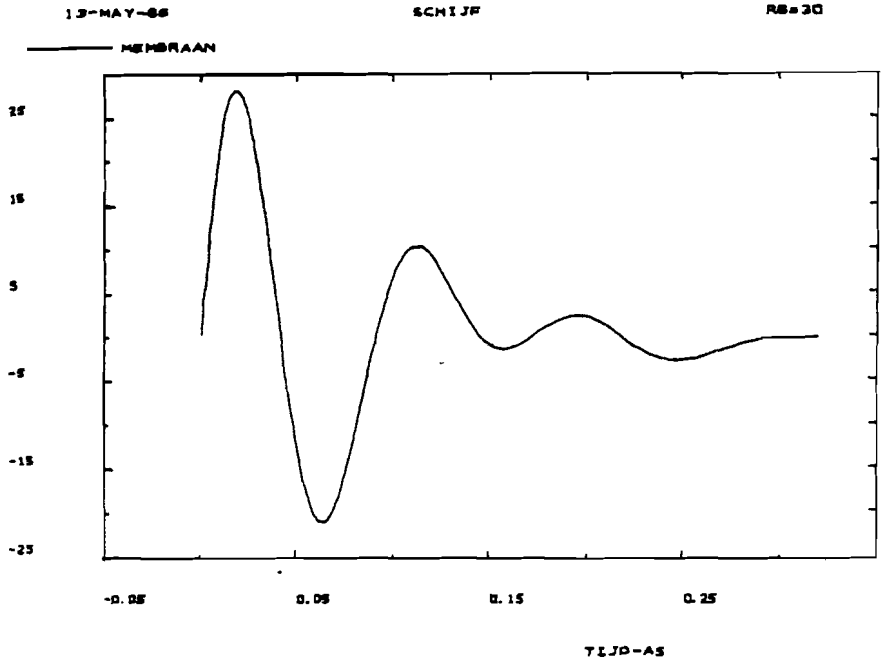

Figure 8.-10c

We see from these figures that the impulse responses are faster and larger in amplitude with increasing stimulus diameter R_{st}.

This is confirmed by the plots of figure 8.-7.

Remark: for higher R_{st} the impulse response start to oscillate, because the Bessel functions with smaller Bessel period j_m becomes larger in amplitude. 10 Bessel functions are not enough to describe the stimulus disk for higher disk diameter.
From the figures 8.-6, 8.-7 and 8.-10c we see that the total response is inseperable.

As a last simulation for the membrane a disk is taken with a sinuoidal time modulation. The transfer function is plotted in figure 8.-11: the amplitude diagrams of the impulse responses of the lateral membrane are illustrated as a function of the temporal frequency. The input signal is a disk stimulus with $R_{st} = R_b$. The stimulus diameter R_{st} is varied between the plots.

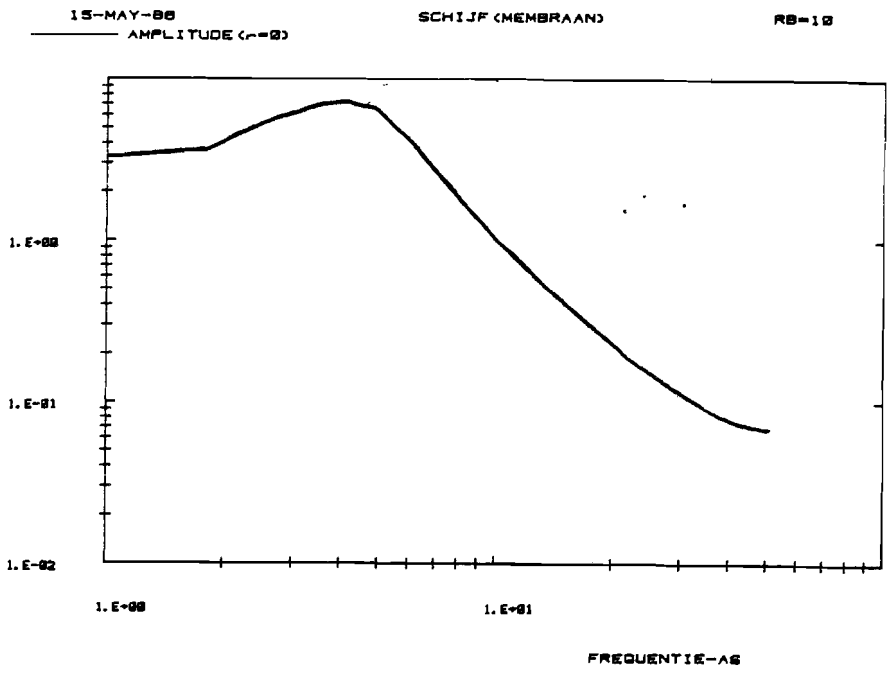

Figure 8.-11a

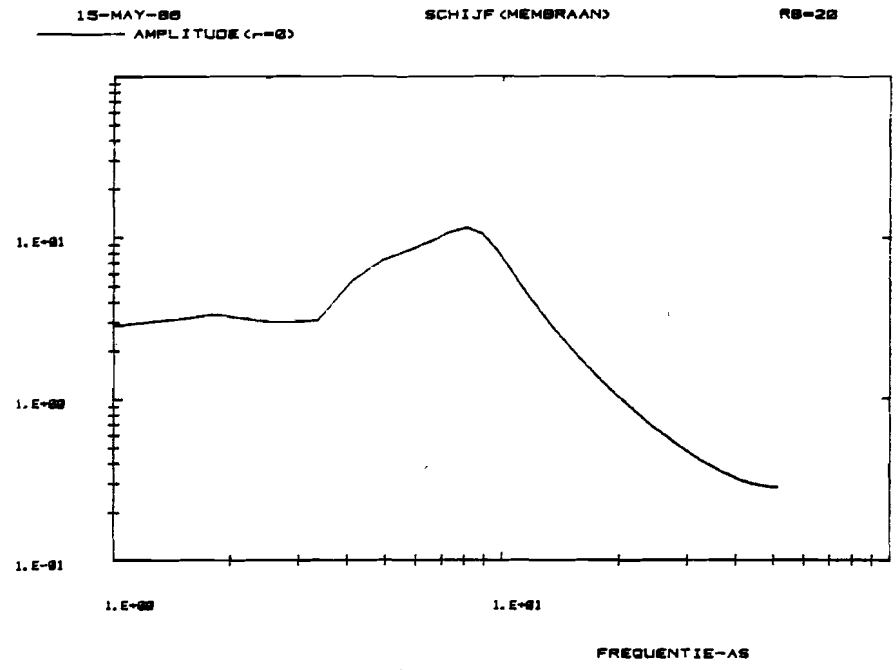

Figure 8.-11b

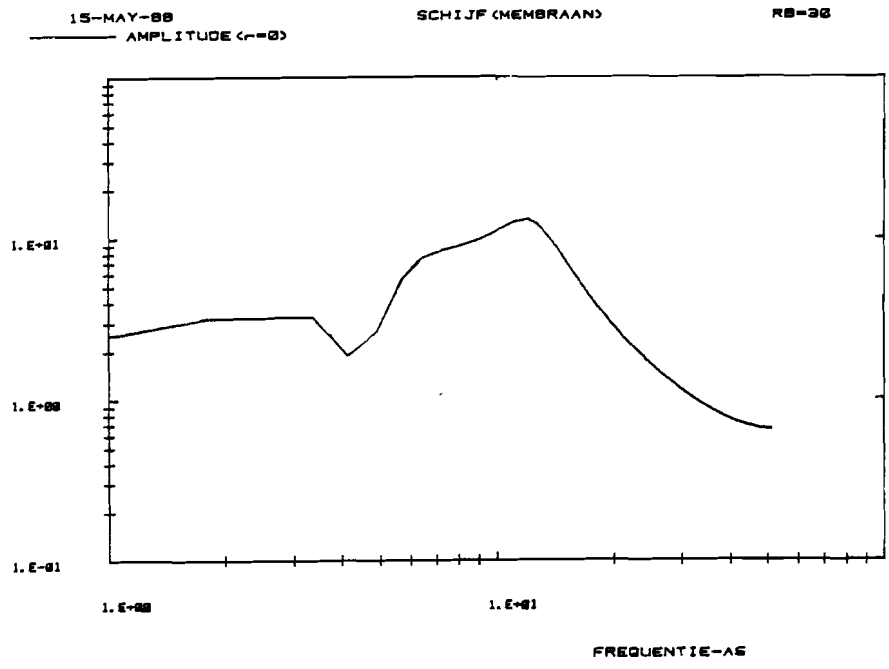

Figure 8.-11c

Remark: we see that for higher disk diameter $R_{st}(=R_b)$ some amplitude components are weakening. We think this is due to the fact that there are not enough Bessel functions used in the summation to describe the stimulus disk adequatly.

Chapter 9: Temporal filter

In chapter 7 the lateral membrane structure was chosen including its parameters. In chapter 8 simulations of the lateral membrane were shown. The only thing that now needs to be done is to choose the temporal filter. This is done in this chapter. Having done this the overall response of the system can be calculated. This will be done in the next chapter.

For simplicity reason the matched filter model is chosen. The temporal filter has an impulse $f_3(t)$ according to this model:

$$f_3(t) = -e^{-b_2 t} \sin(\omega t) \{U(t) - U(t - T)\} \qquad (9.-1)$$

with $T = 2\pi / \omega$ and $b_2 < 0$.

In figure 9.-1 the root-locus of the lateral membrane is sketched with the chosen parameters. The filter $f_3(t)$ is now matched to that point of the root-locus that has the highest peak in its Bode-amplitude plot. This is the point where the tangent at the circle goes through the origin of the s-plane (see chapter 6). This point is also approximately, the 1^o-field, because the first term from the Bessel-serie for the 1^o-field was chosen right there in chapter 7. So only for a 1^o-field there is real matching.

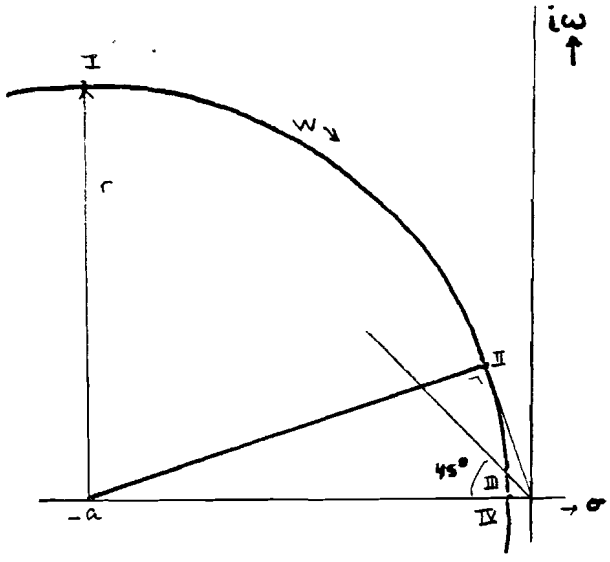

Figure 9.-1. Part of the root-locus of case II.

We find that the point of highest Bode-plot-peak occurs for w=0.07 (min. arc)$^{-1}$ and with damping ratio β and (temporal) natural frequency ω_o of:

$w = 0.07$ (min. arc)$^{-1}$
$\omega_o = 83$ rad/s
$\beta = 0.2066$

From this we obtain the damping b_2 and frequency ω of the matched filter by

$$b_2 = -\beta\omega_0 = -17 \ s^{-1}$$
$$\omega = \omega_0\sqrt{1-\beta^2} = 80.57 \ rad/s$$

The simulation of the impulse response of the temporal filter is shown in figure 9.-2.

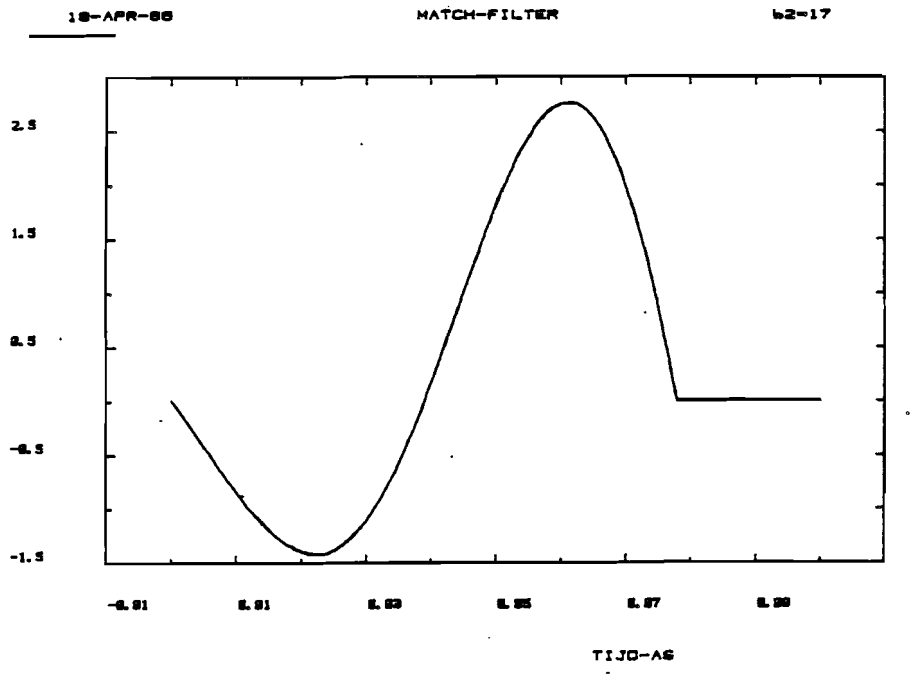

Figure 9.-2. Impulse response of the temporal filter according to the matched filter principle.

It is a damped sinusoid of one period. The maximum of the positive phase is bigger than that of the negative phase. In figure 9.-3 we illustrate the amplitude diagram of the temporal filter as a function of the temporal frequency. And in figure 9.-4 the phase diagram as a function of the temporal frequency is shown.

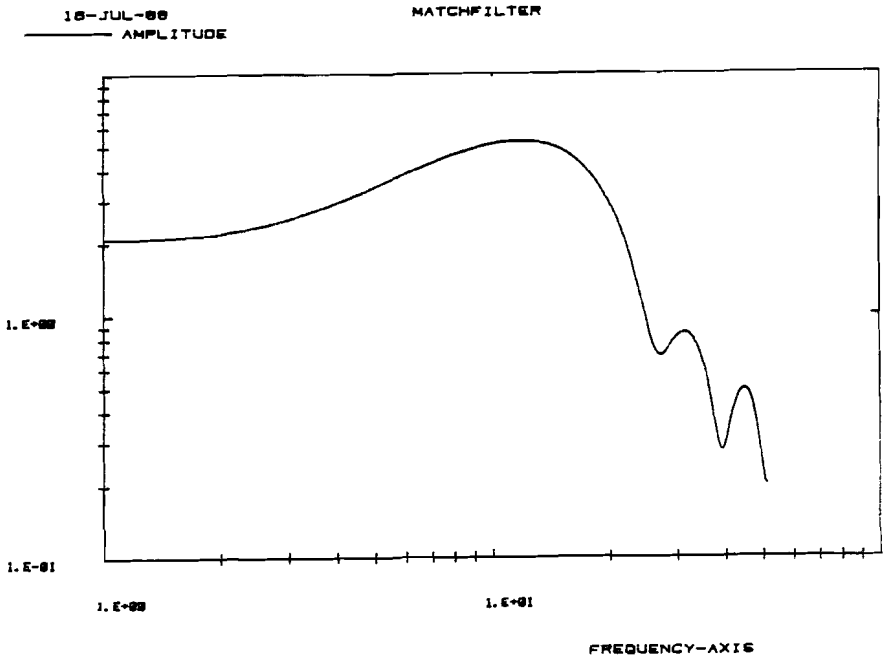

Figure 9.-3. The amplitude diagram of the temporal filter as a function of the temporal frequency.

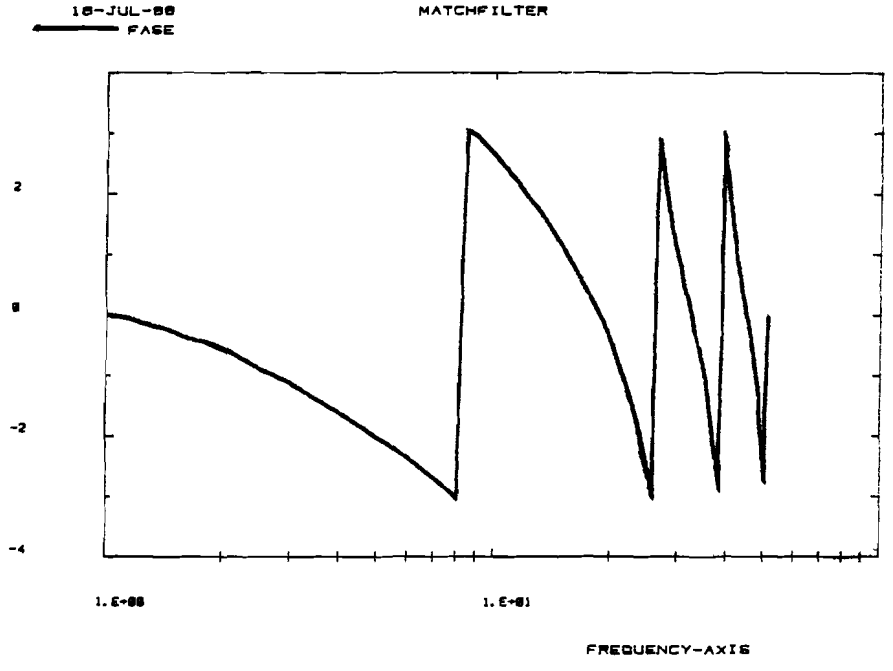

Figure 9.-4. The phase diagram of the temporal filter as a function of the temporal frequency.

Remark: the phase curve makes jumps in figure 9.-4, because the function arctan of the computer is defined for an interval from $-\pi$ to $+\pi$; in this figure the curve passes this limit several times. Thus in reality the phase curve decreases continuously with increasing temporal frequency.

The response of the system with the lateral membrane in serie with the matched filter can now be calculated. The matched filter is tuned to a certain frequency (ω = 80.57 rad/s). We expect that through convolution with the matched filter and other signals the signals with period equal to the temporal filter are amplified the strongest.

Remark: In the original pseudo-matched filter analysis (see chapter 4) also a first order filter was present. This filter is omitted here also for simplicity reasons. The effect of adding such a filter in our model still has to be considered.

Remark: In chapter 10 the computer simulations of the transient model using the matched filter principle are shown. In chapter 4 it was shown that also a second order temporal filter might be considered to be used in serie with the lateral membrane. We did not try this as yet.

Chapter 10: Simulations of the total model

In this chapter we will consider the responses of the system to various excitations.
By putting the temporal filter in cascade with the lateral membrane we can get the output signal of the total visual system by the convolution of the input signal of the temporal filter and the impulse response of this filter.
The excitations are taken the same as in chapter 8. Now these responses are processed by the matched filter, suggested in chapter 9. While showing the simulated responses the similarities to the phycho-physical data are simultaneously discussed.

10.1) Responses to a Bessel function.

flashed inputs.

If the input signal is a Bessel function with a Bessel period $r=\frac{j_1}{j_m}R_b$ and a flash in the time domain we get the impulse responses shown in figure 10.-1a, b and c (for m=1, m=2 and m=3 respectively) at a radius r=0.

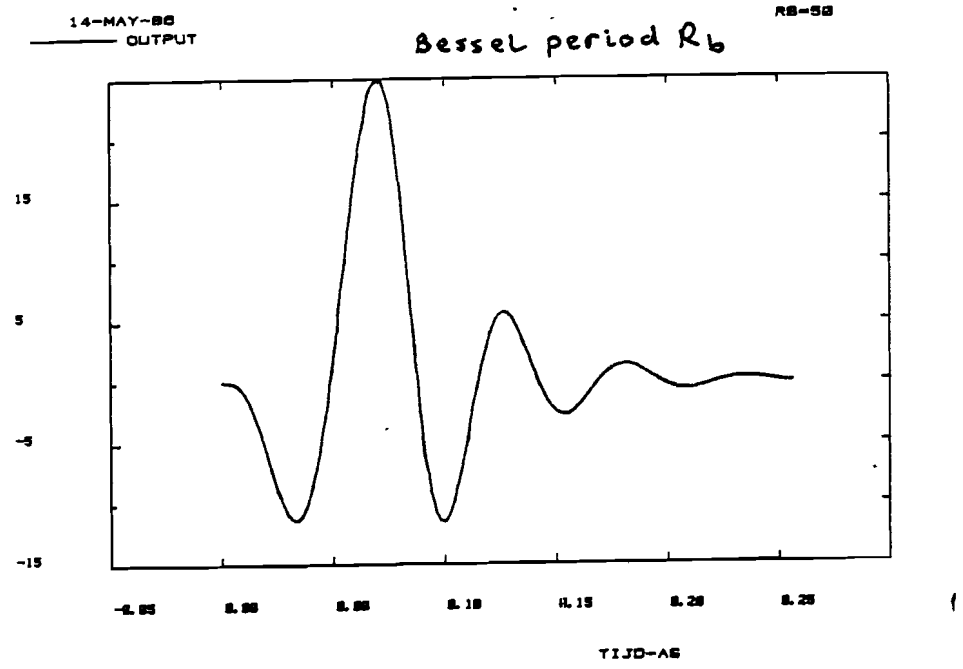

Figure 10.-1a

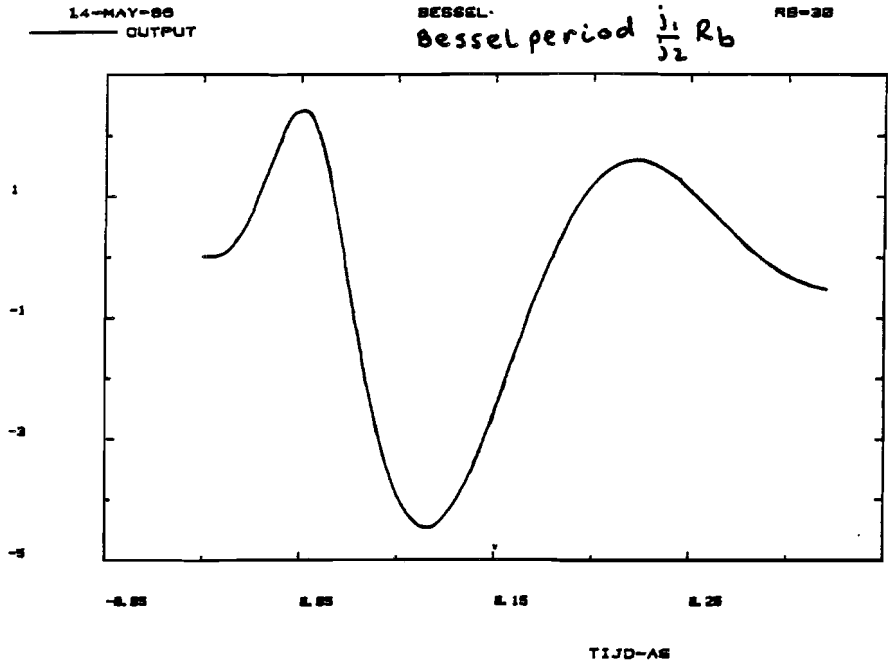

Figure 10.-1b

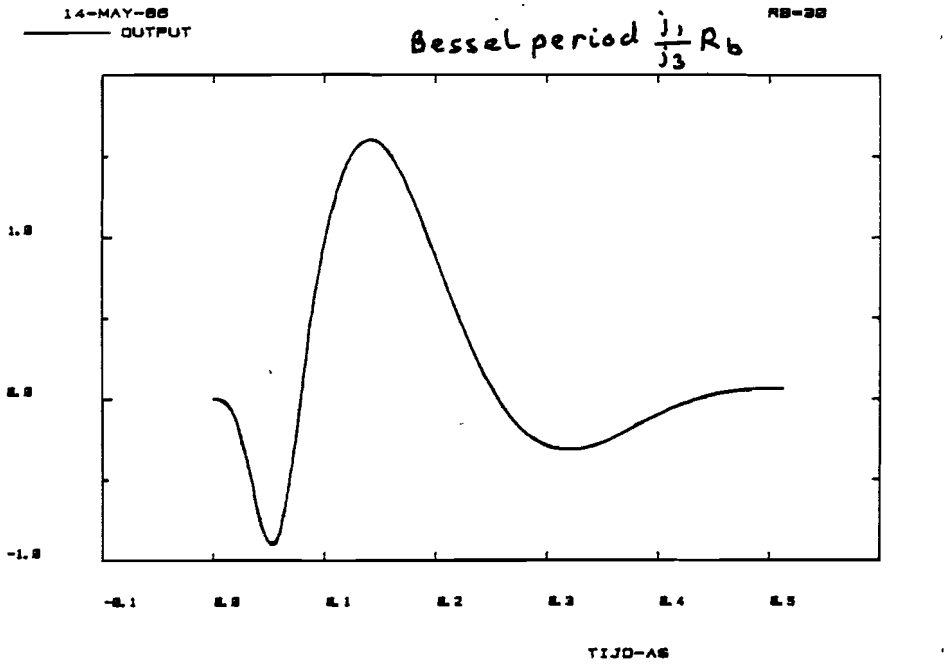

Figure 10.-1c

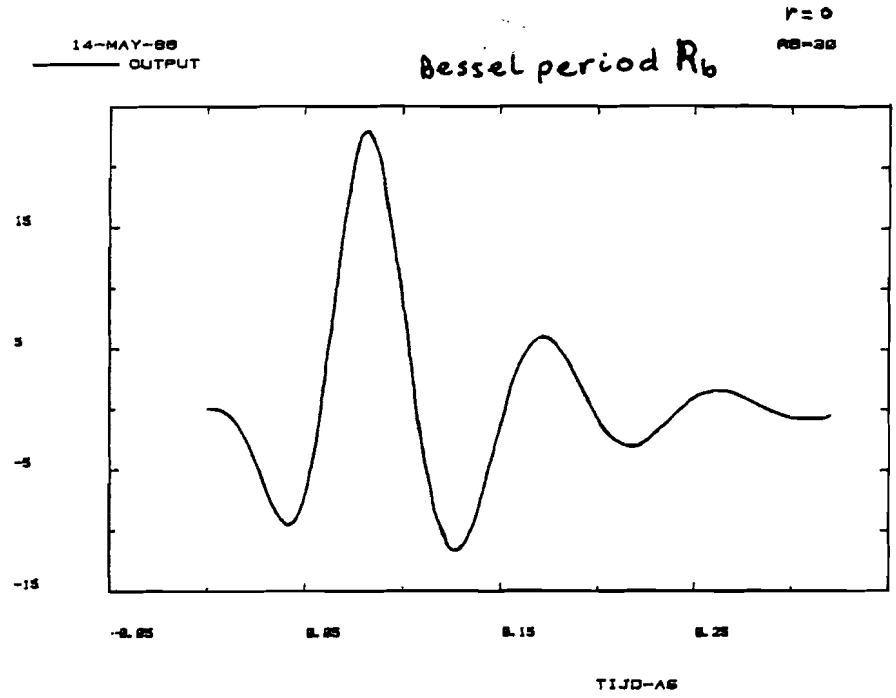

Figure 10.-1d

We have now a triphasic signal with a small oscillation behind.

The amplitude diagrams of the impulse responses of figure 10.-1 are shown in figure 10.-2 as a function of the temporal frequency.

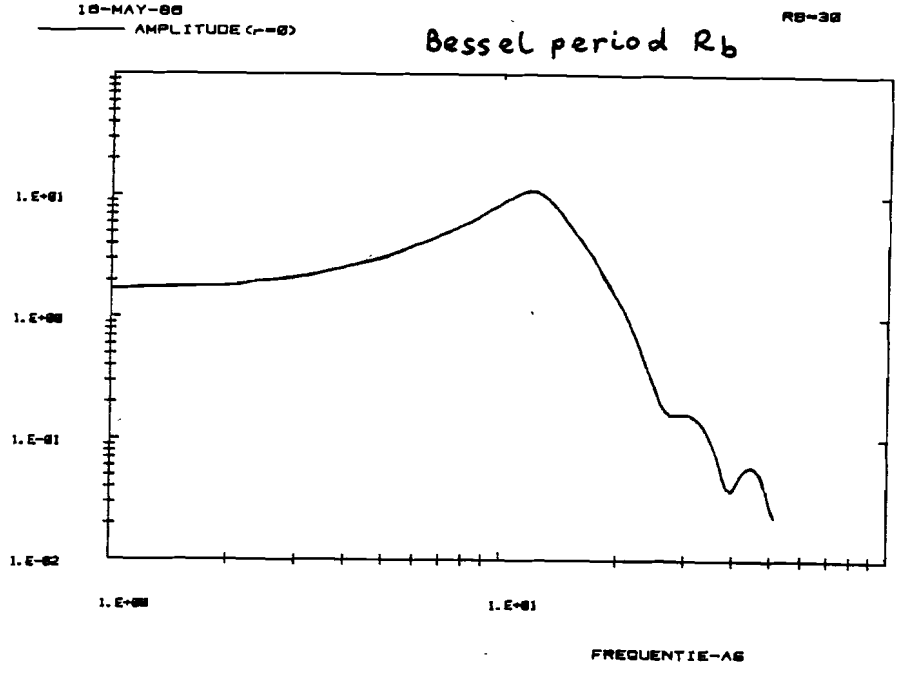

Figure 10.-2a

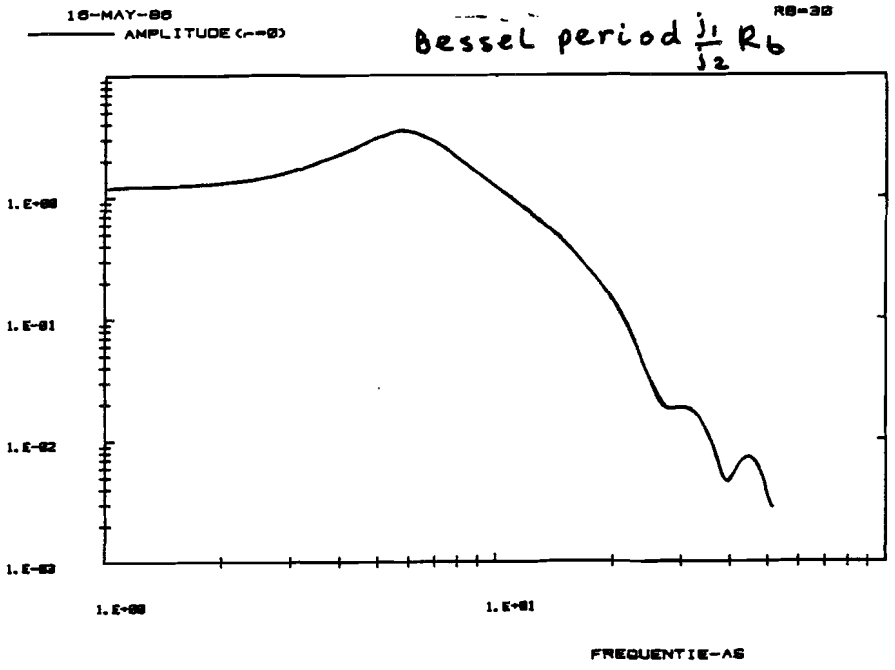

Figure 10.-2b

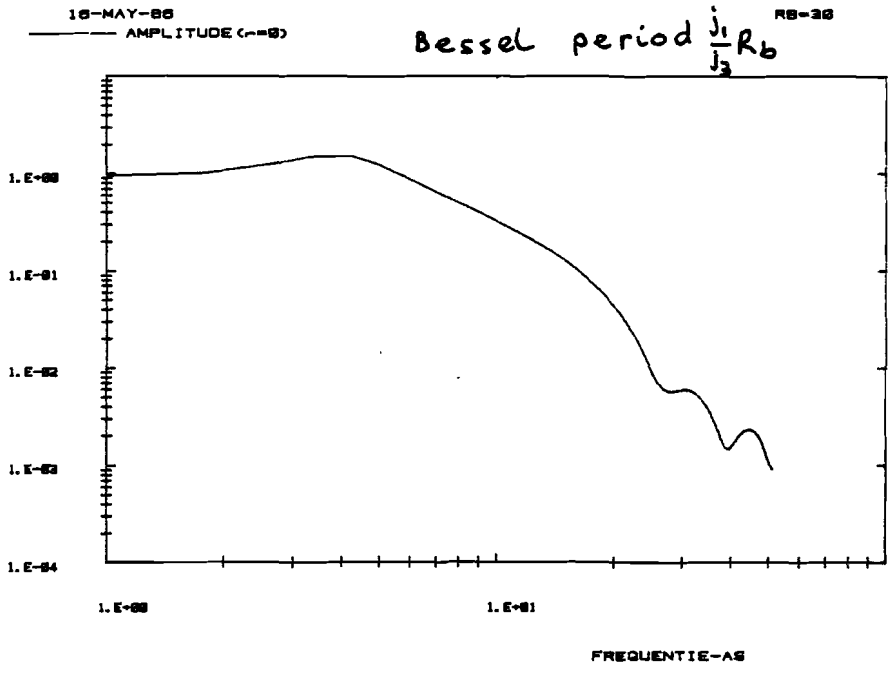

Figure 10.-2c

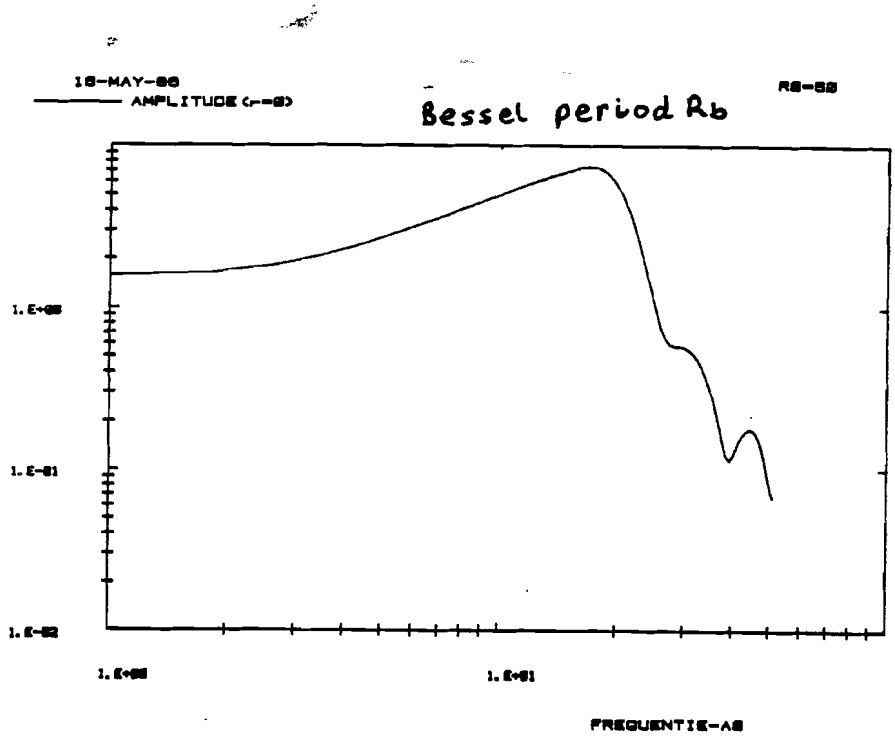

Figure 10.-2d

The ripple in the Bode-amplitude diagrams is due to the truncation of the sinus in the temporal filter (see also figure 9.-3).

10.2) Responses to a disk stimulus.

flashed inputs.

In figure 10.-3 the impulse response of the visual system are shown with a disk as input, here we vary the disk diameter (this is equal with the backgroud disk diameter). (the radius r=0)
In Appendix 3 the main programme and the subroutines are given. With this main programme we have simulated the impulse response of the visual system with a disk as input. By some small changing in this programme we get the other simulations of this report.

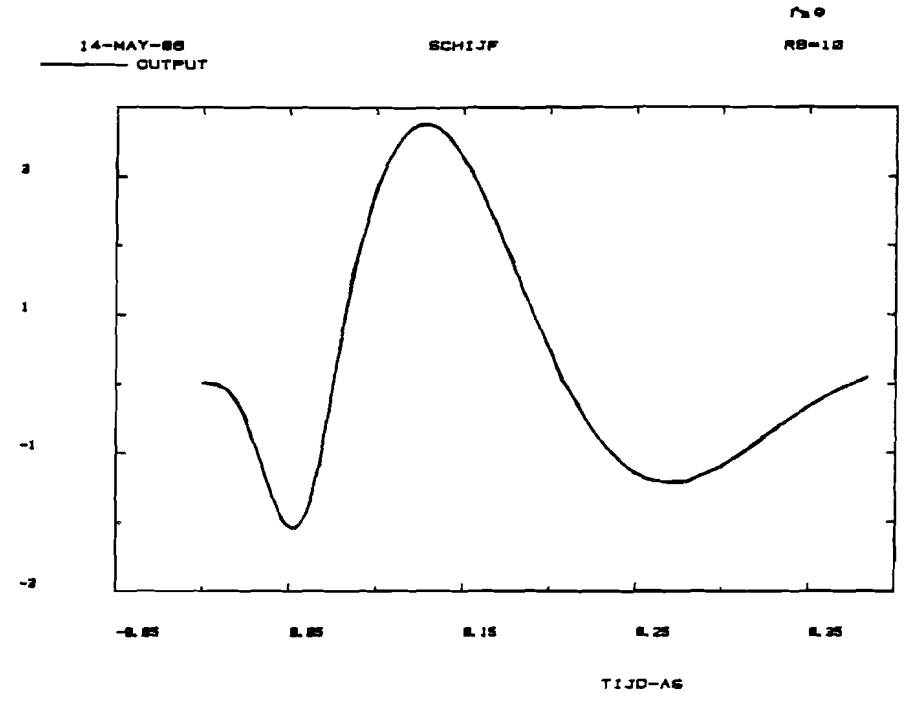

Figure 10.-3a

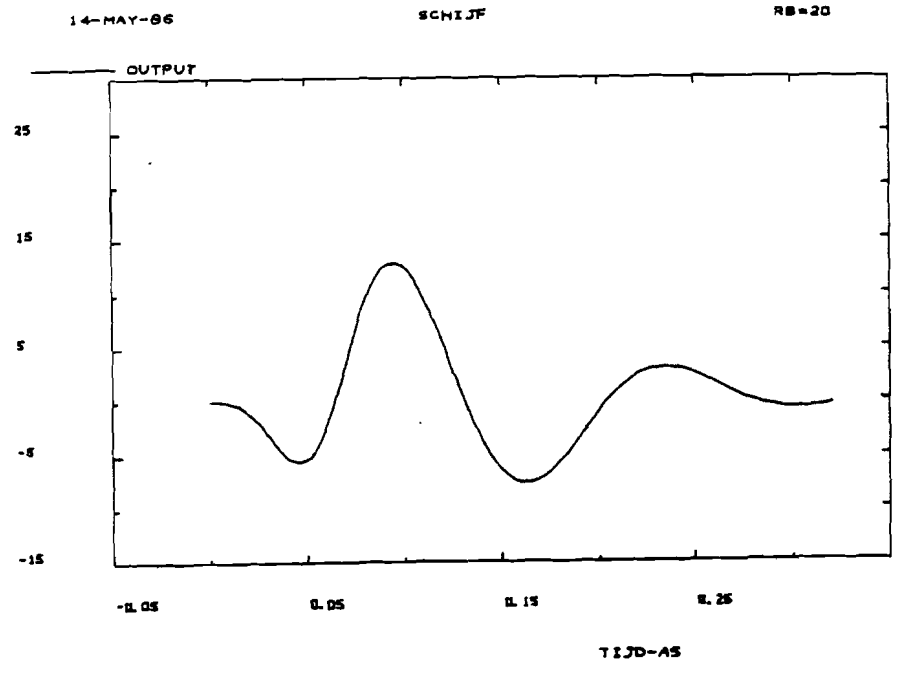

Figure 10.-3b

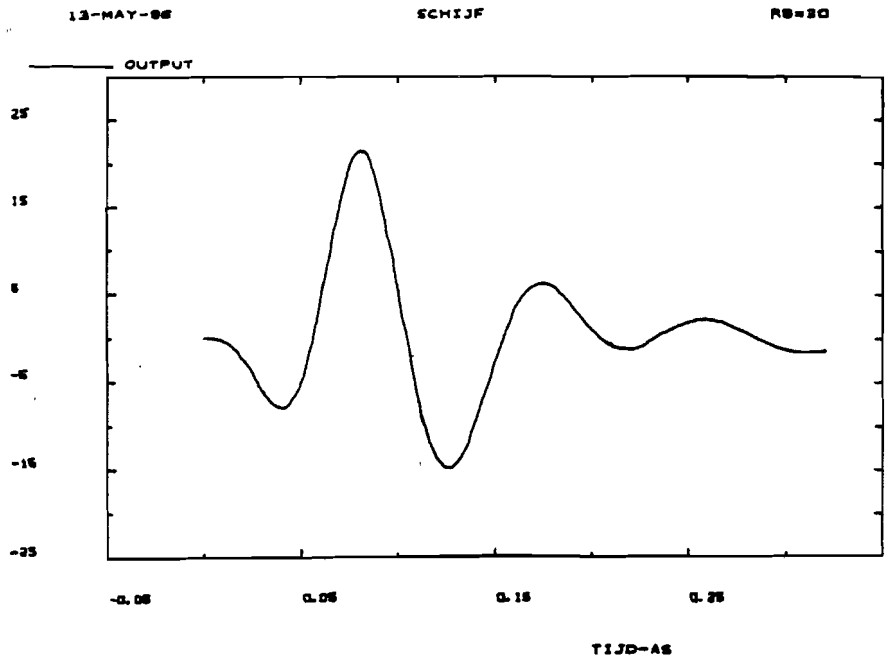

Figure 10.-3c

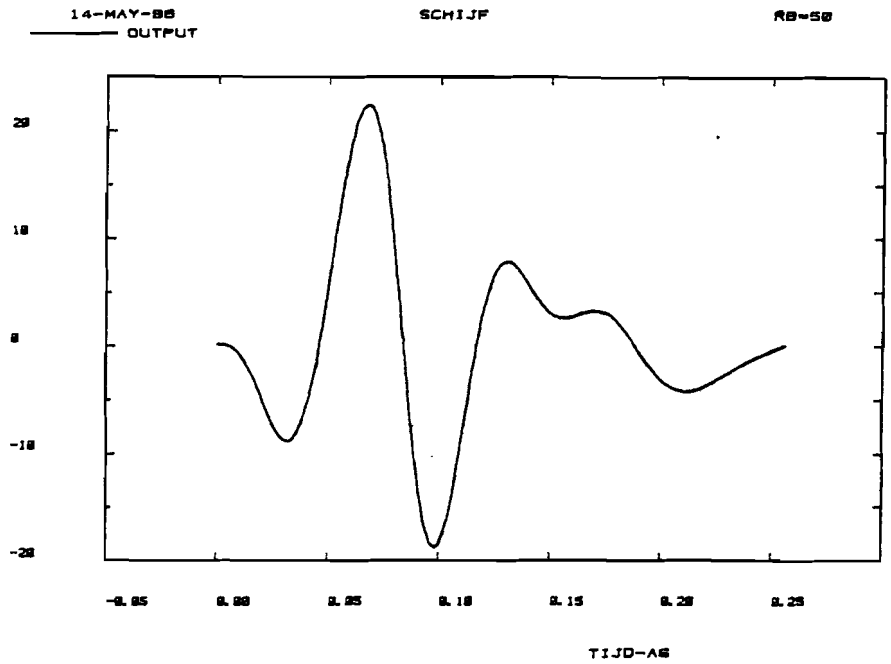

Figure 10.-3d

For increasing disk diameter R_{st} ($=R_b$) the triphasic impulse response is faster (smaller period) and the magnitude also increases hereby. The second phase becomes deeper than the first

phase. For R_{st} = 10 the first phase is deeper than the second, but this is changed for larger stimulus disk diameter.
For R_{st} ($=R_b$) =50 we see that after the third phase the signal is not a damped sinus anymore.
For much larger R_{st} than 50 we get a heavy oscillating signal. This is maybe due to that the summation of 10 Bessel functions is not enough to describe the disk stimulus. Which means that more Bessel functions are needed to describe the disk.

We will compare the simulations of the impulse response of the disk stimulus with different stimulus diameter R_{st} (see figure 10.-3; here R_{st} <50) with the data of the impulse response in figure 3.-1.
The simulations have the same form as the data: triphasic and a damped sinus hereafter . See figure 3.-1e and 10.-2c for 1^{e} -field.
The data of subject H.D. has a deeper first phase than the third phase. His data has the same form as the simulation of a smaller stimulus diameter($R_{st}=R_b=10$) .

In figure 10.-4 the impulse response of the disk stimulus (figure 10.-3) are illustrated as a function of the temporal frequency with parameter the stimulus disk diameter R_{st} ($=R_b$) .

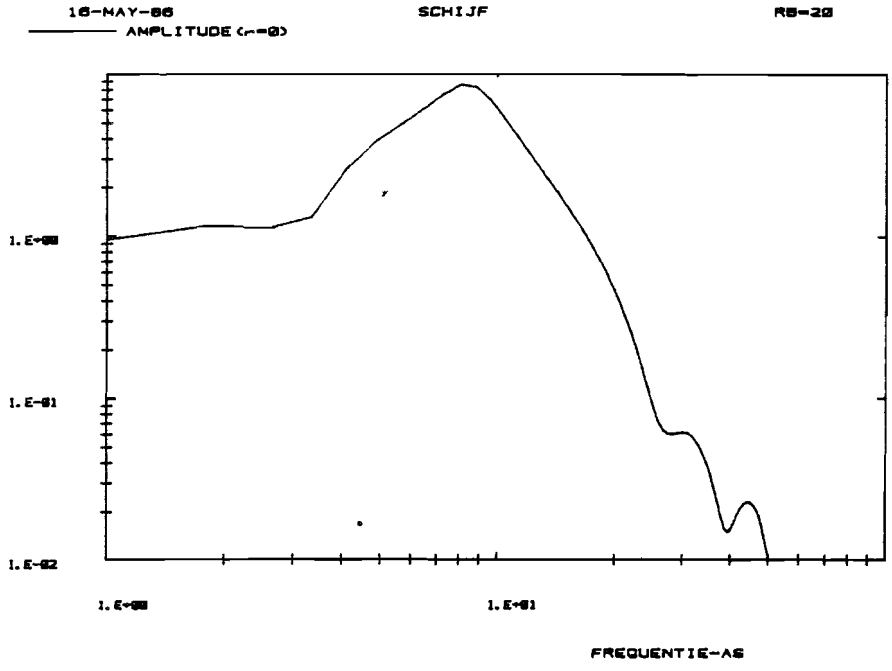

Figure 10.-4a

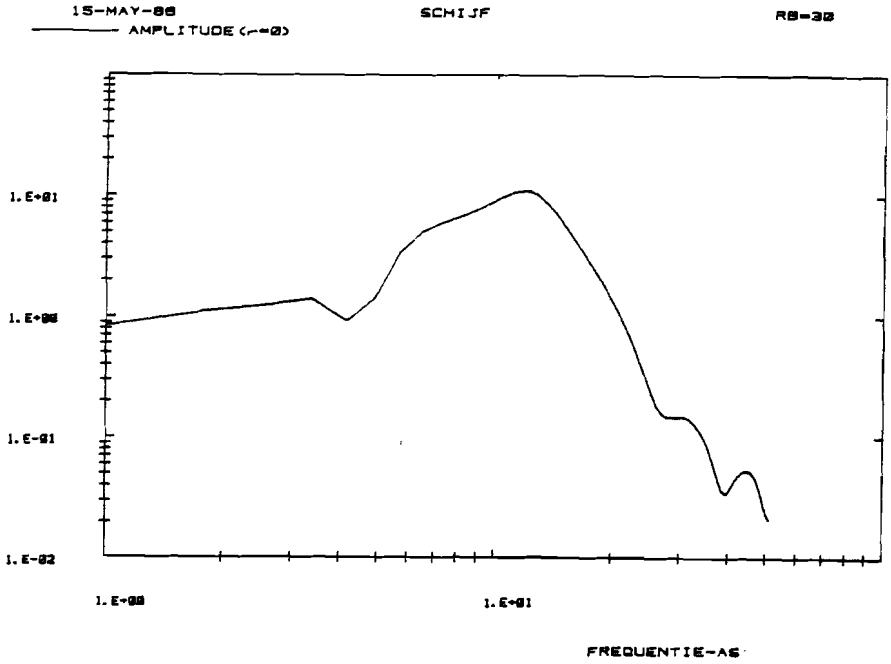

Figure 10.-4b

The weakening of some amplitude components of figure 8.-11 also appears in figure 10.-4. Plus the ripples of figure 10.-2 , this is due to the one period sinus of the temporal filter.
For larger stimulus diameter the simulations of the Bode-amplitude diagrams also have a higher top just like the data of figure 3.-2 (De Lange characteristics).

The maximum of the impulse response is plotted against the stimulus disk diameter ($R_{st}=R_b$) in figure 10.-5.

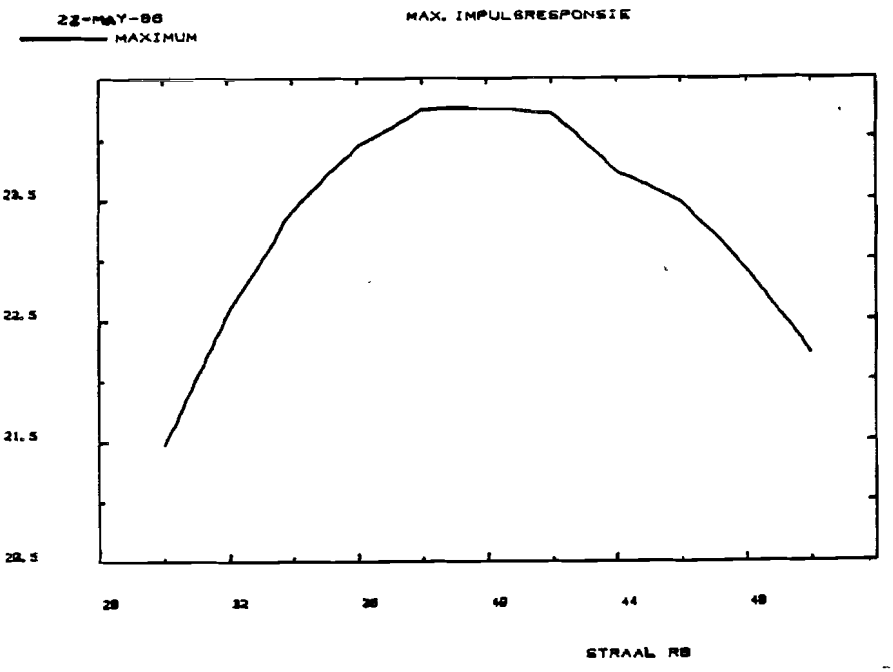

Figure 10.-5. Maximum of the impulse responses as a function of the stimulus diameter R_{st}.

We see there is a maximum in figure 10.-5 for a stimulus diameter $R_{st}=35$. Here after the curve decreases for larger stimulus diameter.

We will compare now the simulation of figure 10.-5 with the upper curve S of figure 3.-3: the maximum of the impulse responses as a function of the stimulus diameter R_{st}.
Both curves are increasing with increasing of the stimulus diameter. Curve S of the data is for a certain stimulus diameter nearly constant, meanwhile the simulation begins to decrease for a certain stimulus diameter; the maximum is about at $R_{st}=35$.
The figure 3.-3 has a horizontal axis with the stimulus diameter in an angle-dimension ($=R_{st}/30$ degrees).

In figure 10.-6 we plot the cutoff frequency $1/f_h$ by varying the stimulus diameter $R_{st}=R_b$. The cutoff values of f_h we get from the Bode amplitude diagrams of the impulse response with different stimulus diameter R_{st}.

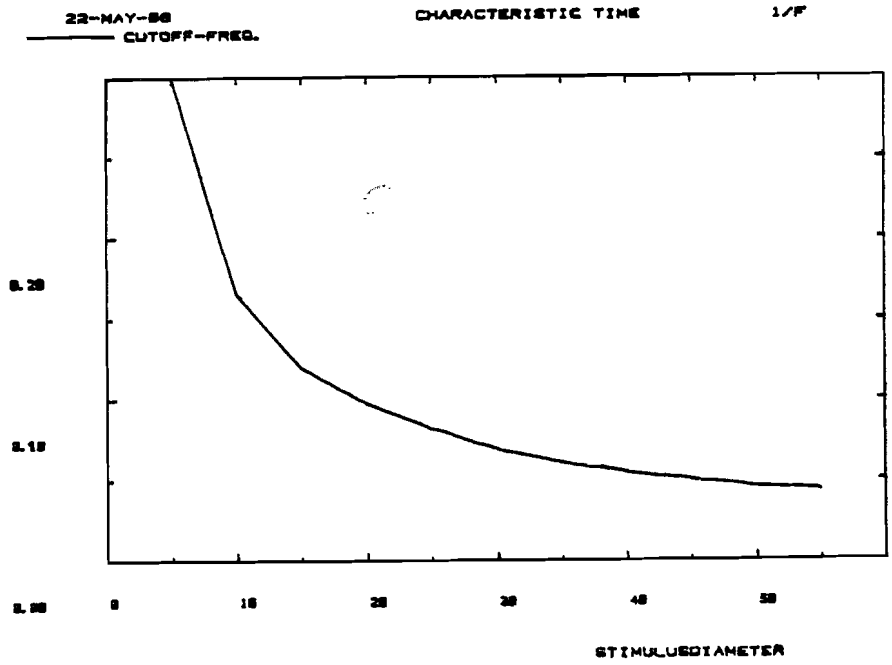

Figure 10.-6. The cutoff frequency $1/f_h$ as a function of the stimulus diameter R_{st}.

The cutoff frequency $1/f_h$ decreases with increasing stimulus diameter.

The simulation of the reciprocal of the cutoff frequency as a function of the stimulus diameter is shown in figure 10.-6 and the data in figure 3.-4 (upper curve). Both curves decreases with increasing of the stimulus diameter.
For small stimulus diameter the simulation curve of $1/f_h$ decreases very rapidly.
For large stimulus diameter the data curve begins to go up: the bandwidth becomes smaller after increasing at the beginning.

10.3) Responses to pulses.

If we modulate the stimulus of the disk as a pulse in the time domain, we will get the pulse response of figure 10.-7 with a pulse width θ = 0.05 s and a stimulus diameter $R_{st}=R_b=30$.

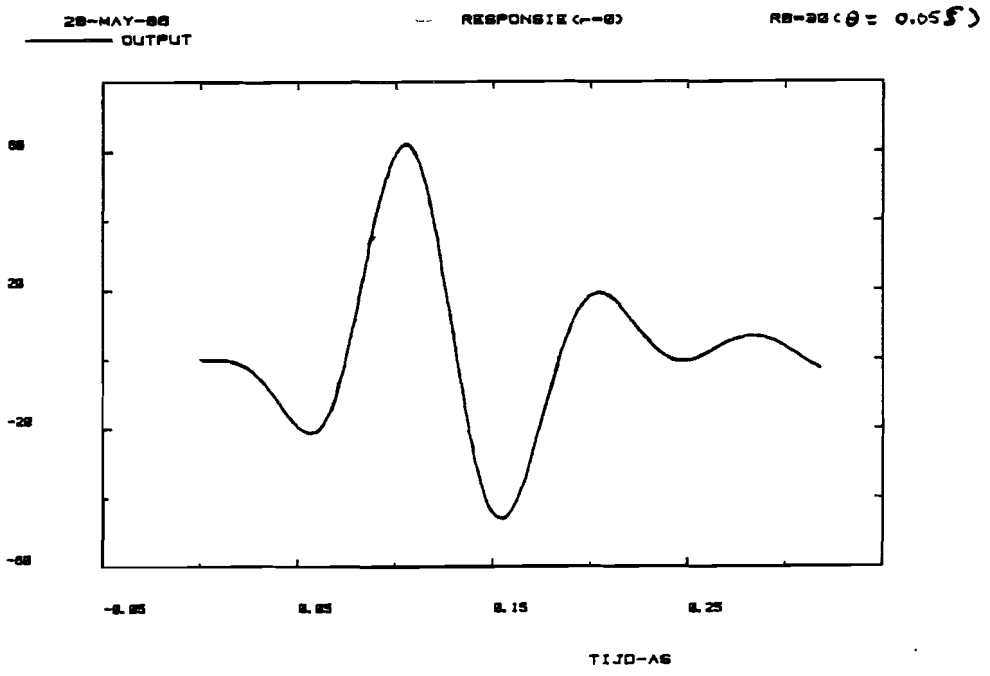

Figure 10.-7

In figure 10.-8 the pulse duration is longer, the transients of the two flanks of the pulse don't influence each other anymore. The last phase is from the oscillation, which occurs behind the triphasic signal.
For small pulse duration the pulse output can be seen as an impulse response: the pulse response has the same shape as the impulse response.

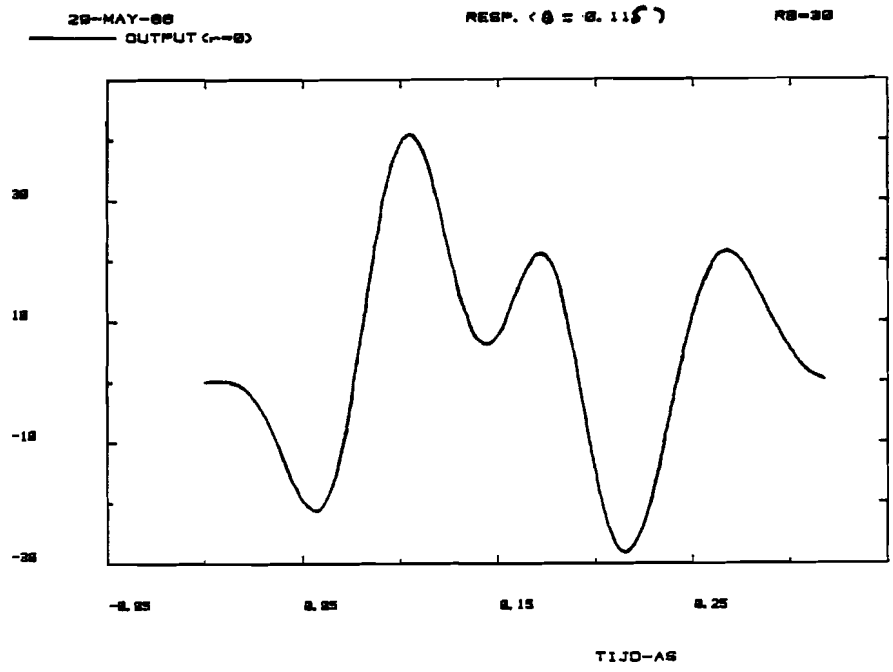

Figure 10.-8

In figure 10.-9 the simulations of the reciprocal of the maximum of the pulse response as a function of the pulse duration are illustrated with as parameter the stimulus disk diameter.

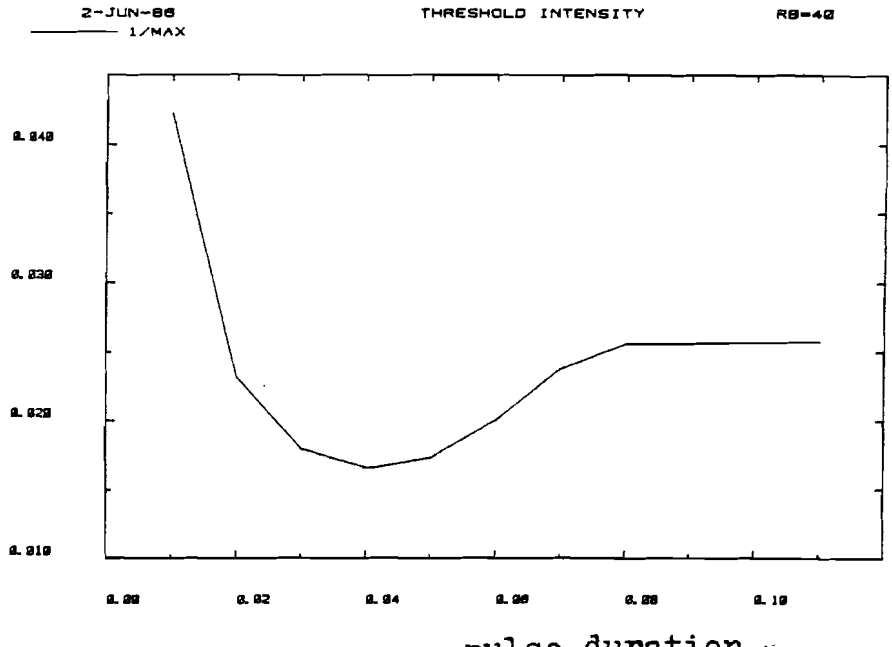

Figure 10.-9a

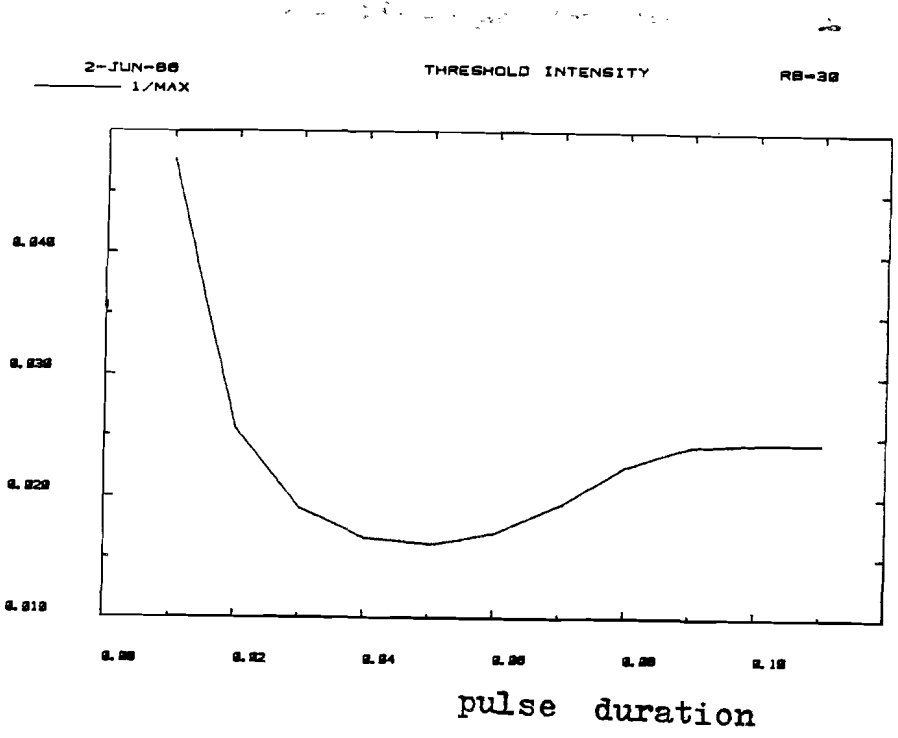

Figure 10.-9b

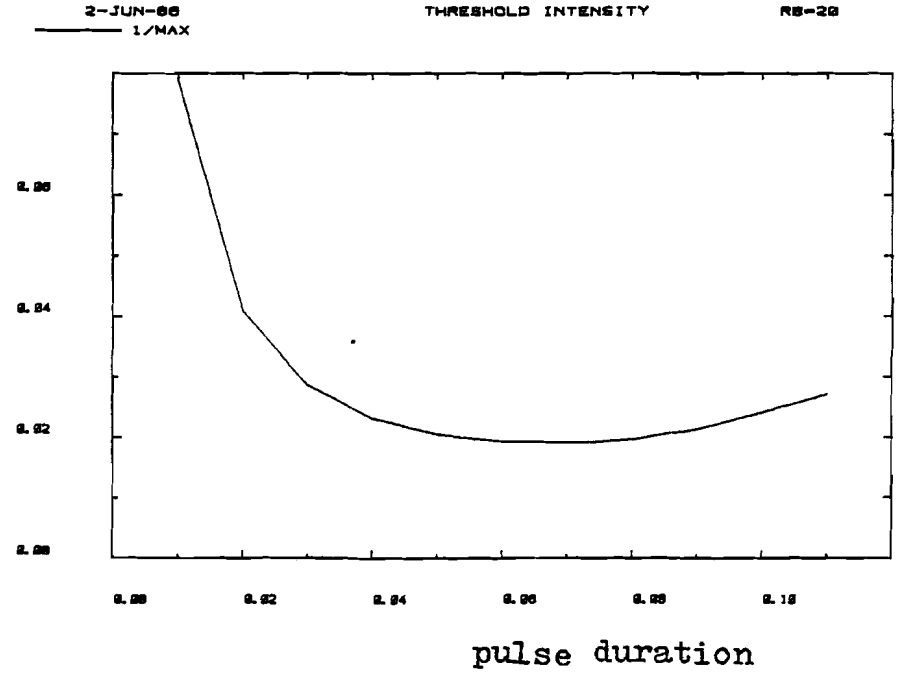

Figure 10.-9c

For greater pulse duration the two transient of the two flanks of the pulse don't influence each other thus the maximum is constant

(the maximum is then the maximum of the first flank or the second flank). Thus the curve is horizontal for larger pulse durations. The negative phase is deeper for increasing stimulus diameter, but longer for smaller stimulus diameter.

Comparison of figure 10.-9 and figure 3.-5 shows that the shapes of both curves are alike. The negative phase of these curves is longer and less deep for larger stimulus diameter. The negative phase of the simulation also has a minimum for a certain stimulus diameter just as the data.

In figure 10.-10 the critical duration T_c is plotted against the stimulus disk diameter ($R_{st} = R_b$). The input signal is a pulse in the time domain.

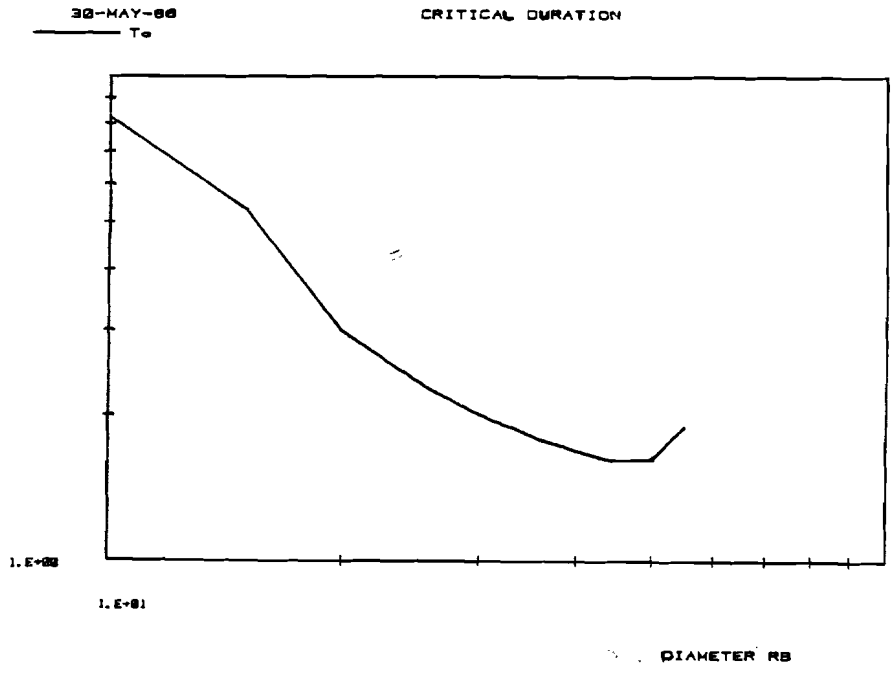

Figure 10.-10

The curve decreases for larger stimulus disk diameter. After R_{st} ($=R_b$) =50 this curve starts to increase. The number of samples is small here, this is due to the long computing time.

When we compare this curve with the data in figure 3.-5 (lower curve), we see that both curves decrease and start to increase for a certain value of the stimulus disk diameter. The range of the stimulus disk diameter of the simulation is smaller than of the data.

In figure 10.-11 the maximum of the pulse response is plotted against the stimulus disk diameter ($R_{st} = R_b$) with a pulse duration of θ =0.11s.
The curve increases by small disk diameter. After R_{st} =15 the

curve varies only in a small interval. The number of samples is here also small (11 samples) due to the long computing time.

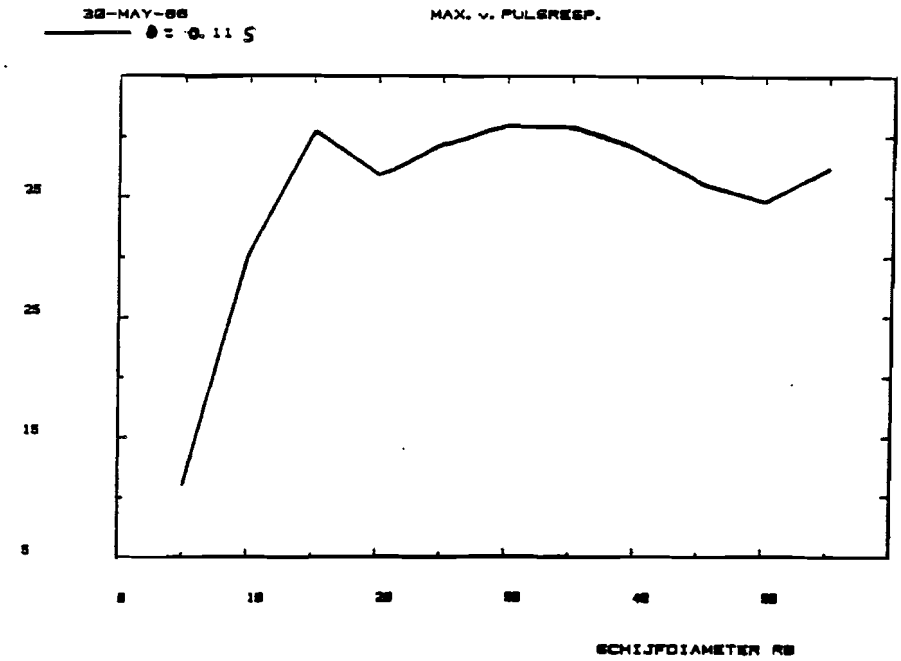

Figure 10.-11

The curve of the maximum of the pulse response as a function of the stimulus disk diameter in figure 10.-11 increases faster than the lower curve of figure 3.-3. The parameter of both curves is the long pulse duration θ , thus at the horizontal line of the curves from figures 3.-5 and 10.-9.

Chapter 11: Conclusions and recommendations

In this report a model for the transient channel of the human visual system is considered. This model consists of two parts: a spatio-temporal plus a temporal filter. The model is based on several assumptions concerning the fovea: linearity, place- and time-invariancy, and rotation symmetry.

For the spatio-temporal filter the class of (two-dimensional) passsive transmission lines of low order is investigated. One type of transmission line was chosen on the ground of quantitative similarities with the measured data.

The chosen transmission line, called the lateral membrane, and the temporal filter can be parametrized on the basis of parameter estimation programs of two sets of temporal impulse responses for different spatial disk diameter (see chapter 4).

The lateral membrane response, and the overall model response to various stimuli, is simulated on a computer. The simulations show that the essential properties of the model agree with the measured data, for stimuli, that are not too large spatially.

Only measurement data of different sources (i.e. different subjects and/or different background levels) are available. Therefore a really quantative test cannot be performed with this model at this moment.

A more general approach (by a more general formula like formula (4.-1)) to the transmission line than the one suggested in chapter 6, might add some degree of freedom to the lateral membrane.

Temporal filters, other than the one chosen have to be investigated; for example a second order temporal filter.

The model gives good results for a limited area ($R_{st} \leq 50$) of the disk diameter R_{st}. We can enlarge this area by adding more Bessel functions in the summation (the stimulus disk is approximated by a summation of Bessel functions). This leads to more calculation time for the computer. It has to be investigated whether this truncation leads to significant errors.
Or we can define that the stimulus is only valid within this area and let the stimulus with larger disk diameter R_{st} also fall within the area. This we can examine with further research with the aid of this model of case II.

Literature:

Aalst, Th.J.P.van, (1981).
A qualitative analysis of a network as a perceptive model of the retina. (in Dutch)
IPO-report no.395.

Blommaert, F.J.J., J.A.J.Roufs and A.C.den Brinker, (1986).
Experimentally determined impulse responses and predictions of thresholds and latency.
To be published.

Boersma, J., (1981).
Applied analysis I. (in Dutch)
Syllabus THE no.2.208.

Brinker, A.C.den, (1985A).
Matched- and pseudo-matched filter approximations of psycho-physical measurement data. (in Dutch)
Internal report THE, ER-1985/03.

Brinker, A.C.den, (1985B).
Two models for the transient system of the spatio-temporal visual perception. (in Dutch)
Internal report THE, ER-1985/04.

Brinker, A.C.den , (1985C).
Matched- and pseudo matched filter approximations of psycho-psysical measurement data. A supplement. (in Dutch)
IPO report no.511.

Brinker, A.C.den and Th.J.P.van Aalst, (1984).
A model of the transient part of the spatio-temporal visual perception, containing a two-dimensional transmission line. (in Dutch)
Internal report THE, ER-1984/02.

Eykhoff, P., (1976).
Control-systems I. (in Dutch)
Syllabus THE no.5.005.

Heynen, H.G.M., (1980).
The pointspreadfunction as basis for a qualitative model for the prediction of the detection thresholds of quasi-static visual details. (in Dutch)
IPO report no. 387.

Koenderink, J.J. and A.J. van Doorn, (1978).
Visual detection of spatial contrast; influence of location in the visual field, target extent and illuminance level.
Biol. Cybernetics 30, pp.157-167.

Oberhettinger, F.
Tables of Bessel transforms.
Berlin: Springer-Verlag.

Papoulis, A., (1968).
Systems and transforms with application in optics.
New York: Mcgraw-Hill.

Roufs, J.A.J. and F.J.J.Blommaert, (1981).
Temporal impulse and step responses of the human eye obtained psycho-physically by means of a drift-correcting perturbation technique.
Vision Research Vol.21, pp.1203-1221.

Roufs, J.A.J. and H.Bouma, (1980).
Towards linking perception research and image quality.
Proceeding of the SID Vol.21/3, pp.247-270.
Roufs, J.A.J. and Duifhuis, (1984).
Light and sound. (in Dutch)
Syllabus THE no.1.148.
Roufs, J.A.J. and H.J.Meulenbrugge, (1967).
The quantitative relation between flash threshold and the ficker-fusion boundary for centrally fixated fields.
IPO Annual Progress Report no.2, pp.133-139.
Roufs, J.A.J., H.A.L.Piceni and J.A.Pellegrino van Stuyvenberg, (1984).
Phase and gain analysis of the visual transient system.
IPO Annual Progress Report no.19, pp.49-56.
Wilson, H.R. and J.R.Bergen, (1979).
A four mechanism model for threshold spatial vision.
Vision Res. 19, pp.19-32.

Appendix 1: Examined models for the transmission line

Case I

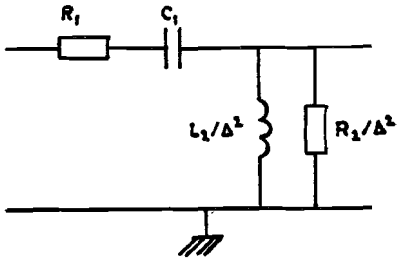

$$Z_1(s) = \frac{1+sR_1C_1}{sC_1}$$

$$Z_2(s) = \frac{sR_2L_2}{R_2+sL_2}$$

Figure A1.-1.

$$\text{Transfer function: } H_1(w,s) = \frac{sR_2L_2\{1+sC_1R_1\}}{\{R_1C_1+C_1R_2w^2\}L_2s^2+\{L_2+R_1R_2C_1\}s+R_2}$$

$$\text{Zeroes: } z_2 = 0 \;;\; z_1 = -\frac{1}{R_1C_1}$$

$$\text{Poles: } p_{1,2} = \frac{-\{L_2+R_1R_2C_1\} \pm \sqrt{\{L_2+R_1R_2C_1\}^2 - 4R_2C_1L_2\{R_1+R_2w^2\}}}{2C_1L_2\{R_1+R_2w^2\}}$$

$$\text{Special cases: } w = 0\text{: } p_1 = -\frac{1}{R_1C_1} \;;\; p_2 = -\frac{R_2}{L_2}$$

$$w \to \infty\text{: } p_1 = 0 \;;\; p_2 = 0$$

$$\text{Breakawaypoints: } \sigma_1 = 0 \text{ and } \sigma_2 = -\frac{2R_2}{L_2+R_1R_2C_1}$$

$$\text{Circle: } \omega^2 + \left\{\sigma + \frac{R_2}{L_2+R_1R_2C_1}\right\}^2 = \left\{\frac{R_2}{L_2+R_1R_2C_1}\right\}^2$$

$$\text{Centre: } \left(-\frac{R_2}{L_2+R_1R_2C_1}, 0\right) \qquad \text{radius: } \frac{R_2}{L_2+R_1R_2C_1}$$

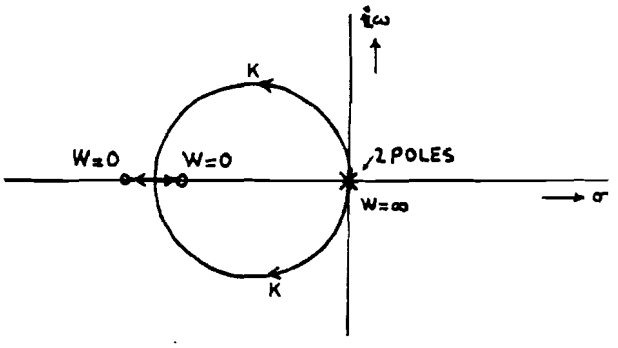

Figure A1.-2.

Case II

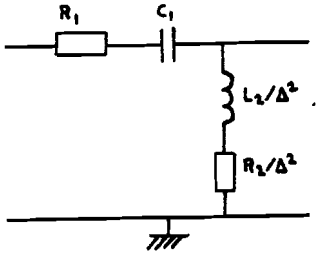

$$Z_1(s) = \frac{1+sR_1C_1}{sC_1}$$

$$Z_2(s) = R_2+sL_2$$

Figure A1.-3.

Transfer function: $$H_1(w,s) = \frac{\{1+sC_1R_1\}\{R_2+sL_2\}}{L_2C_1w^2s^2+\{R_1+R_2w^2\}C_1s+1}$$

Zeroes: $$z_1 = -\frac{1}{R_1C_1} \quad ; \quad z_2 = -\frac{R_2}{L_2}$$

Poles: $$p_{1,2} = \frac{-\{R_1+R_2w^2\}C_1 \pm \sqrt{\{R_1+R_2w^2\}^2C_1^2-4L_2C_1w^2}}{2L_2C_1w^2}$$

Special cases: $w = 0$: $p_1 = -\frac{1}{R_1C_1}$; $p_2 = -\infty$

$w \to \infty$: $p_1 = 0$; $p_2 = -\frac{R_2}{L_2}$

Breakawaypoints: $$\sigma_{1,2} = -\frac{1}{R_1C_1} \pm \sqrt{\frac{1}{R_1C_1}\left\{\frac{1}{R_1C_1}-\frac{R_2}{L_2}\right\}}$$

Circle: $$\omega^2+\left\{\sigma+\frac{1}{R_1C_1}\right\}^2 = \left\{\frac{1}{R_1C_1}-\frac{R_2}{L_2}\right\}\frac{1}{R_1C_1}$$

Centre: $\left(-\frac{1}{R_1C_1}, 0\right)$ radius: $\sqrt{\frac{1}{R_1C_1}\left\{\frac{1}{R_1C_1}-\frac{R_2}{L_2}\right\}}$

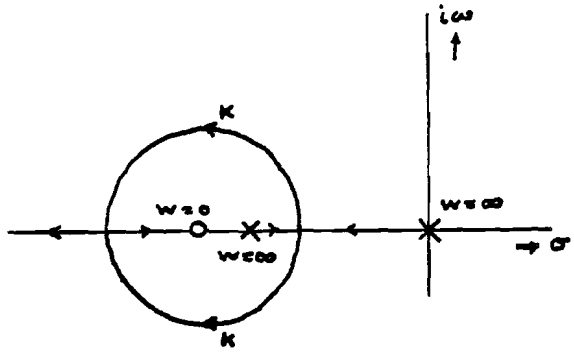

Figure A1.-4. $\frac{1}{R_1 C_1} > \frac{R_2}{L_2}$

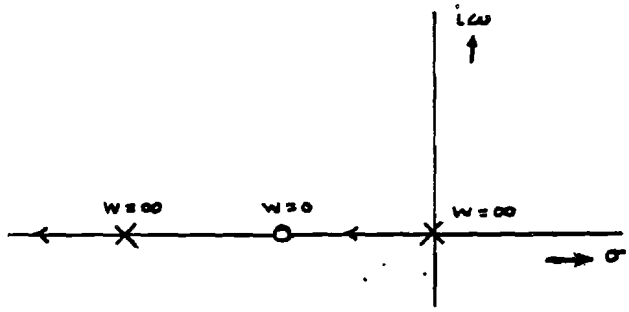

Figure A1.-5. $\frac{1}{R_1 C_1} \leq \frac{R_2}{L_2}$

Case III

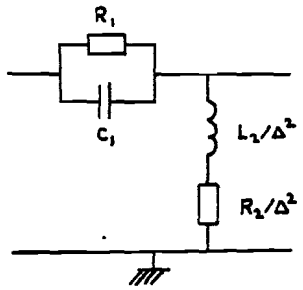

$$Z_1(s) = \frac{R_1}{1+sR_1C_1}$$

$$Z_2(s) = R_2+sL_2$$

Figure A1.-6.

Transfer function: $H_1(w,s) = \frac{R_1\{R_2+sL_2\}}{R_1C_1L_2w^2s^2+\{L_2+R_1R_2C_1\}w^2s+R_2w^2+R_1}$

Zeroes: $z_1 = \infty$; $z_2 = -\frac{R_2}{L_2}$

$$\text{Poles: } p_{1,2} = \frac{-\{R_1 R_2 C_1 + L_2\}w^2 \pm \sqrt{\{R_1 R_2 C_1 + L_2\}^2 w^4 - 4R_1 C_1 L_2 w^2 \{R_2 w^2 + R_1\}}}{2C_1 R_1 L_2 w^2}$$

$$\text{Special cases: } w = 0: \; p_1 = \left\{ -\frac{R_1 R_2 C_1 + L_2}{2R_1 C_1 L_2} \pm i\infty \right\}$$

$$w \to \infty: \; p_1 = -\frac{1}{R_1 C_1} \; ; \; p_2 = -\frac{R_2}{L_2}$$

$$\text{Breakawaypoints: } \sigma = -\frac{1}{2}\left\{ \frac{R_2}{L_2} + \frac{1}{R_1 C_1} \right\}$$

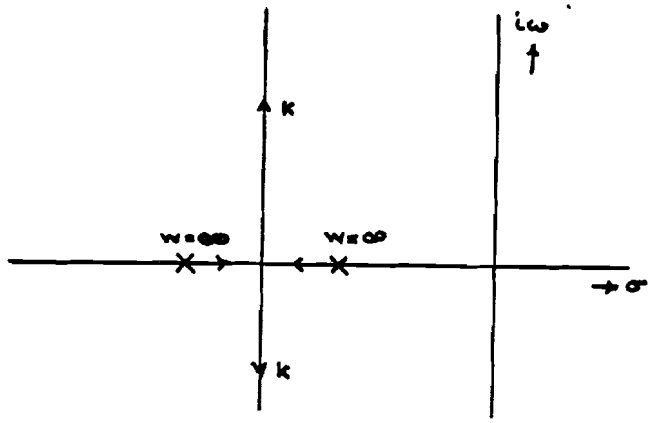

Figure A1.-7.

Case IV

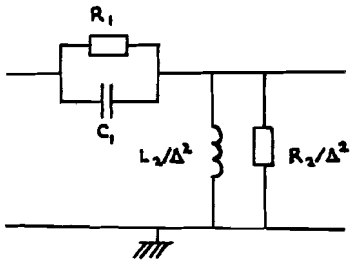

$$Z_1(s) = \frac{R_1}{1 + sR_1 C_1}$$

$$Z_2(s) = \frac{sR_2 L_2}{R_2 + sL_2}$$

Figure A1.-8.

$$\text{Transfer function: } H_1(w,s) = \frac{R_1 R_2 L_2 s}{R_1 R_2 C_1 L_2 w^2 s^2 + \{R_2 w^2 + R_1\}L_2 s + R_1 R_2}$$

Zeroes: $z = 0$; $z = \infty$

$$\text{Poles: } p_{1,2} = \frac{-\{R_2 w^2 + R_1\}L_2 \pm \sqrt{L_2^2 \{R_2 w^2 + R_1\}^2 - 4R_1^2 R_2^2 C_1 L_2 w^2}}{2R_1 R_2 C_1 L_2 w^2}$$

Special cases: $w = 0$: $p_1 = -\infty$; $p_2 = -\frac{R_2}{L_2}$

$w \to \infty$: $p_1 = -\frac{1}{R_1 C_1}$; $p_2 = 0$

Breakawaypoints: $\sigma_{1,2} = -\frac{R_2}{L_2} \pm \sqrt{\frac{R_2}{L_2}\left\{\frac{R_2}{L_2} - \frac{1}{R_1 C_1}\right\}}$

Circle: $\omega^2 + \left\{\sigma + \frac{R_2}{L_2}\right\}^2 = \frac{R_2}{L_2}\left\{\frac{R_2}{L_2} - \frac{1}{R_1 C_1}\right\}$

Centre: $\left(-\frac{R_2}{L_2}, 0\right)$ radius: $\sqrt{\frac{R_2}{L_2}\left\{\frac{R_2}{L_2} - \frac{1}{R_1 C_1}\right\}}$

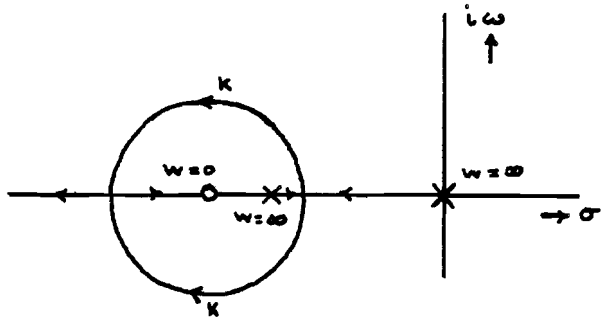

Figure A1.-9. $\frac{R_2}{L_2} > \frac{1}{R_1 C_1}$

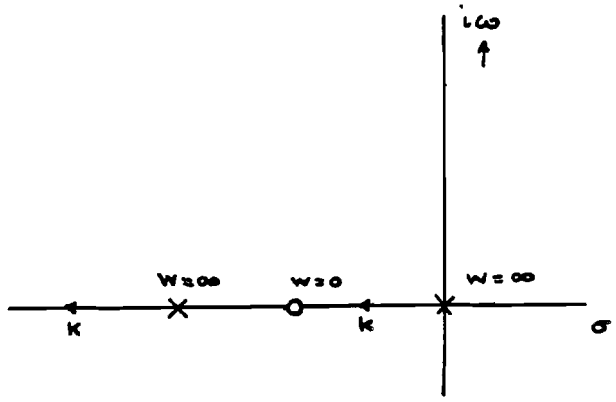

Figure A1.-10. $\frac{R_2}{L_2} \leq \frac{1}{R_1 C_1}$

Case V

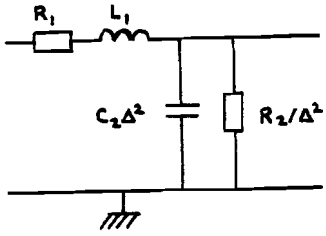

$$Z_1(s) = R_1 + sL_1$$

$$Z_2(s) = \frac{R_2}{1+sR_2C_2}$$

Figure A1.-11.

Transfer function: $$H_f(w,s) = \frac{R_2\{R_1+sL_1\}}{R_2C_2L_1s^2+\{R_1R_2C_2+L_1\}s+R_1+R_2w^2}$$

Zeroes: $$z_1 = -\frac{R_1}{L_1} \; ; \; z_2 = \infty$$

Poles: $$p_{1,2} = \frac{-\{R_1R_2C_2+L_1\} \pm \sqrt{\{R_1R_2C_2+L_1\}^2 - 4R_2C_2L_1\{R_1+R_2w^2\}}}{2R_2C_2L_1}$$

Special cases: $w = 0$: $$p_1 = -\frac{R_1}{L_1} \; ; \; p_2 = -\frac{1}{R_2C_2}$$

$$w \to \infty: \; p_{1,2} = \left[-\frac{1}{2}\left\{\frac{R_1}{L_1}+\frac{1}{R_2C_2}\right\} \pm i\,\infty\right]$$

Breakawaypoints: $$\sigma = -\frac{1}{2}\left\{\frac{R_1}{L_1}+\frac{1}{R_2C_2}\right\}$$

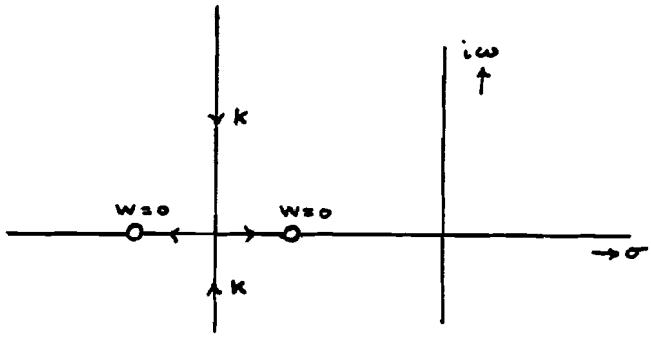

Figure A1.-12.

Case VI

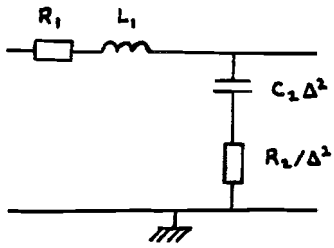

$$Z_1(s) = R_1 + sL_1$$

$$Z_2(s) = \frac{1+sR_2C_2}{sC_2}$$

Figure A1.-13.

$$\text{Transfer function: } H_1(w,s) = \frac{\{R_1+sL_1\}\{1+sR_2C_2\}}{L_1C_2s^2+\{R_1+R_2w^2\}C_2s+w^2}$$

$$\text{Zeroes: } z_1 = -\frac{R_1}{L_1} \; ; \; z_2 = -\frac{1}{R_2C_2}$$

$$\text{Poles: } p_{1,2} = \frac{-\{R_1+R_2w^2\}C_2 \pm \sqrt{\{R_1+R_2w^2\}^2C_2^2 - 4L_1C_2w^2}}{2L_1C_2}$$

$$\text{Special cases: } w = 0\text{: } p_1 = -\frac{R_1}{L_1} \; ; \; p_2 = 0$$

$$w \to \infty\text{: } p_1 = -\infty \; ; \; p_2 = -\frac{1}{R_2C_2}$$

$$\text{Breakawaypoints: } \sigma_{1,2} = -\frac{1}{R_2C_2} \pm \sqrt{\frac{1}{R_2C_2}\left\{\frac{1}{R_2C_2} - \frac{R_1}{L_1}\right\}}$$

$$\text{Circle: } \omega^2 + \left\{\sigma + \frac{1}{R_2C_2}\right\}^2 = \frac{1}{R_2C_2}\left\{\frac{1}{R_2C_2} - \frac{R_1}{L_1}\right\}$$

$$\text{Centre: } \left(-\frac{1}{R_2C_2}, 0\right) \text{ radius: } \sqrt{\frac{1}{R_2C_2}\left\{\frac{1}{R_2C_2} - \frac{R_1}{L_1}\right\}}$$

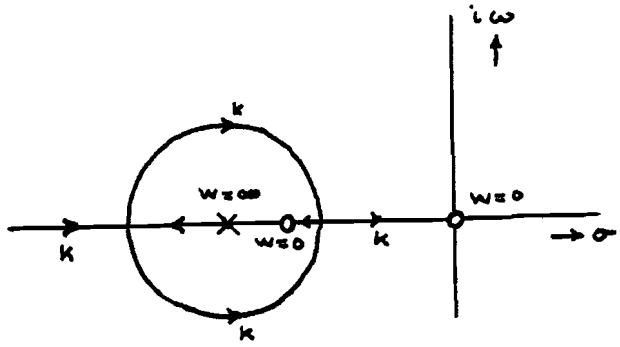

Figure A1.-14. $\frac{1}{R_2 C_2} > \frac{R_1}{L_1}$

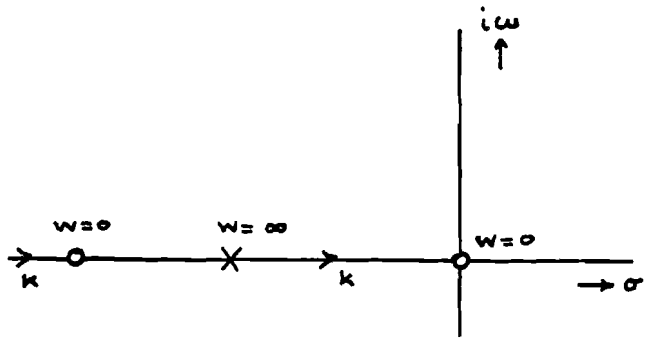

Figure A1.-15. $\frac{1}{R_2 C_2} \leq \frac{R_1}{L_1}$

Case VII

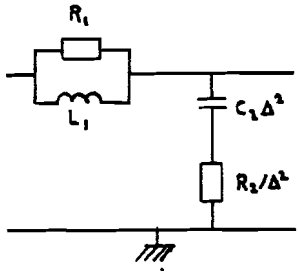

$$Z_1(s) = \frac{sR_1L_1}{R_1+sL_1}$$

$$Z_2(s) = \frac{1+sR_2C_2}{sC_2}$$

Figure A1.-16.

Transfer function: $H_1(w,s) = \dfrac{R_1L_1s\{1+sR_2C_2\}}{\{R_1+R_2w^2\}L_1C_2s^2+\{R_1R_2C_2+L_1\}w^2s+R_1w^2}$

Zeroes: $z_1 = 0$; $z_2 = -\dfrac{1}{R_2C_2}$

$$\text{Poles: } p_{1,2} = \frac{-\{L_1+R_1R_2C_2\}w^2 \pm \sqrt{\{L_1+R_1R_2C_2\}^2 w^4 - 4w^2 R_1 L_1 C_2\{R_1+R_2w^2\}}}{2L_1C_2\{R_1+R_2w^2\}}$$

Special cases: $w = 0$: $p_1 = 0$; $p_2 = 0$

$$w \to \infty\text{: } p_1 = -\frac{R_1}{L_1} \text{ ; } p_2 = -\frac{1}{R_2C_2}$$

Breakawaypoints: $\sigma_1 = 0$ and $\sigma_2 = -\frac{2}{R_2C_2+L_1/R_1}$

Circle: $\omega^2 + \left\{\sigma + \frac{1}{R_2C_2+L_1/R_1}\right\}^2 = \left\{\frac{1}{R_2C_2+L_1/R_1}\right\}^2$

Centre: $\left(-\frac{1}{R_2C_2+L_1/R_1}, 0\right)$ radius: $\frac{1}{R_2C_2+L_1/R_1}$

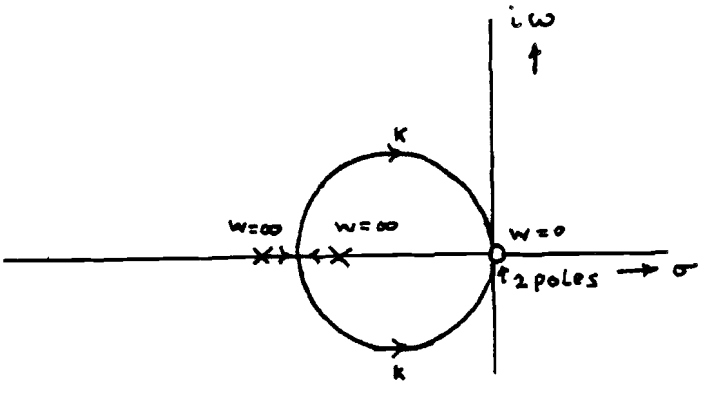

Figure A1.-17.

Case VIII

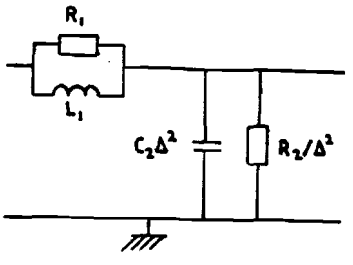

$$Z_1(s) = \frac{sR_1L_1}{R_1+sL_1}$$

$$Z_2(s) = \frac{R_2}{1+sR_2C_2}$$

Figure A1.-18.

$$\text{Transfer function: } H_1(w,s) = \frac{sR_1R_2L_1}{R_1R_2L_1C_2s^2+\{R_1+R_2w^2\}L_1s+R_1R_2w^2}$$

Zeroes: $z_1 = 0$; $z_2 = \infty$

$$\text{Poles: } p_{1,2} = \frac{-\{R_1+R_2w^2\}L_1 \pm \sqrt{\{R_1+R_2w^2\}^2L_1^2 - 4R_1^2R_2^2L_1C_2w^2}}{2R_1R_2L_1C_2}$$

Special cases: $w = 0$: $p_1 = 0$; $p_2 = -\dfrac{1}{R_2 C_2}$

$w \to \infty$: $p_1 = -\dfrac{R_1}{L_1}$; $p_2 = -\infty$

Breakawaypoints: $\sigma_{1,2} = -\dfrac{R_1}{L_1} \pm \sqrt{\left\{\dfrac{R_1}{L_1} - \dfrac{1}{R_2 C_2}\right\}\dfrac{R_1}{L_1}}$

Circle: $\omega^2 + \left\{\sigma + \dfrac{R_1}{L_1}\right\}^2 = \left\{\dfrac{R_1}{L_1} - \dfrac{1}{R_2 C_2}\right\}\dfrac{R_1}{L_1}$

Centre: $\left(-\dfrac{R_1}{L_1}\ ,\ 0\right)$ radius: $\sqrt{\dfrac{R_1}{L_1}\left\{\dfrac{R_1}{L_1} - \dfrac{1}{R_2 C_2}\right\}}$

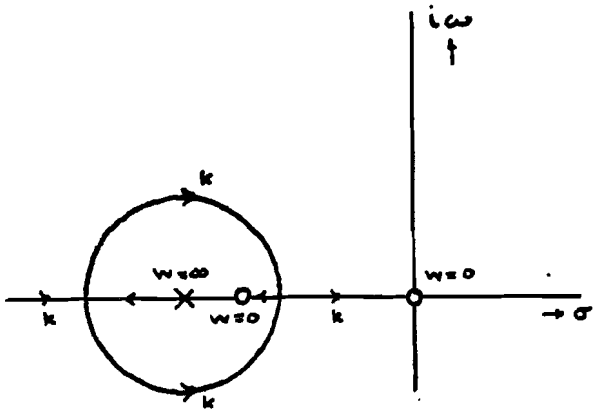

Figure A1.-19. $\dfrac{R_1}{L_1} > \dfrac{1}{R_2 C_2}$

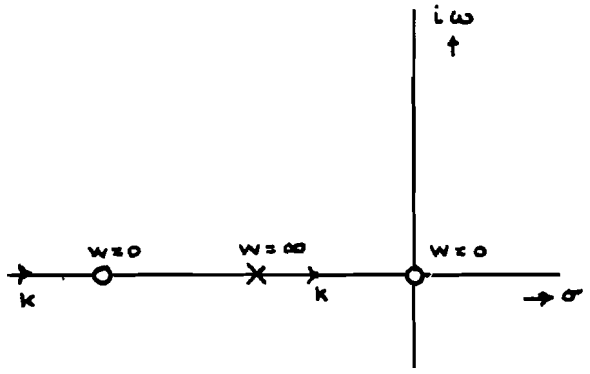

Figure A1.-20. $\dfrac{R_1}{L_1} \leqslant \dfrac{1}{R_2 C_2}$

Case IX

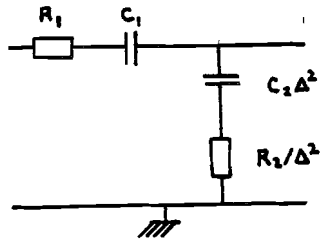

$$Z_1(s) = \frac{1+sR_1C_1}{sC_1}$$

$$Z_2(s) = \frac{1+sR_2C_2}{sC_2}$$

Figure A1.-21.

Transfer function: $H_1(w,s) = \dfrac{\{1+sR_1C_1\}\{1+sR_2C_2\}}{\{R_1+R_2w^2\}C_1C_2s^2+\{C_2+C_1w^2\}s}$

Zeroes: $z_1 = -\dfrac{1}{R_1C_1}$; $z_2 = -\dfrac{1}{R_2C_2}$

Poles: $p_1 = 0$

$$p_2 = -\frac{C_2+C_1w^2}{\{R_1+R_2w^2\}C_1C_2}$$

Special cases: $w = 0$: $p_1 = -\dfrac{1}{R_1C_1}$; $p_2 = 0$

$w \to \infty$: $p_1 = 0$; $p_2 = -\dfrac{1}{R_2C_2}$

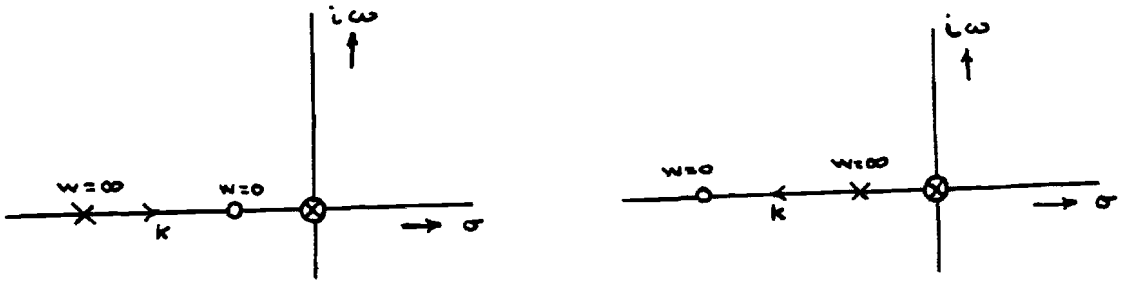

Figure A1.-22.

Case X

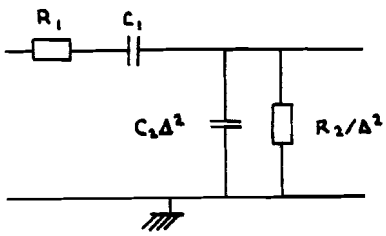

$$Z_1(s) = \frac{1+sR_1C_1}{sC_1}$$

$$Z_2(s) = \frac{R_2}{1+sR_2C_2}$$

Figure A1.-23.

Transfer function:

$$H_1(w,s) = \frac{R_2\{1+sR_1C_1\}}{R_1R_2C_1C_2s^2+\{R_1C_1+R_2C_2+R_1C_2w^2\}s+1}$$

Zeroes: $z_1 = -\frac{1}{R_1C_1}$; $z_2 = \infty$

Poles:

$$p_{1,2} = \frac{-\{R_1C_1+R_2C_2+R_2C_1w^2\} \pm \sqrt{\{R_1C_1+R_2C_2+R_2C_1w^2\}^2-4R_1R_2C_1C_2}}{2R_1R_2C_1C_2}$$

Special cases: $w = 0$: $p_1 = -\frac{1}{R_1C_1}$; $p_2 = -\frac{1}{R_2C_2}$

$w \to \infty$: $p_1 = 0$; $p_2 = -\infty$

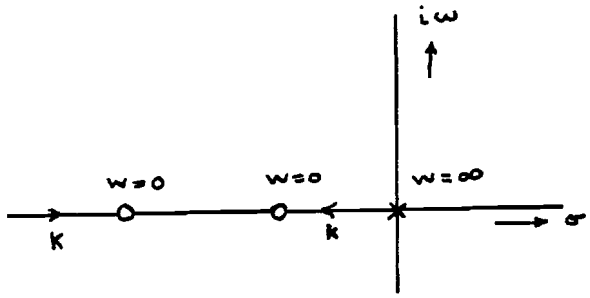

Figure A1.-24.

Case XI

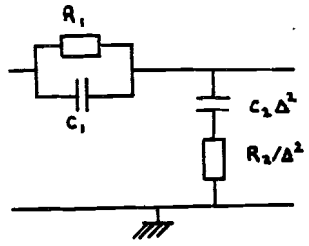

$$Z_1(s) = \frac{R_1}{1+sR_1C_1}$$

$$Z_2(s) = \frac{1+sR_2C_2}{sC_2}$$

Figure A1.-25.

Transfer function:

$$H_1(w,s) = \frac{R_1\{1+sR_2C_2\}}{R_1R_2C_1C_2w^2s^2+\{R_1C_2+R_1C_1w^2+R_2C_2w^2\}s+w^2}$$

Zeroes: $z_1 = \infty \quad ; \quad z_2 = -\frac{1}{R_2C_2}$

Poles: $p_{1,2} =$

$$= \frac{-\{R_1C_2+R_1C_1w^2+R_2C_2w^2\} \pm \sqrt{\{R_1C_2+R_1C_1w^2+R_2C_2w^2\}^2-4w^4R_1R_2C_1C_2}}{2w^2R_1R_2C_1C_2}$$

Special cases: $w = 0$: $p_1 = 0 \quad ; \quad p_2 = -\infty$

$w \to \infty$: $p_1 = -\frac{1}{R_1C_1} \quad ; \quad p_2 = -\frac{1}{R_2C_2}$

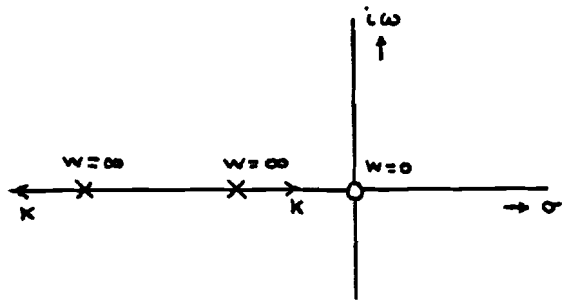

Figure A1.-26.

Case XII

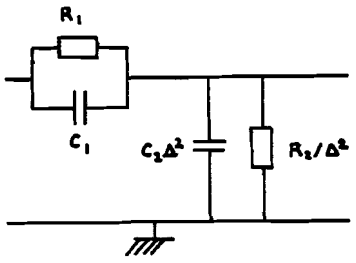

$$Z_1(s) = \frac{R_1}{1+sR_1C_1}$$

$$Z_2(s) = \frac{R_2}{1+sR_2C_2}$$

Figure A1.-27.

Transfer function: $H_1(w,s) = \dfrac{R_1R_2}{\{C_2+C_1w^2\}R_1R_2s+R_1+R_2w^2}$

Zeroes: $z = \infty \;;\; z = \infty$

Poles: $p_1 = -\infty$

$$p_2 = -\frac{R_1+R_2w^2}{\{C_2+C_1w^2\}R_1R_2}$$

Special cases: $w = 0$: $p_1 = -\infty \;;\; p_2 = -\dfrac{1}{R_2C_2}$

$w \to \infty$: $p_1 = -\infty \;;\; p_2 = -\dfrac{1}{R_1C_1}$

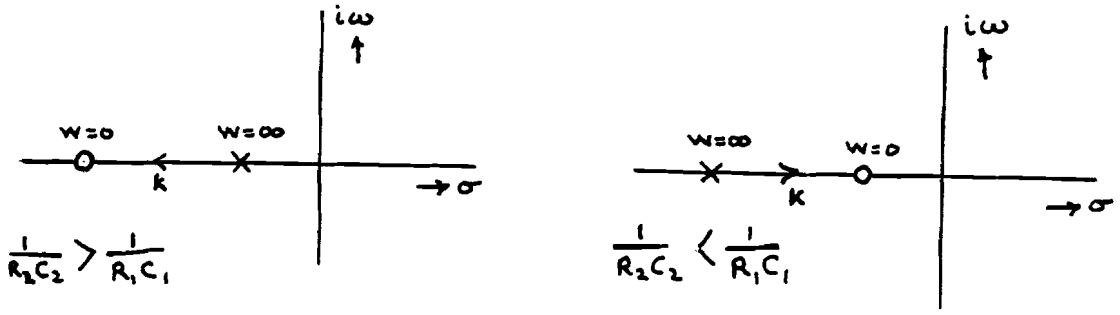

Figure A1.-28.

Case XIII

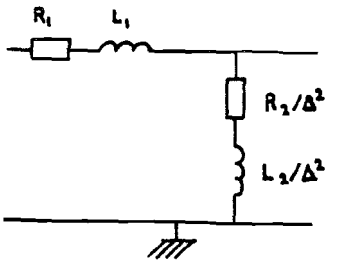

$$Z_1(s) = R_1 + sL_1$$

$$Z_2(s) = R_2 + sL_2$$

Figure A1.-29.

Transfer function: $$H_1(w,s) = \frac{\{R_1+sL_1\}\{R_2+sL_2\}}{\{L_1+L_2w^2\}s+\{R_1+R_2w^2\}}$$

Zeroes: $$z_1 = -\frac{R_1}{L_1} \; ; \; z_2 = -\frac{R_2}{L_2}$$

Poles: $$p_1 = -\infty$$

$$p_2 = -\frac{R_1+R_2w^2}{L_1+L_2w^2}$$

Special cases: $w = 0$: $p_1 = -\infty$; $p_2 = -\frac{R_1}{L_1}$

$w \to \infty$: $p_1 = -\infty$; $p_2 = -\frac{R_2}{L_2}$

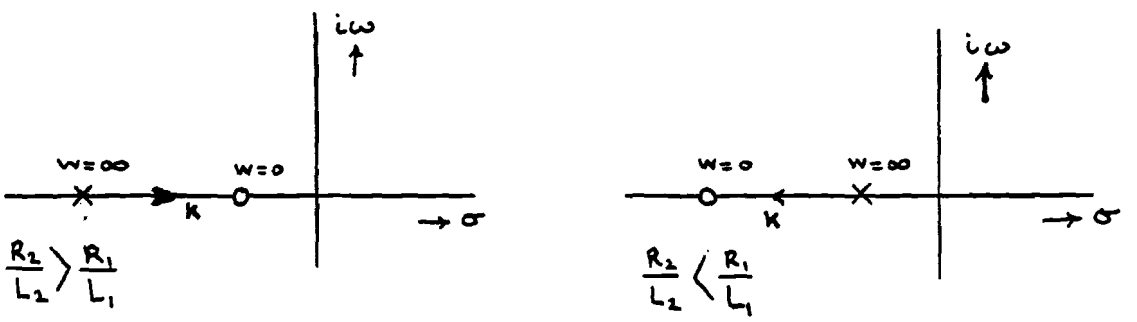

Figure A1.-30.

Case XIV

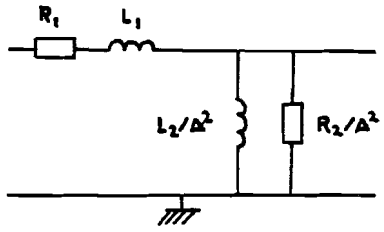

$$Z_1(s) = R_1 + sL_1$$

$$Z_2(s) = \frac{sR_2L_2}{R_2 + sL_2}$$

Figure A1.-31.

Tranfer function:

$$H_1(w,s) = \frac{sR_2L_2\{R_1 + sL_1\}}{L_1L_2s^2 + \{R_1L_2 + R_2L_1 + R_2L_2w^2\}s + R_1R_2}$$

Zeroes: $z_1 = 0$; $z_2 = -\frac{R_1}{L_1}$

Poles:

$$p_{1,2} = \frac{-\{R_1L_2 + R_2L_1 + R_2L_2w^2\} \pm \sqrt{\{R_1L_2 + R_2L_1 + R_2L_2w^2\}^2 - 4R_1R_2L_1L_2}}{2L_1L_2}$$

Special cases: $w = 0$: $p_1 = -\frac{R_1}{L_1}$; $p_2 = -\frac{R_2}{L_2}$

$w \to \infty$: $p_1 = -\infty$; $p_2 = 0$

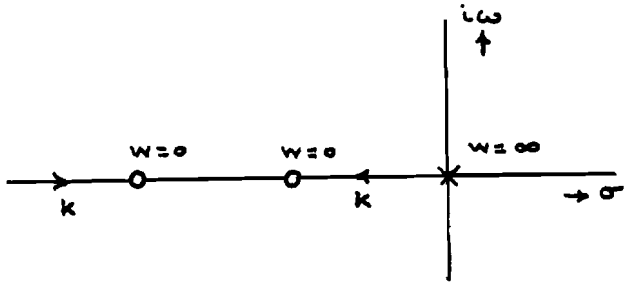

Figure A1.-32.

Case XV

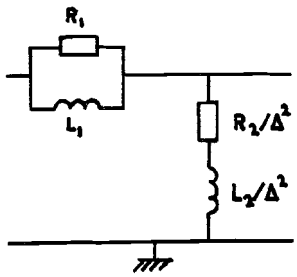

$$Z_1(s) = \frac{sR_1L_1}{R + sL}$$

$$Z_2(s) = R_2 + sL_2$$

Figure A1.-33.

Transfer function:

$$H_1(w,s) = \frac{sR_1L_1\{R_2+sL_2\}}{L_1L_2w^2s^2+\{R_1L_1+R_2L_1w^2+R_1L_2w^2\}s+R_1R_2w^2}$$

Zeroes: $z_1 = 0$; $z_2 = -\frac{R_2}{L_2}$

Poles: $p_{1,2} =$

$$= \frac{-\{R_1L_1+R_2L_1w^2+R_1L_2w^2\} \pm \sqrt{\{R_1L_1+R_2L_1w^2+R_1L_2w^2\}^2 - 4R_1R_2L_1L_2w^4}}{2w^2L_1L_2}$$

Special cases: $w = 0$: $p_1 = 0$; $p_2 = -\infty$

$w \to \infty$: $p_1 = -\frac{R_1}{L_1}$; $p_2 = -\frac{R_2}{L_2}$

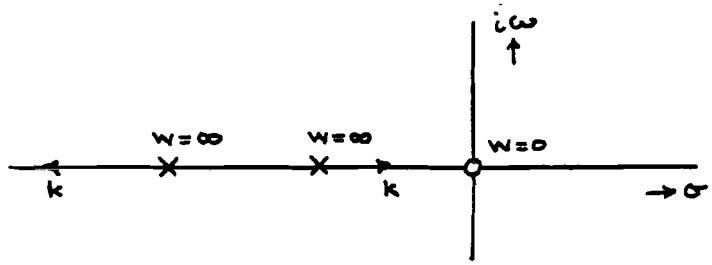

Figure A1.-34.

Case XVI

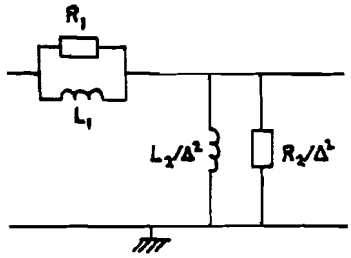

$$Z_1(s) = \frac{sR_1L_1}{R_1+sL_1}$$

$$Z_2(s) = \frac{sR_2L_2}{R_2+sL_2}$$

Figure A1.-35.

Transfer function:

$$H_1(w,s) = -\frac{R_1R_2L_1L_2s^2}{\{R_1+R_2w^2\}L_1L_2s^2+R_1R_2\{L_1+L_2w^2\}s}$$

Zeroes: $z_1 = 0$; $z_2 = 0$

Poles: $p_1 = 0$

$$p_2 = \left\{-\frac{R_1R_2\{L_1+L_2w^2\}}{L_1L_2\{R_1+R_2w^2\}}\right\}$$

Special cases: $w = 0$: $p_1 = 0$; $p_2 = -\frac{R_2}{L_2}$

$w \to \infty$: $p_1 = 0$; $p_2 = -\frac{R_1}{L_1}$

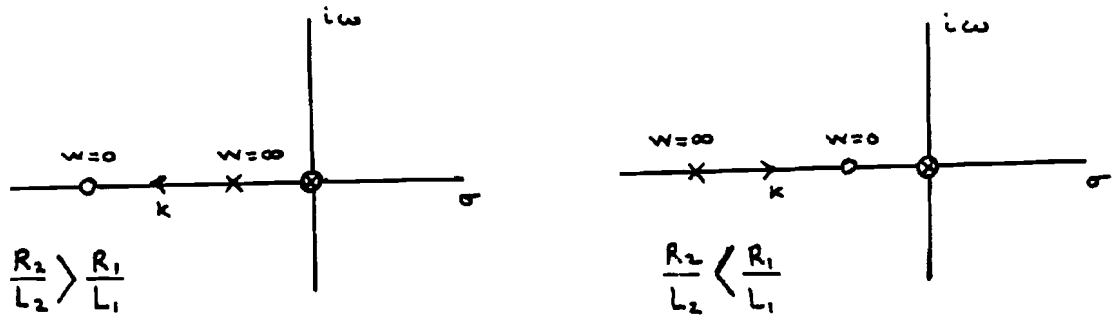

Figure A1.-36.

Appendix 2: Root-locus of the second order system

A characteristic equation of order two dependent on a continuous parameter function B(w) in the following way:

$$B(w)\{s^2 + Q_1 s + Q_0\} + s^2 + R_1 s + R_0 = 0 \qquad (A2.-1)$$

describes a piece of a circular curve in the s-plane for the complex solutions s.

The characteristic equation has complex pole pairs for those w-values with the discriminant D(w) smaller than zero:

$$D(w) = \{B(w)Q_1 + R_1\}^2 - 4\{B(w)Q_0 + R_0\}\{B(w) + 1\} < 0 \qquad (A2.-2)$$

The equation (A2.-1) can be split into its real and imaginary part for D(w)<0; we assume:

$$s_{1,2}(w) = x(w) + iy(w) \qquad (A2.-3)$$

Substitute (A.-3) in formula (A2.-1) and then the imaginary part of the equation is

$$2B(w)xy + B(w)Q_1 y + 2xy + R_1 y = 0 \qquad (A2.-4)$$

$$\text{or } x(w) = -\left\{\frac{R_1 + B(w)Q_1}{2(1 + B(w))}\right\} \qquad (A2.-5)$$

From this B(w) can expressed as a function of x

$$B(w) + 1 = \left\{\frac{Q_1 - R_1}{2x + Q_1}\right\} \qquad (A2.-6)$$

The real part of the equation (A2.-1) becomes:

$$B(w)\{x^2 - y^2 + Q_1 x + Q_0\} + \{x^2 - y^2 + R_1 x + R_0\} = 0 \qquad (A2.-7)$$

$$\text{or } \{B(w) + 1\}y^2 = \{B(w) + 1\}x^2 + \{B(w) + 1\}Q_1 x + (R_1 - Q_1)x + \{B(w) + 1\}Q_0 + R_0 - Q_0 \qquad (A2.-8)$$

Now substitute (A2.-6) in this equation and hereby eliminate B(w):

$$y^2 = x^2 + Q_1 x + \left\{\frac{R_1 - Q_1}{Q_1 - R_1}\right\}x(2x + Q_1) + Q_0 + \left\{\frac{R_0 - Q_0}{Q_1 - R_1}\right\}(2x + Q_1) \qquad (A2.-9)$$

$$y^2 = -\left\{x - \left\{\frac{R_0 - Q_0}{Q_1 - R_1}\right\}\right\}^2 + \left\{\frac{R_0 - Q_0}{Q_1 - R_1}\right\} + Q_1\left\{\frac{R_0 - Q_0}{Q_1 - R_1}\right\} + Q_0 \qquad (A2.-10)$$

substituting $a = -\left\{\frac{R_0 - Q_0}{Q_1 - R_1}\right\}$

$$R^2 = \left\{\frac{R_0 - Q_0}{Q_1 - R_1}\right\}^2 + Q_1\left\{\frac{R_0 - Q_0}{Q_1 - R_1}\right\} + Q_0$$

it is easy to see that (A2.-10) is the equation of a circle:

$y^2 + (x + a)^2 = R^2$

with centre $((-a,0) = (\left\{\frac{R_0 - Q_0}{Q_1 - R_1}\right\}, 0))$ and radius R.

Appendix 3: Computer-programs

```
c
      subroutine GEV(C,D,K)
c
c     Berekening van membraanparameters m.b.v. de elektrische
c     lange leidingparameters voor geval 2.
c
      double precision C(0:2),D(0:2),K
      double precision R1,R2,C1,L2,K1
      write(5,10)
10    format(2x,'Lees R1,R2,C1,L2 in.')
      read(6,20) R1,R2,C1,L2
20    format(4(d11.4))
      write(5,30)
30    format(2x,'Lees de extra versterkingsfactor K1 in.')
      read(6,40) K1
40    format(d11.4)
c
      K = R1*C1*L2*K1
      C(0) = 1
      D(0) = 0
      C(1) = R1*C1
      D(1) = R2*C1
      C(2) = 0
      D(2) = L2*C1
      return
      end


c
      subroutine match(deltat,NT,f2)
c
c     filter achter membraan
c
      integer I,NT
      double precision K,b2,wn,pe,t,deltat,pi,f2(0:NT)
      pi = 3.1416
      K = 10
      b2 = 17
      wn = 80.57
      pe = 2*pi/wn
c
      do 10 I=0,NT
      t = I*deltat
      if (t.gt.pe) go to 100
      f2(I) = -K*dexp(b2*t)*dsin(wn*t)
10    continue
100   return
      end
```

```
c
      subroutine IMPRES(A,K,deltat,N,h)
c
c     Bepaling van de impulsresponsie bij filter met
c     H(s)=K/(A0+A1*s+A2*s**2) op tijdstip t.
c
      integer I,N
      double precision A(0:2),h(0:N),K,deltat
      double precision p1,p2,ALFA,wn,DISCR,t
c
c     Bepaling van de discriminant.
c
      DISCR = A(1)**2-4*A(2)*A(0)
      if (DISCR) 10,50,100
c
c     Complex poolpaar (DISCR<0)
c
10    ALFA = A(1)/(2*A(2))
      wn = dsqrt(-DISCR)/(2*A(2))
      do 20 I=0,N
      t = I*deltat
      h(I) = K*dexp(-ALFA*t)*dsin(wn*t)/(wn*A(2))
20    continue
      go to 200
c
c     Twee samenvallende polen (DISCR=0)
c
50    ALFA = A(1)/(2*A(2))
      do 60 I=0,N
      t= I*deltat
      h(I) = K*t*dexp(-ALFA*t)/A(2)
60    continue
      go to 200
c
c     Twee enkelvoudige reele polen (DISCR>0)
c
100   p1 = (A(1)+dsqrt(DISCR))/(2*A(2))
      p2 = (A(1)-dsqrt(DISCR))/(2*A(2))
      do 110 I=0,N
      t =I*deltat
      h(I) = K*(dexp(-p2*t)-dexp(-p1*t))/(A(2)*(p1-p2))
110   continue
200   return
      end
```

```
c
      subroutine imres(C,D,K,W,deltat,NT,h)
c
c     Bepaling h(W,t) impulsresponsie op Besselfunctie van
c     spatiale frequentie W.
c     Gebruikmaking van subroutine IMPRES.FOR
c
      integer I,NT
      double precision C(0:2),D(0:2),K,deltat,W
      double precision h(0:NT),A(0:2)
c
      do 10 I=0,2
      A(I) = C(I)+D(I)*W**2
10    continue
      call impres(A,K,deltat,NT,h)
      return
      end


c
      subroutine TIR(C,D,K,AM,W,NW,deltat,NT,deltar,NR,hwt,J0,h)
c
c     Berekening impulsresponsie van membraan in r en t
c     hierbij is ingangssignaal een sommatie van nulde
c     order Besselfunctie van de eerste soort.
c
      integer NT,NR,NW,I,J,M,IFAIL
      double precision C(0:2),D(0:2),K,AM(NW),W(NW)
      double precision deltat,deltar,r,h(0:NR,0:NT)
      double precision hwt(0:NT),J0(0:NR)
      external S17AEF
      double precision S17AEF
c
      do 10 J=0,NR
      do 10 M=0,NT
      h(J,M) = 0
10    continue
      do 50 I=1,NW
      call IMRES(C,D,K,W(I),deltat,NT,hwt)
      do 50 J=0,NR
      r = J*deltar
      IFAIL = 0
      J0(J) = S17AEF(W(I)*r,IFAIL)
      if (IFAIL.eq.0) go to 40
      write(5,30)
30    format(2x,'FOUTMELDING IFAIL')
      go to 50
40    do 50 M=0,NT
      h(J,M) = h(J,M)+AM(I)*J0(J)*hwt(M)
50    continue
      return
      end
```

```
c
      subroutine CONV(deltat,NT,X,H,Y)
c
      integer K,I,NT
      double precision S,X(0:NT),Y(0:NT),H(0:NT),deltat
      Y(0) = 0
      do 20 K=1,NT
      S = 0
      do 10 I=1,K
      S = S+X(I)*H(K-I)
10    continue
      Y(K) = deltat*S
20    continue
      return
      end


c
c     Programma hoofd2.for
c     Gebruikmaking van subroutine grad,geval,
c     tir,match en conv.
c
      integer NW,NT,NR,I,J,M,IFAIL1,IFAIL2
      parameter(NW=10,NT=128,NR=4)
      double precision jm(10),AM(NW),C(0:2),D(0:2)
      double precision K,W(NW),deltat,deltar,deltal
      double precision RB,RST,J1,J12,h(0:NR,0:NT),pi
      double precision A1(0:NT),B1(0:NT),C1(0:NT),D1(0:NT)
      double precision E1(0:NT),F1(0:NT),hwt(0:NT),J0(0:NR)
      external S17AFF
      double precision S17AFF
c
      pi = 3.1416
      deltat =  0.0025
      deltar = 10
      deltal =  1
      RB  = 30
      RST = 30
      jm(1)  =  2.404826
      jm(2)  =  5.520078
      jm(3)  =  8.653728
      jm(4)  = 11.791534
      jm(5)  = 14.930918
      jm(6)  = 18.071064
      jm(7)  = 21.211637
      jm(8)  = 24.352472
      jm(9)  = 27.493480
      jm(10) = 30.634606
c
      do 10 M=1,NW
      W(M) = jm(M)/RB
10    continue
      if (RST.gt.RB) go to 100
      do 20 M=1,NW
      IFAIL1 = 0
      J1 = S17AFF(W(M)*RST,IFAIL1)
      if (IFAIL1.ne.0) go to 150
```

```
      IFAIL2 = 0
      J12 = S17AFF( jm( M) ,IFAIL2)
      if ( IFAIL2.ne.0) go to 200
      AM( M) = ( 2*RST*J1) /( jm( M) *RB*J12**2)
20    continue
      call gev( C,D,K)
      call tir( C,D,K,AM,W,NW,deltat,NT,deltar,NR,hwt,J0,h)
      do 30 J=0,NR
      do 30 I=0,NT
      h( J,I) = deltal*2*pi*h( J,I)
30    continue
      call MATCH( deltat,NT,C1)
      J = 0
      do 40 I=0,NT
      B1( I) = h( J,I)
40    continue
      call conv( deltat,NT,B1,C1,D1)
c
      do 50 I=0,NT
      A1( I) = I*deltat
50    continue
c
      call grad( 'responT',NT+1,0,4,A1,B1,C1,D1,E1,F1)
      go to 300
100   write( 5,110)
110   format( 2x,'RST is groter dan RB.')
      go to 300
150   write( 5,160)
160   format( 2x,'FOUTMELDING IFAIL1')
      go to 300
200   write( 5,210)
210   format( 2x,'FOUTMELDING IFAIL2')
300   continue
      stop
      end


c
      subroutine grad( name,npts,minmax,ncols,A,B,C,D,E,F)
c
c     door E.M.M.Ploemen.
c
      character*( *) name
      double precision A,B,C,D,E,F
      integer npts,minmax,ncols length,ip2,I,nrec
      real x,y1,y2,y3,y4,y5
      dimension A( 1) ,B( 1) ,C( 1) ,D( 1) ,E( 1) ,F( 1)
      intinsic sngl,max0
      nrec=max0( ( ncols,3)
      open( unit=9,file=name,status='new',access='direct',
     *  form='unformatted',recl=nrec)
c
      write( 9,rec=1) npts, ncols, 3
c
      if ( minmax.eq.0) then
      write ( 9,rec=2) 1,0,0
      length=npts
```

```
      else
      write (9,rec=2) 1,npts+3,npts+4
      length=npts+2
      end if
c
      do 10 I=1,length
      ip2=I+2
      if (ncols.eq.2) then
      x=sngl(A(I))
      y1=sngl(B(I))
      write (9,rec=ip2) x,y1
      else if (ncols.eq.3) then
      x=sngl(A(I))
      y1=sngl(B(I))
      y2=sngl(C(I))
      write (9,rec=ip2) x,y1,y2
      else if (ncols.eq.4) then
      x=sngl(A(I))
      y1=sngl(B(I))
      y2=sngl(C(I))
      y3=sngl(D(I))
      write (9,rec=ip2) x,y1,y2,y3
      else if (ncols.eq.5) then
      x=sngl(A(I))
      y1=sngl(B(I))
      y2=sngl(C(I))
      y3=sngl(D(I))
      y4=sngl(E(I))
      write (9,rec=ip2) x,y1,y2,y3,y4
      else if (ncols.eq.6) then
      x=sngl(A(I))
      y1=sngl(B(I))
      y2=sngl(C(I))
      y3=sngl(D(I))
      y4=sngl(E(I))
      y5=sngl(F(I))
      write (9,rec=ip2) x,y1,y2,.y3,y4,y5
      end if
10    continue
c
      close (unit=9,status='keep')
      return
      end
```